

INFORMATION TO USERS

This manuscript has been reproduced from the microfilm master. UMI films the text directly from the original or copy submitted. Thus, some thesis and dissertation copies are in typewriter face, while others may be from any type of computer printer.

The quality of this reproduction is dependent upon the quality of the copy submitted. Broken or indistinct print, colored or poor quality illustrations and photographs, print bleedthrough, substandard margins, and improper alignment can adversely affect reproduction.

In the unlikely event that the author did not send UMI a complete manuscript and there are missing pages, these will be noted. Also, if unauthorized copyright material had to be removed, a note will indicate the deletion.

Oversize materials (e.g., maps, drawings, charts) are reproduced by sectioning the original, beginning at the upper left-hand corner and continuing from left to right in equal sections with small overlaps. Each original is also photographed in one exposure and is included in reduced form at the back of the book.

Photographs included in the original manuscript have been reproduced xerographically in this copy. Higher quality 6" x 9" black and white photographic prints are available for any photographs or illustrations appearing in this copy for an additional charge. Contact UMI directly to order.

UMI

A Bell & Howell Information Company
300 North Zeeb Road, Ann Arbor MI 48106-1346 USA
313/761-4700 800/521-0600

Boston College

The Graduate School of Arts and Sciences

Department of Physics

LASER PHOTOACOUSTIC RESONANCE AND
MOLECULAR RELAXATION MEASUREMENT

a dissertation

by

GANG LEI

submitted in partial fulfillment of the requirements

for the degree of

Doctor of Philosophy

September, 1996

UMI Number: 9713051

Copyright 1996 by
Lei, Gang

All rights reserved.

UMI Microform 9713051
Copyright 1997, by UMI Company. All rights reserved.

**This microform edition is protected against unauthorized
copying under Title 17, United States Code.**

UMI
300 North Zeeb Road
Ann Arbor, MI 48103

© copyright by GANG LEI
1996

BOSTON COLLEGE
GRADUATE SCHOOL OF ARTS & SCIENCES

The thesis of Gang Lei

entitled Laser Photoacoustic Resonance and

Molecular Relaxation Measurements

submitted to the Department of Physics

in partial fulfillment of the requirements for the degree of

Doctor of Philosophy

in the Graduate School of Arts and Sciences has been read

and approved by the Committee:

Francesca Di Bartolo

Kevin S. Bedell

John W. Collins

David Broid

Alfred Bedell

Date August 14, 1996

Laser Photoacoustic Resonance and Molecular Relaxation measurements

Abstract

The photoacoustic resonance method was applied to study molecular relaxation in a cylindrical cavity. The profile of the acoustic resonance, excited by the vibrational mode ν_3 of a gas sample SF_6 with a CO_2 laser, was measured as a function of pressure between 1~800 Torr. A general theoretical treatment of the effects of vibrational and rotational relaxations on the acoustically resonant characteristics, such as the resonant frequency and the half-width, taking into account the contributions of surface and volume losses, and the nonideality of the gas, was worked out in detail and was used to frame the discussion of the relaxation processes following the vibrational excitation. The observed overall relaxation times were associated with the internal energy transition rates via an effective two-states model of the gaseous molecule. The analysis of the experimental data yields a value of vibrational relaxation time $(p\tau)_{V-T} = 0.21 \pm 0.01 \mu\text{s atm}$, and a value of $(p\tau)_{R-T} = 0.09 \pm 0.06 \text{ ns atm}$ for the rotational relaxation time of SF_6 at $T=295 \text{ K}$.

This thesis brought all aspects of photoacoustic resonance to the applications of molecular relaxation measurements. In particular, the rotational relaxation time of SF_6 was the first such measurement obtained by the photoacoustic resonance method. The measurements were performed on a newly constructed experimental apparatus with virtualized instrumentation and data acquisition and analysis system. This work appears promising as a basis for developing an infrared laser photoacoustic resonator capable of tracing and monitoring gas molecules, measuring molecular relaxation-times, and evaluating the rate constant and activation energy of photo-induced chemical reaction.

Table of Contents

Table of Contents.....	i
Acknowledgments	iv
List of Publications & Presentations.....	v
List of Tables and Figures	vii
1. INTRODUCTION	1
1.1 Motivation of the Thesis	1
1.2 Organization of the Thesis.....	3
1.3 Developments of the Photoacoustic Techniques	5
1.4 Applications in Environmental Studies	8
References to Chapter 1	11
2. LASER PHOTOACOUSTIC RESONANCE & RELAXATION.....	13
2.1 Absorption of Light.....	14
2.2 Excitation of Acoustic Wave.....	22
2.3 Losses Mechanism (Q factors)	27
2.3.1 Heat Conduction and Viscosity	30
2.3.2 Nonideality of Gas.....	34
2.3.3 Molecular Relaxation	38
2.4 Shift of Frequency & Broadening of Line Width.....	41
2.5 General Consideration on Relaxation	43
2.5.1 Excitation in Parallel	46
2.5.2 Excitation in Series	47
References to Chapter 2	50

3. THEORY OF MOLECULAR ENERGY TRANSFER.....	51
3.1 Molecular Collisions.....	51
3.2 Vibrational-Transitional Transfer.....	56
3.2.1 The Transition Probability (SSH Theory).....	56
3.2.2 V-R and V-(T,R) Transfer	62
3.2.3 Relaxation in Pure Gases	66
3.3 Vibrational-Vibrational Transfer.....	69
3.3.1 The SSH theory for non-and resonant transfer.....	69
3.3.2 Intermode Transfer in Polyatomic Gases.....	70
3.4 Rotational-Transitional Transfer.....	74
References to Chapter 3	78
4. EXPERIMENTAL APPARATUS.....	80
4.1 The Hardware Setup	80
4.1.1 Cylindrical Cavity and Acoustic Modes	82
4.1.2 The instruments.....	91
4.2 The Software Virtualization (VI).....	93
4.2.1 The Operation System.....	93
4.2.2 The Program of the VI.....	94
4.2.3 The Front Panel of the VI.....	100
4.3 Experimental Results.....	101
References to Chapter 4	105
5. RELAXATION AND LOSSES OF SF ₆	106
5.1 Sulfur Hexafluoride Molecules.....	106
5.2 Photoacoustic Resonance in a Cylinder	108

5.3	Experimental Results and Data Handling.....	115
5.4	Discussions of the Results.....	121
5.4.1	V-T and R-T Relaxation Times of SF ₆	121
5.4.2	Losses Mechanisms	122
5.4.3	Nonideality of The Gas.....	123
5.4.4	Relaxation Model in SF ₆	123
	References to Chapter 5	126
6.	CONCLUSIONS AND FUTURE WORK.....	128
6.1	Conclusions Remarks	128
6.2	Continuing Interest & Suggestions for Future Work.....	130
	APPENDIX A CO ₂ Waveguide Laser Line Data Sheet (¹² C ₁₆ O ₂)	132
	APPENDIX B The Cavity Modes Data Sheet.....	135
	APPENDIX C Instrument Driver Programs.....	136
	C-1. EG&G 5210 Lock-in	136
	C-2. HP 3325A Synthesizer/Function Generator.....	142

***A*cknowledgments**

I would like to thank my thesis advisor, Dr. Baldassare Di Bartolo, for his advice and encouragement during the course of the thesis works. I have benefited over the years from his teaching, guidance, and friendship.

I am grateful to Dr. David Broido, Dr. Kevin Bedell, Dr. Clyfe Beckwith, and Dr. John Collins for serving on my thesis committee and helpful discussions.

Many thanks to Dr. Rein A. Uritam, Dr. Kevin Bedell, Dr. Michael J. Graf, and department administrator, Ms. Shirley Lynch for their support and help throughout these years of my graduate studies at Department of Physics, Boston College.

Finally, I am thankful to my wife for her sacrifice and support during my years of study.

List of Publications and Presentations

1. G. Lei and B. Di Bartolo, "Measurement of rotational and vibrational relaxation in gases by photoacoustic resonance: application to SF₆", *J. Appl. Phys.*, **79**, 2890(1996).
2. G. Lei and B. Di Bartolo, "Virtual instrumentation of a resonant spectrophone", *Rev. Sci. Instrum.*, **66**, 5102(1995).
3. G. Lei and B. Di Bartolo, "Relaxation-time measurements by photoacoustic resonance methods", presented at The American Physical Society, APS March Meeting, St. Louis, 1996.
4. G. Lei and B. Di Bartolo, "Relaxation and losses of SF₆ in a photoacoustic resonator", presented at NATO Advanced Study Institute of Atomic and Molecular Spectroscopy, 12th course: Spectroscopy of Collective Excitations in Solids, Erice, Italy, June 1995.
5. X. Xu and G. Lei *et.al*, "Multiplication of carriers by impact ionization", *J. Crystal Growth*, **117**, 935(1992).
6. G. Lei and X. Xu, "An EL device of spatial separation of carrier acceleration and excitation", *J. Luminescence*, **48&49**, 881(1991).
7. X. Xu & G. Lei *et.al*, "New approach to color thin film electroluminescence", *SPIE Proceedings*, **1519**, 525(1991).
8. X. Xu and G. Lei *et.al*, "Preliminary trial of third generation EL", *J. Crystal Growth*, **101**, 1004(1990).

9. G. Lei and X. Xu *et.al*, "Energy distribution of hot electrons in TFEL", *Acta Polytechnica Scandinavica, Appl. Phys.*, **170**, 295(1990).
10. X. Xu & G. Lei *et.al*, "Attempt at the third generation electroluminescence", *Acta Polytechnica Scandinavica, Appl. Phys.*, **170**, 133(1990).
11. G. Lei and X. Xu, "A new electroluminescent device", *J. Electrochem. Soc.*, **137**, 414c(1989).
12. G. Lei, "The dependence of infrared emission of Er^{3+} on frequency", Presented at the International Conference on Luminescence ICL'93, Storrs, CT 1993.
13. G. Lei & X. Xu, "Measurement of light-induced detrapping charge in electroluminescence", presented at the International Conference on Luminescence, ICL'93, Storrs, CT 1993.
14. G. Lei and X. Xu, *et.al*, "New principle of accelerating electrons in electroluminescence", *Proceedings of 2th International Symposium on Rare-Earth Spectroscopy, Changchun (1989)*110, (World Scientific).

List of Figures and Tables

Chapter 2

- FIG. 2.1 (a) Laser excitation of vibrational-rotational molecular levels in the IR spectral region; (b) bottleneck effect in absorption saturation of vibrational-rotational transition.
- FIG. 2.2 The acoustic energy loss/decay in the time domain.
- FIG. 2.3 The energy losses in frequency domain, i.e., resonant line shape.
- FIG. 2.4 The temperature dependence of second Virial coefficient of SF₆.
- Table 2.1 Characteristic values α_{mn} for the cylindrical cavity.
- Table 2.2 Integrals used for the evaluation of Eqs.(2.48, 50).

Chapter 3

- FIG. 3.1 The Lennard-Jones intermolecular potential.
- FIG. 3.2 Schematic representation of the overlap between the distribution of molecular speeds $f(v)$, and the de-excitation probability P_{10} , as a function of molecular speed v .
- FIG. 3.3 “Fitting” of exponential potential.
- FIG. 3.4 Energy level diagram for simultaneous vibrational and rotational transitions.
- FIG. 3.5 Energy-level diagram showing transition for a molecule with two active vibrational modes.
- FIG. 3.6 Energy-level diagram for a molecule with two active vibrational modes, showing double relaxation process.

Chapter 4

- FIG. 4.1 Block diagram of the resonant spectrophone setup.
- FIG. 4.2 (a) Cross sectional view of window flange of the resonant cavity. (b) Side view of the resonant cavity. (c) The side view of the cavity window.
- FIG. 4.3 Pictorial view of resonant acoustic longitudinal, azimuthal, and radial modes.
- FIG. 4.4 The dimensions of *Knowles* BT-1759 microphone
- FIG. 4.5 Performace specification of *Knowles* BT-1759 microphone.
- FIG. 4.6 The manifold of gas handling system.
- FIG. 4.7 The program block diagram of the resonant spectrophone VI .
- FIG. 4.8 The block diagram of the laser resonant specctrophone VI at the 3th sequence.
- FIG. 4.9 The front panel of the resonant spectrophone VI.
- FIG. 4.10 The resonant profile of the first radial mode (100) of SF₆ at pressure 40 Torr and temperature T=295 K.
- FIG. 4.11 The resonant profile of the second longitudinal mode (002) of SF₆ at pressure 600 Torr and T=289 K.

Chapter 5

- FIG. 5.1 The normal vibrations of an octahedral XY₆ molecule (SF₆) with corresponding degeneracy factors (*g*), and wave numbers (cm⁻¹).
- FIG. 5.2 An overview of the resonance profile of the mode (034) of SF₆ as function of pressure, (a) 50~1000 Torr, (b) 1~50 Torr. With the

pressure decreasing, the resonant frequency shifts up and down through the vibrational dispersion region, and the accumulated energy in the mode spreads out, resulting in an increase of the half-widths.

FIG. 5.3 The pressure dependence of resonant frequency of the combination mode (034) for SF₆. The upper S-shaped thin curve is the calculated vibrational dispersion, the surface losses make large contribution at low pressure, and the non-ideal correction becomes significant at high pressure.

FIG.5.4 The pressure dependence of the half-width of the combination mode (034) for SF₆. The lower bell-shaped thin curve is the calculated vibrational relaxation and the difference on its left wing as pointed by an arrow is the rotational relaxation contribution. The surface losses make a large contribution to the half-width, and the volume losses make its correction at low pressure.

FIG. 5.5 The effective two-states relaxation model of SF₆, following the CO₂ (P₂₀) laser excitation of the ν_3 vibrational mode, the system relaxes by rapid R-T to translational and V-V down to the lowest vibrational ν_6 level; the whole excess vibrational temperature relaxes via a slow rate V-T transfer process from ν_6 level to the translational temperature, and heat the entire gas translationally.

Table 5.1 Summary of the constants used to evaluate Eq.(5.17) and Eq.(5.18).

Chapter 1

Introduction

1.1 Motivation of the Thesis

The photoacoustic effect may be used to study molecular relaxation processes, in addition to other methods based on spectroscopic and ultrasonic absorption techniques. The photoacoustic process is initiated by exciting intermittently a transition with a modulated radiation beam; molecular collisions relax the excited states; in turn this results in an increased translational temperature and causes an induced pressure fluctuation within a closed cavity, i.e. an acoustic wave. Two things make the photoacoustic method different from the others: i) Unlike spectroscopy, photoacoustics deals with the ubiquitous non-radiative processes, which often provides an effective conversion of absorbed photon energy into translational energy; and ii) with laser radiation, the relaxation process of individual states of polyatomic molecule can be investigated selectively (this situation is different than that provided by the ultrasonic absorption method where only the low-lying vibrational modes are accessible).

Relaxation time measurements have been traditionally carried out with photoacoustic "non-resonant" methods, mainly by measuring the phase lag between the modulated radiation input and the resulting acoustic wave. This phase lag, however, includes the effects of the heat loss from the measuring

system (i.e. cavity), and of the molecular relaxation; it is possible to sort out their separate contributions only if the two relevant time constants are sufficiently different. An acoustic resonance, however, could be promoted by using a laser beam spatially confined and temporally modulated at a frequency coincident with one of the natural frequencies of the cavity; in this way the energy accumulates in a standing acoustic wave that makes the cavity act as an acoustic amplifier.

The initial interest in laser photoacoustic resonance was primarily due to the high sensitivities attainable in the detection of trace amounts of gaseous molecules by monitoring their vibrational spectra in the infrared region.¹⁻³ This has led to an increasing number of applications, such as molecular relaxation processes⁴⁻⁶, photon-induced chemical reactions⁷ and gas absorption line profiles,⁸ mainly due to its high sensitivity and the capability of dealing with the non-radiative processes. The measurements of the rate constants of energy transfer between different degrees of freedom are carried out by analyzing the characteristics of an acoustically resonant curve (a *Lorentzian* profile), such as the resonant frequency and the half-width as a function of pressure. The advantage of this method is that it utilizes the measurement of a resonance frequency instead of that of a sound velocity, a parameter especially difficult to appraise in the dispersion region, with a considerable improvement of the accuracy. On the other hand, the photoacoustic signal in a resonator may depend on the various losses present in the cavity and on the deviation of the gas from the ideal condition. Therefore, one has to take into account a number of factors in order to extract from the data the information related to the relaxation processes. Since a large set of experimental data has to be collected, an automatic data acquisition system seems to be mandatory.

The photoacoustic resonance method has received some attention in the investigations of molecular relaxation and photo-induced chemical reactions,⁵⁻⁷ but it has not been widely applied. One difficulty is that the observed relaxation times do not represent the average lifetime of the mode excited, but the time it takes the excitation photon energy to be converted into translational (heat) energy.

The purpose of this thesis is to examine the photoacoustic resonant method and its application to the measurement of relaxation times. Firstly, a theoretical treatment relating the molecular vibrational and rotational relaxation processes to the characteristics of the acoustic resonance is presented. Secondly, the experiments on the well-known gas system SF₆, a symmetrical molecule with fifteen vibrational degrees of freedom and six fundamental modes, are reported. Finally the appropriate parameters related to the various relaxation processes in this system are extracted from the experimental data.

1.2 Organization of the Thesis

Chapter 2 presents the theory of photoacoustic resonance. The light absorption processes of a simple two vibrational level system with rotational structure are discussed. The generation of acoustic waves, the occurrence of resonance, and the loss mechanisms which affect the resonance line shape in terms of a mode dependent Q_j factor, are treated in detail. The last section presents a general discussion of relaxation, following the excitation "in parallel" and "in series".

In Chapter 3, the theories of molecular vibrational-translational, vibrational-vibrational and rotational-translational energy transfers are outlined to back the interpretations of experimental photoacoustic results, since photoacoustics deals with translational temperature, a final energy reservoir, ultimate destination of the relaxation of excited molecules through a number of intermediate states.

Chapter 4 presents a description of the apparatus which has been constructed with the aim of developing versatile techniques and instrumentation, which can perform the tasks of tracing and monitoring gas molecules, measuring molecular relaxation time, and evaluating the rate constant and active energy of photo-induced chemical reaction in a resonator. The way to pursue this goal is to use the so-called "Virtual Instrument", in which the software plays the key role conventionally played by the hardware in traditional experimental setups. Through the GPIB(IEEE 488.2) interface, all the instruments work as one virtual instrument that can be easily defined as an application-oriented system.

Chapter 5 presents a thorough study of molecular relaxation of gas sample SF₆ via the cavity mode (034). The profile of the acoustic resonance, excited by the vibrational mode ν_3 with a CO₂ laser, was measured as a function of pressure between 1~800 Torr. The analysis of the experimental data yields a value of vibrational relaxation time $(p\tau)_{V-T} = 0.21 \pm 0.01 \mu\text{s atm}$, and a value of $(p\tau)_{R-T} = 0.09 \pm 0.06 \text{ ns atm}$ for the rotational relaxation time of SF₆ at T=295 K. The latter piece of data may be considered the first reported result on rotational relaxation by the photoacoustic resonance method.

Chapter 6 summarizes all the results and conclusions of this research, presents the reasons for the continuing interest in this type of studies, and put forward suggestions for future works.

1.3 Developments of the Photoacoustic Techniques

The photoacoustic effect was independently discovered, around 1880, by a number of workers.⁹⁻¹¹ They found that, when certain gases were exposed to radiation modulated at the correct frequency, they emitted sound. Tyndall established that sound was caused by energy beyond the red end of the visible spectrum, now known of course as the IR region. The effect is caused by the periodic heating and cooling of the IR absorbing gas, which, in a constant-volume system, give rise to a pressure wave, a consequently a sound wave. Attempts by Tyndall to develop the method for gas analysis were curtailed by the lack of a convenient sound detector.

In 1938 a number of photoacoustic gas analyzers were constructed using modern electronic and microphone techniques.¹² Over the years development had continued and commercial gas analyzers using this principle became available which would detect a few ppmV of an absorbing gas molecule in air.

The use of the photoacoustic effect to measure the rate of energy transfer between vibrational and translational modes was first suggested by Gorelik.¹³ A gas absorbs energy into an IR-active vibration; after a time delay determined by the rate of energy transfer, this energy will appear in the translational modes and cause the gas to heat up. If the modulation frequency is such that the time of

irradiation is less than the time required for energy transfer to take place then the phase of the pressure fluctuations will be different than that of the incident radiation. Thus a study of the phase of the acoustic pressure as a function of modulation frequency should give information about the rate of intermolecular energy transfer. All attempts to use the photoacoustic effect to measure relaxation times were based on Gorelik's original suggestion until the 1970s.

In the early 1970s,¹⁴ the initial resurgence of interest in photoacoustic spectroscopy was primarily due to the high sensitivity attained by the usage of laser sources of excitation. These sources include optical parametric oscillators, dye lasers, and current-tunable diode lasers. Later, further improvements were proposed in two essential ways.^{15,16} Firstly, the sample cell was designed as an acoustic resonance chamber so that the pressure fluctuations produced by spatially and temporally nonuniform excitation contribute to standing acoustic waves within the chamber. Secondly, the excitation beam was modulated at a frequency coincident with one of the natural resonant acoustic frequencies of the chamber. The fact that molecular vibrational absorption cross sections are generally not large, coupled with the requirement for low-level detection, means that long absorption path lengths must be used. This has led to the design of multipaths resonators.¹⁷ A photoacoustic resonator may allow the identification by means of IR absorption spectra of a concentration at ppbV level and the measurement of gas absorption coefficients as low as 10^{-8} cm^{-1} .

The usage of the photoacoustic resonant method to measure the rate of energy transfer between different degrees of freedoms appeared in 1979,^{18,19} and to study chemical relaxation in 1990.²⁰ The analysis of the characteristics of a

resonant curve (i.e. a *Lorentzian* profile), such as the shift of the resonant frequency and the broadening of the half-width as a function of pressure, may allow one to extract the parameters of molecular relaxation with high accuracy. The theory of such analysis is formally discussed in detail in Chapter 2; here we make a few simple points to indicate roughly what happens. The resonant frequencies of a cylindrical cavity are directly proportional to the velocity of sound wave c , according to²¹

$$\omega_{mnl} = c \left[(\pi \alpha_{mn} / R)^2 + (\pi l / L)^2 \right]^{1/2} \quad (1.1)$$

where the labels m , n and l refer to radial, azimuthal and longitudinal modes, respectively. R is the radius and L the length of the cavity, α_{mn} is the n th zero of the derivative of the m th *Bessel* function divided by π . For an ideal gas, the velocity of sound is

$$c^2 = \frac{\gamma RT}{M} = \frac{RT}{M} \left(1 + \frac{R}{C_v} \right) \quad (1.2)$$

where C_v is the heat capacity at constant volume, R is the gas constant, and M is the molecular weight. On the other hand, the thermodynamic parameters of a gas, such as C_v , depend on all the contributions from the different modes of motion, so that

$$C_v = C_{trans} + C_{rot} + C_{vib} + C_{other} \quad (1.3)$$

Molecular relaxation effects arise because of the finite time required for the internal degrees of freedom of the molecules to come into thermal equilibrium with the translational degrees of freedom, as described by:

$$\frac{dE_n}{dt} = - \frac{(E_n - E_n^e)}{\tau_n} \quad (1.4)$$

where E_n is the ensemble average energy in the n th mode of the molecule, E_n^e is its equilibrium value, and τ_n is the relaxation time for that mode. If E_n varies as a harmonic function of time, $E_n = E_0 e^{i\omega t}$, the solution of the above differential equation leads us to the dynamic heat capacity $C_n(\omega)$ for the n th mode,

$$C_n(\omega) = \frac{dE_n(\omega)}{dT} = \frac{C_n}{1 + i\omega\tau_n} \quad (1.5)$$

Thus information regarding the relaxation times of different modes can be extracted from the dispersion of the resonance frequency, and also the absorption of half-width of an acoustically resonance profile.

1.4 Applications in Environmental Studies

The present techniques oriented toward the detection of small concentrations of pollutants do not seem to meet the needs in today's situation, when complex mechanisms like the formation of acid rain or the generation of photochemical smog are dominant. One of the motivating incentives for our investigations in the field of photoacoustics has been the attempt to develop a laser photoacoustic resonant spectrophone which can perform the three tasks of tracing and monitoring gas molecules, measuring molecular relaxation-time, and evaluating the rate constant and active energy of photo-induced chemical reaction. Through these measurements one should be also able to gain a deeper insight into the molecular and chemical processes occurring in gases.

Since the beginning of the industrial revolution the burning of fossil fuels for energy production has increased drastically. As a consequence, growing

amounts of gaseous air pollutants have been emitted into the atmosphere, influencing natural physicals and chemical regulation cycles previously untouched over long periods. The long-term increase of global air pollution is documented by studies on polar snow and ice samples which contain small air bubbles and thus preserve a unique and chronological record of the past composition of the earth's atmosphere. On the basis of these studies an increase of the concentrations of methane (CH_4) and carbon dioxide (CO_2) from pre-industrial data of approximately 0.7 and 260 ppmV to present-day data of 1.6 and 340 ppmV, respectively, has been verified.²²⁻²⁴ For both gases, the largest concentration gradients were obtained from 1950 to the present time.

The gaseous pollutants sulfur dioxide (SO_2), nitrogen oxide (NO_x), and hydrocarbons (HC) as well as their reaction products like acids and oxidants are of main importance. SO_2 , NO_x , and HC are called primary pollutants while the reaction products are denoted as secondary pollutants. In earlier times, the effects of air pollution were restricted to industrial areas where increased concentrations of toxic compounds occurred near their source. More recently, large-area damages to nature, e.g., the acidification of soils and waters²⁵ or the serious forest decline were related to the increase of air pollution. However, the primary pollutants cannot be the primary origin of these damages. Today, complex mechanism like the formation of acid rain or the generation of photochemical smog are dominant. In the former process the primary pollutants SO_2 and NO_x are converted to sulfuric and nitric acids which subsequently are deposited on the earth as acid rain or fog. In the latter process solar UV irradiation causes the conversion of NO_x and HC to toxic oxidants such as ozone (O_3) or peroxyacetylnitrate (PAN). In the course of these conversion processes

the resultant secondary pollutants can be transported over large distances. Therefore, their concentrations may be smaller in the vicinity of emission sources, e.g., near roads or large cities, than in rural areas which were previously regarded as clean-air regions.

The sensitive and selective detection of the numerous trace constituents is a prerequisite for the understanding of the various tropospheric air pollution processes. Hence, the development of novel physical or chemical techniques of detection in addition to conventional methods is required. A typical example for the importance of novel schemes was the discovery of the substance PAN in smog-simulation chambers by the use of inferred absorption spectroscopy.²⁶ Spectroscopic techniques are of growing interest due to the recent development of powerful lasers tunable over large-wavelength ranges which permits the detection of numerous substance at low concentrations. In contrast to conventional, e.g., wet-chemical or chromatographic schemes, spectroscopic methods exhibit some unique advantages. In general, they allow the contactless simultaneous detection of many substance. Furthermore, some of the novel techniques, e.g., the different versions of light detection and ranging permit the three-dimensional profiling of air pollutants.

One of the most promising spectroscopic techniques developed in recent years is photoacoustic spectroscopy. It offers some obvious advantages like simple setup, easy calibration, high sensitivity, and wide dynamic range. In conjunction with tunable lasers, the *in situ* monitoring of many substances of environmental concern occurring at ppbV concentrations appears feasible, although it should be mentioned that absorption interferences in

multicomponents mixtures often may restrict the present applications either to specific components or to measurements near emission sources.

References to Chapter 1

- 1.1 L.B.Kreuzer, J. Appl. Phys. **42**, 2934 (1971).
- 1.2 C.F.Dewey, Jr., R.D. Kamm, and C.E.Hackett, Appl. Phys. Lett. **23**, 633 (1973).
- 1.3 Roger D.Kamm, J. Appl. Phys. **47**, 3550 (1976).
- 1.4 K. Frank and P. Hess, Chem. Phys. Lett. **68**, 540 (1979).
- 1.5 R.H.Johnson, R.Gerlach, L.J.Thomas III and N.M.Amer, Applied Optics **21**, 81 (1982).
- 1.6 A.Karbach and P. Hess, J. Chem. Phys. **83**, 1075 (1985).
- 1.7 M.Fiedler & P.Hess, J. Chem. Phys. **93**, 8693 (1990).
- 1.8 R.P.Fiegel, P.B.Hays & W.M.Wright, Applied Optics **28**, 1401 (1989).
- 1.9 J. Tyndall, Proc. Roy. Soc. (London), **31**, 307(1881).
- 1.10 W.C. Röntgen, Phil. Mag., **11**, 308(1881).
- 1.11 A.G. Bell, Phil. Mag., **11**, 510(1881).
- 1.12 A.H. Pfund, Science, **90**, 326(1939).
- 1.13 G. Gorelik, Dolk. Akad. Nauk SSSR, **54**, 779(1946).
- 1.14 L.B.Kreuzer, J. Appl. Phys. **42**, 2934 (1971).
- 1.15 C.F.Dewey, Jr., R.D. Kamm, and C.E.Hackett, Appl. Phys. Lett. **23**, 633 (1973).
- 1.16 P. D. Goldan & K. Goto, J. Appl. Phys., **45**, 4350(1974).
- 1.17 Roger D.Kamm, J. Appl. Phys. **47**, 3550 (1976).

- 1.18 K. Frank and P. Hess, Chem. Phys. Lett. **68**, 540 (1979).
- 1.19 R.H.Johnson, R.Gerlach, L.J.Thomas III and N.M.Amer,
Applied Optics **21**, 81 (1982).
- 1.20 M.Fiedler & P.Hess, J. Chem. Phys. **93**, 8693 (1990).
- 1.21 P.M.Morse & K.U.Ingard, *Theoretical Acoustics*,
(McGraw-Hill, New York, 1968).
- 1.22 E.W. Wolff and D.A. Peel, Nature **313**, 535(1985).
- 1.23 B. Stauffer, G. Fischer, A. Neftel, and H. Oeschger, Science **229**, 1386(1985).
- 1.24 H.Friedli, et al., Nature **324**, 237(1986).
- 1.25 J.O. Reuss & D.W. Johnson,
Eccological Studies (Springer, New York, 1986), vol.59.
- 1.26 W.E. Scott, et al, Procc. Am. Petro. Instrum. Sec. III **37**, 171(1957).

Chapter 2

Laser Photoacoustic Resonance and Relaxation

When a molecule absorbs infrared radiation, the energy taken up appears directly as quanta of vibrational energy. A molecule, having absorbed such energy, may lose it by spontaneous emission of radiation, by induced emission, or by converting it into thermal energy. This last process occurs via collisions; the excitation energy may occasionally reappear as vibrational energy of the collision partner, but usually it becomes translational energy. This means that, if an absorbing gas is illuminated by infrared radiation, it will warm up, and reach a new average (translational) temperature determined by the number of quanta absorbed per unit time and by the rate of heat loss from the system. If the system is illuminated by infrared radiation which is periodically interrupted, or the intensity of which is modulated, the gas will heat and cool, and a periodic change of pressure will be observed in a constant volume system (a cavity). These periodic pressure changes will lead to sound emission.

When the frequency of the periodic change of pressure coincides with the natural frequency of the cavity, an acoustic resonance is promoted. The analysis of such a resonant system differs from that of a non-resonant one in that the acoustic phenomena can no longer be described in terms of a response to a single excitation cycle repeated periodically and averaged over time. The steady state resonant response is a consequence of an initial transient state during which energy is stored in the acoustic standing wave. Upon reaching a steady

state the energy lost by way of the various dissipation mechanisms is balanced by that gained by way of molecular absorption.

This chapter provides a physical description of how this resonance could afford a method for the measurement of the rate constants of energy transfer among different degrees of freedom. Section 2.1 uses a simple mathematical formulation to describe the optical absorption process in a gas molecule with two vibrational level system with rotational structure; it considers the effect of the pulse duration of the excitation source on the resulting photoacoustic (PA) signal. Section 2.2 presents the formalism employed for treating generation of acoustic wave and the acoustic resonance. Section 2.3 deals with the loss mechanisms which affects the resonance line shape in terms of a mode dependent Q_j factor, the molecular relaxation has been treated as one of them as bulk viscosity, a detailed theoretical treatment has been given to the molecular relaxation. Section 2.4 summarizes final expressions of resonance characteristics in terms of a shift of the resonance frequency and a broadening of the half width. The last section presents general considerations on relaxation, and on three different modes of excitation, the excitation in parallel, in series, and in complex.

2.1 Absorption of Light

The physical processes responsible for the photoacoustic phenomenon are the same for both coherent and incoherent radiation sources. They include optical resonant excitation of the medium followed by radiation absorption, non-radiative relaxation of excited molecules, heating of the medium, and formation of acoustic oscillations. The use of laser radiation sources has a number of

advantages and leads to essential features both in the processes of generating photoacoustic signals and in the principles of designing proper measuring schemes; the high radiation power makes it possible to excite a considerable fraction of molecules, thereby realizing the ultimate sensitivity of the system. The high monochromaticity of the beam and the possibility of frequency tuning allow the running of the absorption spectra of many molecules with high resolution, realizing the selective excitation of individual molecular species and of particular quantum states of a molecule. The spatial coherence provides a well collimated laser-beam with a consequent increase in sensitivity.

To estimate the amplitude and shape of the PA signal it is necessary to calculate: a) the number of molecules excited by radiation, b) the gas temperature variation, caused by the nonradiative relaxation of molecules, and c) the variation of gas pressure.

The primary action which initiates the PA process in gases is the variation in population of the molecular energy levels resonating with the radiation: electron levels in the ultraviolet and visible spectral regions, vibrational-rotational levels in the IR region and purely rotational ones from the far-IR to the microwave region. The procedure by which the PA signal is calculated is similar for all the spectral regions, but there are specific features for each case. For instance, when using an electronic excitation an account must be taken of possible photochemical processes; as a result, the portion of absorbed energy causing gas heating decreases. It should also be noted that the relaxation of excited molecules through a number of intermediate states is rather complex; this

makes it more difficult to estimate the temporal parameters of PA signals; we will deal with this problem in Chapter 3.

Very generally, the radiation power absorbed in a unit of volume is given by

$$H_{abs}(t) = \alpha(\nu, t, I)I(t) \tag{2.1}$$

where $I(t)$ is the radiation intensity, $\alpha(\nu, t, I)$ is the absorption coefficient of the gas per unit length that depends on the intensity I and on time t on account of possible nonlinear and transient interaction effects between radiation and gas. In pre-laser PA spectroscopy the gas absorption coefficient did not vary with radiation intensity: it was always assumed that $\alpha(\nu, t, I) = \alpha(\nu)$.

Let us consider the simplest model of absorption of IR laser radiation via a vibrational-rotational molecular transition. The Figure 2.1 illustrates this model.

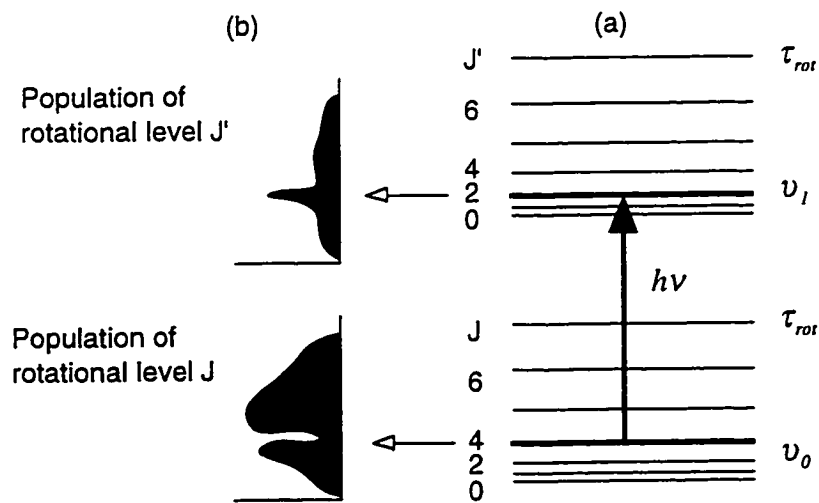


FIG. 2.1 (a) Laser excitation of vibrational-rotational molecular levels in the IR spectral region; (b) bottleneck effect in absorption saturation of vibrational-rotational transition.

Collisions lead to a Boltzmann equilibrium distribution of molecules over the rotational levels with characteristic rate τ_{rot}^{-1} . At the same time the laser radiation with the rate $w = \sigma_j I/h\nu$ (σ_j being the cross section of the radiative transition $\nu = 0, j$ and $\nu = 1, j'$ between the levels concerned) excites the molecules from rotational sublevel j of the ground vibrational state $\nu = 0$ to the rotational sublevel j' of the excited vibrational state $\nu = 1$. This changes both the rotational and vibrational distributions of molecules. The vibrationally excited molecules relax to the ground state from all rotational sublevels in the characteristic time τ_{vib} . For simplicity, we neglect here the possible excitation of molecules to higher vibrational levels and vibrational-rotational exchange between molecules.

The rate equations describing the rotational distribution of molecules under laser excitation have the form

$$\frac{dn_{1,j'}}{dt} = w(n_{0,j} - n_{1,j'}) + \frac{q_{1,j'}N_1 - n_{1,j'}}{\tau_{rot}} \quad (2.2.a)$$

$$\frac{dn_{0,j}}{dt} = w(n_{1,j'} - n_{0,j}) + \frac{q_{0,j}N_0 - n_{0,j}}{\tau_{rot}} \quad (2.2.b)$$

where $n_{\nu,j}$ is the molecular density in the vibration-rotational state (ν, j) , N_ν is the total density of molecules in the vibrational state ν , i.e., $N_\nu = \sum_j n_{\nu,j}$. The value $q_{\nu,j}$ describes the fraction of molecules in the vibrational state ν at the rotational state j under consideration. In another word, the factor $q_{\nu,j}$ describes the rotational distribution equilibrium of molecules in the vibrational state ν ,

$$q_{\nu,j} = \frac{1}{z^{rot}} g_j \exp\left(-\frac{E_j}{k_B T}\right) \quad (2.3)$$

where z^{rot} is the statistical sum of the rotational states, g_j is the degeneracy of the rotational sublevel j with rotational energy E_j and k_b is the Boltzmann constant. The density variation of vibrationally excited molecules is determined by the excitation rate w and the time of vibrational relaxation τ_{vib} ,

$$\frac{dN_1}{dt} = w(n_{0,j} - n_{1,j'}) + \frac{N_1^0 - N_1}{\tau_{vib}} \quad (2.4.a)$$

The population of the lowest vibrational state N_0 is determined from the total population of the vibrational levels $v = 0, 1$:

$$N_0 + N_1 = N_0^0 + N_1^0 = const. \quad (2.4.b)$$

The value of N_v^0 is the equilibrium population of the vibrational state v without excitation.

The time τ_{vib} of vibrational relaxation of excited molecules to the ground state is described by

$$\tau_{vib} = \left(\tau_{V-T}^{-1} + \tau_{rad}^{-1} + \tau_w^{-1} \right)^{-1} \quad (2.5)$$

where τ_{V-T} is the time of vibrational rotational relaxation responsible for the transfer of the molecular excitation energy to heat, τ_{rad} is the time of radiative relaxation, τ_w is the relaxation time of molecules onto the cell walls. For vibrational rotational molecular state at gas pressure typical for PA cells (hundreds of Torr) the following relation is valid

$$\tau_{rot} \ll \tau_{V-T} \ll \tau_{rad} \leq \tau_w \quad (2.6)$$

Eqs (2.2~4) describe the population kinetics of the excited vibrational state and the depletion of the ground vibrational state. Knowing the level population, it is possible to determine the absorption coefficient per unit length

$$\alpha(\nu, t, I) = \sigma_j(\nu)(n_{0,j} - n_{1,j'}), \quad (2.7)$$

and, according to Eq.(2.1), the absorbed radiation power per unit volume. Here we use the cross section of the transition between rotational-vibrational states. In the literature the transition cross section determined by total population of vibrational levels is also given as follows:

$$\alpha = \sigma(\nu)(N_0 - N_1). \quad (2.8)$$

From Eqs. (2.7,8) it follows that both cross section σ and σ_j are related by the fraction q or relative population of the rotational state j

$$\sigma = q\sigma_j \quad (2.9)$$

for simplicity we have assumed that $q_{0,j} \approx q_{1,j'} = q$.

Instead of solving Eq.(2.2~4) in the general case and thus calculating $\alpha(\nu, t, I)$, we consider only three different particular cases which give a clear picture of molecular absorption saturation by IR radiation.

a) Short Laser Pulse ($t_p \leq \tau_{rot}$). For $t_p \leq \tau_{rot}$. The rotational relaxation during a laser pulse is negligible. Therefore, in the molecular distribution over rotational states a "peak" is formed at the level $\nu = 1$, and conversely a "hole" at $\nu = 0$. In other words, the vibrational-rotational transition $V = 0, j \rightarrow V = 0, j'$ resonating with the laser radiation becomes saturated, and rate of further

excitation of the molecules is limited by the so-called "rotational bottleneck". After the pulse is over, the absorbed energy is distributed over all the rotational sublevels by rotational relaxation. And, finally, during τ_{vib} the excited molecules return back to their initial state.

In this regime the population of the upper level depends weakly on the shape of the laser pulse. The population fully depends on the pulse energy flux ϕ

$$\phi = \int_0^{t_p} I dt \quad (2.10)$$

and

$$N_1 \approx N_0 \frac{q}{2} \left[1 - \exp(-\phi/\phi_s^j) \right] \quad (2.11)$$

where, for simplicity, we assumed that $N_1^0 \ll N_0$ and introduce the absorption saturation energy

$$\phi_s^j = q \frac{h\nu}{2\sigma} = \frac{h\nu}{2\sigma_j} \quad (2.12)$$

At the radiation fluency $\phi = \phi_s^j$ the absorption coefficient decreases by e times. When $\phi \ll \phi_s^j$, the absorption is linear. In the other limiting case ($\phi \gg \phi_s^j$), absorption is highly saturated and the maximum population of the upper state can be expressed as

$$N_1^{\max} \approx q \frac{N_0}{2}. \quad (2.13)$$

With polyatomic molecules one must be careful with Eqs.(2.11, 13) at $\phi \gg \phi_s$, because multistep and multiphoton processes may participate even at a low energy fluency of the laser pulse. The average energy absorbed in a unit volume is determined by

$$E_{abs} = h\nu(N_1 - N_1^0) \approx h\nu N_1, \quad (2.14)$$

where N_1 is the population of the upper vibrational level after the laser pulse described by Eq.(2.11).

b) Laser Pulse of Intermediate Duration ($\tau_{rot} \leq t_p \leq \tau_{vib}$). For a laser of intermediate duration, rotational relaxation occurs during the pulse which reduces the "rotational bottleneck" effect and increases the energy absorbed in the gas. On the other hand, the pulse duration is not long, so the vibrational-rotational relaxation of excited molecules in a laser pulse is still negligible. Such a case can be realized in typical experiments on molecules diluted in an atomic inert buffer gas. Since rotational relaxation redistributes molecules during a laser pulse, the population of the vibrational state $v=1$ by the end of the laser pulse is approximately described by an expression similar to Eq.(2.11)

$$N_1 = N_0 \frac{1}{2} [1 - \exp(-\phi/\phi_s)] \quad (2.15)$$

where ϕ_s is the saturation energy of the vibrational transition, i.e.,

$$\phi_s = \frac{h\nu}{2\sigma} \approx \frac{\phi_s^j}{q} \quad (2.16)$$

and $t_p \geq \tau_{rot}/q$. Under high saturation ($\phi \gg \phi_s$) the population of the excited vibrational level reaches its maximum

$$N_1^{\max} \approx \frac{1}{2} N_0. \quad (2.17)$$

The energy absorbed with fast rotational relaxation increases by $1/q$ times at most, when $t_p \geq \tau_{rot}/q$.

c) Long Laser Pulse ($t_p \gg \tau_{vib}$). When $t_p \gg \tau_{vib}$. The population of the upper vibrational level and the absorption factor depend on radiation intensity since during a laser pulse relaxation of vibrational excitation takes place and

$$\alpha = \frac{\alpha_0}{1 + I/I_s} \quad (2.18)$$

where α_0 is the linear absorption coefficient, I_s is the intensity of absorption saturation under which the absorption decreases twice, the value of I_s is determined by

$$I_s = \frac{h\nu}{2\sigma\tau_{vib}} \quad (2.19)$$

During a long laser pulse absorbed energy turns into heat during the pulse.

In our experimental situation the acoustic resonant profiles are studied as a function of pressure. Since the product of collision relaxation time and gaseous pressure is a constant, actually one is changing the relaxation time around the range where the acoustic dispersion could occur, while at the laser modulated frequencies range where a resonance of a particular cavity mode could happen. The details will be given in later sections.

2.2 Excitation of Acoustic Wave

Sound in the gas can be described by the acoustic pressure $p(r,t)$ which is the difference between the total pressure P and its average value P_0 :

$$p = P - P_0$$

Associated with acoustic pressure p is an acoustic velocity $u(r,t)$ and an acoustic temperature $\Theta(r,t)$. The acoustic velocity is the fluid velocity of the gas at position r and time t caused by sound. The acoustic temperature is the departure from the average temperature T caused by the sound.

The heat $H(r,t)$ produced by the absorption of light acts as a source for the generation of sound . This is described by¹

$$\nabla^2 - c^{-2} \partial^2 p / \partial t^2 = -[(\gamma - 1)/c^2] \partial H / \partial t \quad (2.20)$$

where c is the velocity of sound and γ is the ratio of the specific heat of the gas at constant pressure C_p to that at constant volume C_v . This equation does not include the effects of acoustic loss produced by heat conduction and viscosity. In order to properly discuss the photoacoustic effect, it is necessary to include these mechanisms. Although this could be done by modifying Eq.(2.20), the resulting equation and its solution are unnecessarily complex. The approach followed here consists of including the loss as a perturbation of the loss-free solutions of Eq.(2.20).

Eq.(2.20) is an inhomogeneous wave equation that may be solved in the usual manner by taking the time Fourier transform of both sides and expressing the solution p as an infinite series expansion of the normal mode solution p_j of the homogeneous wave equation. The Fourier transform of Eq.(2.20) is given by

$$(\nabla^2 + \omega^2/c^2)p(r, \omega) = [(\gamma - 1)/c^2] i\omega H(r, \omega) \quad (2.21)$$

where

$$\begin{aligned} p(r, t) &= \int p(r, \omega) e^{-i\omega t} d\omega \\ H(r, t) &= \int H(r, \omega) e^{-i\omega t} d\omega \end{aligned} \quad (2.22)$$

The normal mode solutions of the homogeneous wave equation are determined by the boundary conditions. If the walls of the gas container are rigid, the acoustic velocity component normal to the wall must vanish at the wall. Since the acoustic velocity u is proportional to the gradient of p as expressed by

$$u(r, \omega) = (i\omega\rho_0)^{-1} \nabla \cdot p(r, \omega) \quad (2.23)$$

it follows that the gradient of p normal to the boundary must vanish at the boundary. This boundary condition determined the normal mode solutions p_j of the homogeneous wave equation

$$(\nabla^2 + k_j^2)p_j(r) = 0 \quad (2.24)$$

Let the resonant frequency of the normal mode $p_j(r)$ be ω_j . These modes will be orthogonal and may be normalized with the normalization condition given by

$$\int p_j^* p_j = V_c \delta_{ij} \quad (2.25)$$

The volume integral is over the volume V_c of the gas container.

If, for example, the gas container is a cylinder of radius R , and length L , then it is convenient to write Eq.(2.24) in cylindrical coordinates:

$$r^{-1} \frac{\partial}{\partial r} \left(r \frac{\partial p_j}{\partial r} \right) + r^{-2} \frac{\partial^2 p_j}{\partial \phi^2} + \frac{\partial^2 p_j}{\partial z^2} + \frac{\omega_j^2}{c^2} p_j = 0. \quad (2.26)$$

The solution of this equation is given by¹

$$p_j = \frac{\cos}{\sin}(m\phi) [AJ_m(k_r r) + BN_m(k_r r)] [C \sin(k_z z) + D \cos(k_z z)] \quad (2.27)$$

where J_m and N_m are Bessel functions of the first and second kind, respectively. Since N_m becomes infinite as r approached zero, it follow that $B=0$, if Eq.(2.26) is to represent the pressure inside a cylindrical container. In order to satisfy the

boundary condition imposed by the rigid gas container, the gradient of p normal to the container walls must vanish at the walls. If one end of the gas container is at $z=0$, and the other end is at $z=L$, then it follows that $C=0$ and the allowed values of k_z are given by

$$k_z = (\pi/L)n_z \quad (n_z = 1, 2, 3, \dots) \quad (2.28)$$

Applying the same boundary condition to the walls at $r=R$ leads to the condition that the derivative of $J_m(k_r r)$ with respect to r must vanish at $r=R$:

$$\left[dJ_m(k_r r)/dr \right]_{r=R} = 0 \quad (2.29)$$

This is equivalent to

$$\left[dJ_m(k_r \alpha)/d\alpha \right]_{\alpha=\alpha_{mn}} = 0 \quad k_r = \pi\alpha_{mn}/R \quad (2.30.a)$$

where α_{mn} , the n th root of the equation involving the m th order Bessel function, has been tabulated in Table 1.

Table 2.1 Characteristic values α_{mn} for the cylindrical cavity.

$n \backslash m$	0	1	2	3	4
0	0.0000	1.2197	2.2331	3.2383	4.2411
1	0.5861	1.6970	2.7140	3.7261	4.7312
2	0.9722	2.1346	3.1734	4.1923	5.2036
3	1.3373	2.5513	3.6115	4.6428	5.2036
4	1.6926	2.9547	4.0368	5.0815	6.1103

The requirement that p be continuous limits m to integral values. Substitution of Eq.(27) into Eq.(26) gives the resonant frequency of the modes:

$$\omega_j = c\sqrt{k_r^2 + k_z^2} = c\left[(\pi\alpha_{mn}/R)^2 + (\pi n_z/L)^2\right]^{1/2}, \quad (2.30.b)$$

the acoustic pressure p can be expressed as an expansion over the modes p_j with mode amplitudes A_j :

$$p(r, \omega) = \sum_j A_j(\omega) p_j(r) \quad (2.31)$$

Substituting Eq.(2.31) into Eq.(2.21) and making use of Eqs.(2.24 ~ 26), gives

$$A_j(\omega) = -\frac{i\omega}{\omega_j^2} \frac{[(\gamma-1)/V_c] \int p_j^* H dV}{(1 - \omega^2/\omega_j^2)} \quad (2.32)$$

which gives the mode amplitudes. The integral in the numerator on the right side of Eq.(2.32) represents the coupling between the heat source H and the normal mode p_j . The denominator represents the mode resonance with A_j becoming infinite as ω approaches the natural resonant frequency ω_j . This physically unreasonable situation is the result of the absence of any loss mechanism in Eq.(2.20). It may be corrected by modifying Eq.(2.32) to include a mode damping described by the quality factor Q_j :

$$A_j(\omega) = -\frac{i\omega}{\omega_j^2} \frac{[(\gamma-1)/V_c] \int p_j^* H dV}{(1 - \omega^2/\omega_j^2 - i\omega/\omega_j Q_j)}. \quad (2.33)$$

Take the absolute value of Eq.(2.33), and let

$$A_j^0 = [(\gamma-1)/V_c] \int p_j^* H dV, \quad (2.34)$$

we obtain the following symmetric *Lorentzian* profile which gives us that the expression of photoacoustic signal vs. frequency,

$$A_j(\omega) = \frac{A_j^0}{\sqrt{(\omega_j^4 / \omega^2) - 2\omega_j^2 + \omega^2 + \Delta\omega_j^2}}, \quad (2.35)$$

where $\Delta\omega_j = Q_j^{-1}\omega_j$ is the half-width of the resonant profile and the amplitude A_j^0 . Eq.(2.34) which we will discuss more later. The next section will discuss the method of calculating Q_j and its physical meanings.

2.3 Loss Mechanisms (Q factors)

In the preceding section it was found that resonant cavities had discrete frequencies of oscillation with a definite acoustic field configuration for each resonance frequency. This implies that, if one was attempting to excite a particular mode of oscillation in a cavity by some means, no acoustic fields of the right sort could be build up unless the exciting frequency were exactly equal to the chosen resonant frequency. In actual fact there is not a delta function singularity, but rather a narrow band of frequencies, described by a *Lorentzian* profile Eq.(2.35), around the eigenfrequency over which appreciable excitation can occur. An important source of this smearing out of the sharp frequency of oscillation is the dissipation of energy by a number of losses mechanisms, such as cavity losses, gaseous molecular relaxation, and nonideality of gases.

A measure of the sharpness of response of the cavity to external excitation is the quality factor Q of the cavity, defined as 2π times the ratio of the time-average energy stored in the cavity to the energy loss per cycle:

$$Q_j = -\omega_j \frac{du}{(du/dt)} \quad (2.36.a)$$

with solution

$$u(t) = u_0 e^{-\frac{\omega}{Q}t} \quad (2.36.b)$$

If an initial amount of energy u_0 is stored in the cavity, it decays away exponentially with a constant inversely proportional to Q . The time dependence in the Eq.(2.36.b) implies that the oscillation of the cavity are damped as follows

$$P(t) = P_0 e^{-\frac{\omega_j t}{2Q}} e^{-i(\omega_j + \delta\omega)t} \quad (2.37)$$

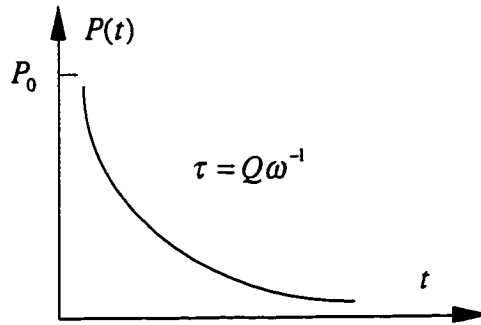


FIG. 2.2 The acoustic energy loss/decay in the time domain.

where we have allowed for a shift $\delta\omega$ of resonant frequency as well as damping. A damped oscillation such as this has not a pure frequency, but a superposition of frequencies around $\omega = \omega_j + \delta\omega$. thus,

$$P(t) = \frac{1}{\sqrt{2\pi}} \int_{-\infty}^{\infty} P(\omega) e^{-i\omega t} d\omega \quad (2.38.a)$$

where

$$P(\omega) = \frac{1}{\sqrt{2\pi}} \int_0^{\infty} P_0 e^{-\frac{\omega_j t}{2Q}} e^{-i(\omega - \omega_j - \delta\omega)t} dt \quad (2.38.b)$$

The integral in Eq.(2.38) is elementary and leads to a frequency distribution for the energy in the cavity having a resonant line shape:

$$|P(\omega)| \propto \frac{1}{\sqrt{(\omega - \omega_j - \delta\omega)^2 + (\omega_j/2Q)^2}} \quad (2.39)$$

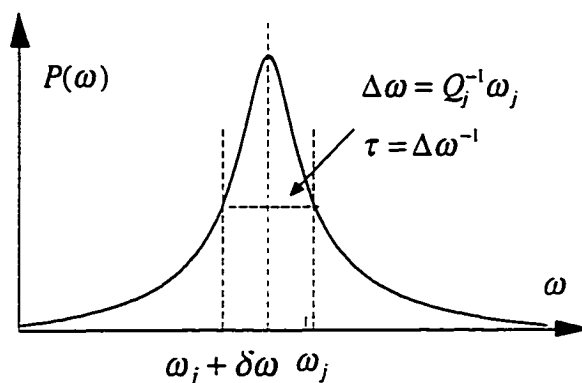


FIG. 2.3 The energy losses in frequency domain, i.e., resonant line shape.

The resonance shape Eq.(2.39), shown in the Fig.2.3, has a full width $\Delta\omega$ at half-maximum (confusingly called the half-width) equal to ω_j / Q_j . For a constant input, the energy of oscillation in the cavity as function of frequency will follow the resonance curve in the neighborhood of a particular resonant frequent. Thus, the frequency separation $\delta\omega$ between half-power points determines the width $\Delta\omega$ and the Q_j of cavity is

$$Q_j = \omega_j \Delta\omega^{-1} = \frac{1}{2} \omega_j \delta\omega^{-1}, \quad (2.40)$$

the Q_j values of several hundreds and up to one thousand are common for photoacoustic resonators. This mode dependent finite Q_j is usually the result of loss caused by heat conduction and viscosity, nonideality of gases, and molecular relaxation. For example, the finite time required for rotational and vibrational degrees of freedom of the gas molecules to come to equilibrium with

translational degrees of freedom can also introduce loss. The following we will discuss them in details.

2.3.1 Heat Conduction and Viscosity of Gases

Loss produced by viscosity and heat conduction can be separated into surface losses and a volume losses.

Surface losses. The surface losses, due to wave interactions with solid boundaries of the cavity, account for a large part of the energy dissipation. The loss mechanisms can be categorized as follows: (1)compliance of the chamber walls, (2)dissipation at the microphone diaphragm, (3)scattering at surface imperfections, or (4)viscous and thermal dissipation in the boundary layer at the smooth internal surfaces.

The first three effects are minimized by suitable design of the spectrophone. The fourth loss mechanism is then the dominant one. The surface loss occurs in a thin region near the walls. This region may be considered to be composed of two layers that extend out from the wall. One of thickness l_v in which the viscosity effects take place and one of thickness l_h in which heat conduction effects occur. These skin depths are given by¹

$$l_v^2 = 2\eta/\omega\rho_0 \quad \text{and} \quad l_h^2 = 2\kappa/\rho_0\omega C_p \quad (2.41)$$

In these equations, η is the viscosity and κ the thermal conductivity of the gas, ρ_0 is the density of the gas and C_p the pressure constant heat capacity. The nature of these layers can be understood in the following manner. The container wall will have thermal conductivity much greater than the gas and thus near the

wall the gas will have a constant temperature and expand and contract in an isothermal manner. Far from the walls, the expansion and contraction caused by the sound is very nearly adiabatic. Acoustic loss from heat conduction occurs in the region where the gas expansion is partly adiabatic and partly isothermal. At the wall surface, the component of the acoustic velocity u_t tangent to the wall surface vanishes owing to viscosity. Far from the wall, the acoustic velocity is proportional to the gradient of p and is given by Eq.(2.23). Loss occurs owing to viscosity in the region near the walls where the transition from the condition of Eq.(2.23) to the condition $u_t = 0$ occurs. the total surface loss L_j^{sur} is given by²

$$L_j^{sur} = |A_j|^2 \int \left[\frac{1}{2} R_{v,j} |u_{ij}|^2 + \frac{1}{2} R_{h,j} |p_j|^2 \right] ds, \quad (2.42)$$

where j stands for a particular mode, and u_{ij} is the component of acoustic velocity tangential to the walls that would be present if there were no viscosity or heat conduction. The integration is over the surface of the container, $R_{v,j}$ and $R_{h,j}$, which represent the loss from viscosity and heat conduction are given by

$$R_{v,j} \equiv \sqrt{\eta \omega_j \rho_0 / 2}$$

and

$$R_{h,j} = [(\gamma - 1) / \rho_0 c^2] \sqrt{\kappa \omega_j / 2 \rho_0 C_v} \quad (2.43)$$

The energy E_j stored in the mode j is given by

$$E_j = V_c |A_j|^2 / \rho_0 c^2 \quad (2.44)$$

where V_c , ρ_0 , A_j are the volume of the cavity, density of gases, and the mode amplitude respectively. Thus the Q factor due to the surface loss

$$Q_j = \omega_j \frac{E_j}{L_j^{sur}} = \omega_j \frac{(1/\rho v^2) \int |p_j|^2 dV}{\int \left[\frac{1}{2} R_{v,j} |u_{t,j}|^2 + \frac{1}{2} R_{h,j} |p_j|^2 \right] dS}, \quad (2.45)$$

where the component parallel to the resonator surface of the acoustic velocity is

$$u_{t,j} = (\omega_j \rho)^{-2} |\nabla_t p_j|^2, \quad (2.46)$$

and make uses of Eqs.(2.41 ~ 44).

Taking into account the boundary conditions and the cylindrical symmetry of the problem, the following choice have been made for the resonator modes:³

$$p_j(r, z) = \begin{cases} \cos(k_z z) & (n = 0, n_z \neq 0) \\ J_0(k_r r) & (n \neq 0, n_z = 0) \\ J_0(k_r r) \cos(k_z z) & (n \neq 0, n_z \neq 0) \end{cases} \quad (2.47)$$

where

$$\begin{cases} k_z = (\pi/L)n_z & n_z = 0, 1, 2, \dots \\ k_r = \frac{x_{0n}}{R} \left. \frac{dJ_0(x)}{dx} \right|_{x=x_{0n}} & (x_{0n} = \pi\alpha_{0n}) \\ \omega_{n_0 n_z} = c [k_z^2 + k_r^2]^{1/2} \end{cases}$$

where R and L are the radius and length of the cylinder. The functions here are not normalized. This is allowed because Eq.(2.46) is a quotient and normalization constants cancel. To solve the problem, one must calculate the volume and surface integrals in Eq.(2.46). This can be done analytically using elementary calculus and the integral relations of the Bessel functions. The results for the various integrals and straightforward calculations yields:³

$$Q_{sur,j}^{-1} = \begin{cases} \frac{1}{R} [l_{v,j} + l_{h,j}(\gamma - 1)(1 + \frac{2R}{L})] & (n_z \neq 0, n = 0) \\ \frac{1}{L} [l_{v,j} + l_{h,j}(\gamma - 1)(1 + \frac{1}{k})] & (n_z = 0, n \neq 0) \\ \frac{2}{L} [l_{v,j} + l_{h,j}(\gamma - 1)(1 + \frac{1}{2k})f(\frac{R}{L}, n, n_z)] & (n_z, n \neq 0) \end{cases} \quad (2.48)$$

where

$$f(\frac{R}{L}, n, n_z) = \frac{1 + \frac{1}{2}(R/L)(\pi n_z / \chi_{on})^2}{1 + \frac{1}{2}(R/L)^2(\pi n_z / \chi_{on})^2}$$

For our choice of resonator dimensions $R/L = 1/2$, $f(\frac{R}{L}, n, n_z) = 1$.

Volume loss. The volume losses, associated with internal acoustic processes, originate from the nonequilibrium nature of the propagating wave and can be divided into the following categories: (1) free space viscous and thermal dissipation, (2) diffusion effects, (3) radiation effects, and (4) molecular relaxation losses. The diffusion and radiation effects are very small, and molecular relaxation effects will be treated separately. Friction due to compression motion results in viscous losses, while the volumetric thermal losses are attributable to the transfer of organized energy into dispersed heat due to the resulting temperature gradients in the gas. the combination of these damping, termed the "Stokes-Kirchhoff losses", are small when compared with surface damping, but in some extreme cases at low pressure it can become significant. The volume loss L_v is given by

$$L_{vj} = (\omega_j^2 / \rho^2 c^4) [(\gamma - 1)(\kappa / 2C_p) + (2n/3)] V_c |A_j|^2 \quad (2.49)$$

The Q_j of the mode can easily be calculated from Eqs.(2.41 ~ 44, 49), and the definition of Q_j :

$$Q_j = \omega_j \frac{E_j}{L_{vj}} = \omega_j \frac{(1/\rho v^2) \int |p_j|^2 dV}{(\omega_j^2/\rho^2 c^4) [(\gamma-1)(\kappa/2C_p) + (2n/3)] V_c |A_j|^2}$$

The rest of the calculations are similar as that for surface Q_j . We obtain⁴

$$Q_{vol,j}^{-1} = \frac{\omega_j}{\gamma p} \left[\frac{4}{3} \eta + (\gamma-1) \kappa M / C_p \right] \quad (2.50)$$

Table 2.2 given all the results of integrals for the final expressions of the surface quality factor Eq.(2.48) and the volume quality factor Eq.(2.50).

Table 2.2 Integrals used for the evaluation of Eqs.(2.48, 50).³

	$n_z \neq 0, n = 0$	$n_z = 0, n \neq 0$	$n_z \neq 0, n \neq 0$
$\int (p_{non_z})^2 dV$	$\frac{1}{2} \pi R^2 L$	$\pi R^2 L J_0^2(\chi_{on})$	$\frac{1}{2} \pi R^2 L J_0^2(\chi_{on})$
$\int (p_{non_z})^2 dS$	$2 \pi R (R + \frac{L}{2})$	$2 \pi R (R + L) J_0^2(\chi_{on})$	$2 \pi R (R + \frac{L}{2}) J_0^2(\chi_{on})$
$\int (\nabla_t p_{non_z})^2 dS$	$\pi^3 \frac{R n_z^2}{L}$	$2 \pi \chi_{on}^2 J_0^2(\chi_{on})$	$2 \pi (\chi_{on}^2 + \frac{\pi^2 R n_z^2}{2L}) J_0^2(\chi_{on})$

2.3.2 Nonideality of Gases

The nonideal behavior of gases manifests itself at high pressures where intermolecular forces give rise to a change in the compressibility and consequently in the sound velocity. The correction for the deviation of the gas from the behavior of ideal gases on the resonant frequency is given by⁵

$$\delta \omega^{vir} = -\frac{p \omega_j}{RT} \left(B + \frac{RT}{C_v} \frac{dB}{dT} + \frac{(RT)^2}{2C_v C_p} \frac{d^2 B}{dT^2} \right) \quad (2.51)$$

where R is the gas constant and B the second Virial coefficient. The followings is the derivation of Eq.(2.51). Assuming the deviations are small, the equation of state can be written as

$$pV/RT = 1 + B'p \quad (2.52)$$

B' is simply connected with the second Virial coefficient in the Kammerling-Onnes equation of state

$$pV/RT = 1 + B/V \quad (2.53)$$

Since the term $B'p$ is a small correction, one can use the ideal gas equation for p in this term, getting

$$B'p = B'pT/V = B/V \quad \text{or } B' = B/RT \quad (2.54)$$

With the Van der Waals notation

$$B = b - a/RT \quad \text{or } B' = b/RT - a/(RT)^2 \quad (2.55)$$

In the equation for the low-frequency sound velocity, $c^2 = C_p/C_v(dp/d\rho)_T$, here $(dp/d\rho)_T$, C_p , and C_v have to be corrected. Rewrite Eq.(2.52)

$$V = RT(1/p + B'). \quad (2.56)$$

Then

$$\left(\frac{\partial V}{\partial p}\right)_T = -\frac{RT}{p^2} - \frac{1}{V^2} \left(\frac{\partial V}{\partial p}\right)_T = \frac{1}{M} \frac{\partial \rho}{\partial p} = \frac{RT}{p^2} \frac{1}{(RT)^2} \frac{p^2}{(1 + B'p)^2}$$

Therefore

$$\left(\frac{\partial p}{\partial \rho}\right)_T = \frac{RT}{M} (1 + B'p)^2. \quad (2.57)$$

We know $\partial C_p/\partial p = -T(\partial^2 V/\partial^2 T)_p$; with the form of Eq.(2.56) for V

$$\partial C_p / \partial p = -RT [\partial^2 (B'T) / \partial T^2]. \quad (2.58)$$

Since we keep in the region where all deviations are linear in p ,

$$C_p = C_p^0 - pRT [\partial^2 (B'T) / \partial T^2]. \quad (2.59)$$

and

$$C_p - C_v = -TV \frac{1}{V^2} \left(\frac{\partial V}{\partial T} \right)_p^2 V \left(\frac{\partial p}{\partial V} \right)_T = -T \left(\frac{\partial V}{\partial T} \right)_p^2 \left(\frac{\partial p}{\partial V} \right)_T. \quad (2.60)$$

From Eq.(2.56)

$$\left(\frac{\partial V}{\partial T} \right)_p = \frac{R}{p} + R \frac{\partial (B'T)}{\partial T} = \frac{R}{p} \left[1 + p \frac{\partial (B'T)}{\partial T} \right].$$

According to the equation following Eq.(2.56), $(\partial p / \partial V)_T = -p^2 / RT$. Inserting all this in Eq.(2.59)

$$C_p - C_v = T \frac{R^2}{p^2} \left[1 + p \frac{\partial (B'T)}{\partial T} \right] \frac{p^2}{RT} = R \left[1 + p \frac{\partial (B'T)}{\partial T} \right]^2. \quad (2.61)$$

Since we have kept only the first power of p to describe the deviations from the ideal gas law in the equation of state, Eq.(2.52), it would not be justified to keep higher powers in the corrections just calculated. Therefore, Eqs.(2.57, 61) should be replaced by

$$\left(\frac{\partial p}{\partial \rho} \right) = \frac{RT}{M} (1 + 2B'p) \quad (2.57')$$

$$C_p - C_v = R \left[1 + 2p \frac{\partial (B'T)}{\partial T} \right]. \quad (2.61')$$

From Eqs.(2.61') and (2.59)

$$C_v = C_p - (C_p - C_v) = C_p^0 - pR \left[2 \frac{\partial (B'T)}{\partial T} + T \frac{\partial^2 (B'T)}{\partial T^2} \right] \quad (2.62)$$

From Eq.(2.59) and (2.62) one has

$$\begin{aligned}
 \gamma &= \frac{C_p^0 - pRT \left[\partial^2(B'T) / \partial T^2 \right]}{C_p^0 - pR \left[2 \frac{\partial(B'T)}{\partial T} + T \frac{\partial^2(B'T)}{\partial T^2} \right]} \\
 &= \frac{C_p^0}{C_v^0} \left\{ 1 + \frac{pRT}{C_p^0} \frac{\partial^2(B'T)}{\partial T^2} + \frac{pR}{C_v^0} \left[2 \frac{\partial(B'T)}{\partial T} + T \frac{\partial^2(B'T)}{\partial T^2} \right] \right\} \\
 &= \gamma_0 \left\{ 1 + p \frac{R}{C_v^0} \left[\frac{2R}{C_v^0} \frac{\partial(B'T)}{\partial T} + T \frac{\partial^2(B'T)}{\partial T^2} \right] \right\} \quad (2.63)
 \end{aligned}$$

and with Eq.(2.57')

$$c^2 = c_0^2 \left\{ 1 + 2p \left[B' + \frac{R}{C_v^0} \frac{\partial(B'T)}{\partial T} + \frac{1}{2} \frac{R^2 T}{C_v^0 C_p^0} \frac{\partial^2(B'T)}{\partial T^2} \right] \right\}. \quad (2.64)$$

Recall Eq.(2.30.b), $\omega_j = c \left[(\pi \alpha_{mn} / R)^2 + (\pi n_z / L)^2 \right]^{1/2}$, Eq.(2.54), $B' = B/RT$, and make the approximation $c^2 - c_0^2 = \Delta c 2c_0$, one could obtain the deviation of the resonant frequency ω_j caused by the nonideality of the gas, i.e.,

$$\delta \omega^{vir} = -\frac{p \omega_j}{RT} \left(B + \frac{RT}{C_v} \frac{dB}{dT} + \frac{(RT)^2}{2C_v C_p} \frac{d^2 B}{dT^2} \right). \quad (2.51')$$

Fig.(2.5) gives the best fit of the second Virial coefficient B of SF_6 as a function of temperature, the data were from ref. 6, and the fitting function⁵ is

$$B(T) = a - bT^{-1.37} - cT^{-4.45} \quad (2.65)$$

with fitted parameters: $a = 129.69$ $b = 9.55 \times 10^5$ $c = 2.52 \times 10^{12}$.

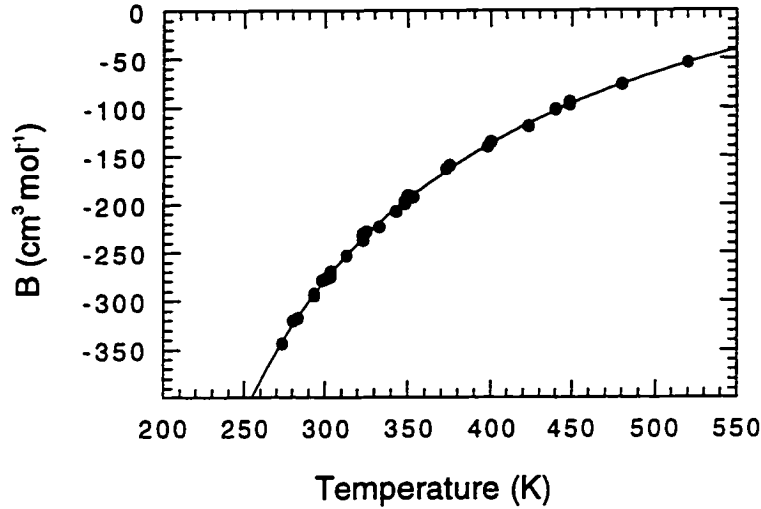


FIG. 2.4 The temperature dependence of second Virial coefficient of SF₆.

2.3.3 Molecular relaxation

Molecular relaxation effects arise because of the finite time required for the internal degrees of freedom of the molecules to come into thermal equilibrium with the translational degrees of freedom, as described by:

$$\frac{dE_n}{dt} = -\frac{(E_n - E_n^e)}{\tau_n} \quad (2.66)$$

where E_n is the ensemble average energy in the n th mode of the molecule, E_n^e is its equilibrium value, and τ_n is the relaxation time for that mode. If E_n varies as a harmonic function of time, $E_n = E_0 e^{i\omega t}$, the solution of above differential equation leads us to the dynamic heat capacity $C_n(\omega)$ for the n th mode,

$$C_n(\omega) = \frac{dE_n(\omega)}{dT} = \frac{C_n}{1 + i\omega\tau_n}. \quad (2.67)$$

Considering all degrees of freedom, we have:

$$C_v(\omega) = C_v + \frac{1}{2} \sum_n [C_n(\omega) - C_n]$$

$$C_p(\omega) = C_p + \frac{1}{2} \sum_n [C_n(\omega) - C_n],$$

thus, the dynamic heat capacity ratio is,

$$\begin{aligned} \gamma(\omega) &= \frac{C_p(\omega)}{C_v(\omega)} = \frac{C_p - \frac{1}{2} \sum_n [i\omega\tau_n C_n / (1 + i\omega\tau_n)]}{C_v - \frac{1}{2} \sum_n [i\omega\tau_n C_n / (1 + i\omega\tau_n)]} \\ &= \frac{\gamma - \frac{(\gamma-1)}{2R} \sum_n [i\omega\tau_n C_n / (1 + i\omega\tau_n)]}{1 - \frac{(\gamma-1)}{2R} \sum_n [i\omega\tau_n C_n / (1 + i\omega\tau_n)]} \end{aligned} \quad (2.68)$$

where C_p and C_v are the molar static heat capacities. Since the C_n 's for the vibrational modes are small at room temperatures, we can expand the fraction of Eq.(2.68) for these terms also, but we cannot neglect the higher orders of $\omega\tau_n$. The root square of the expression can be approximated to the first power in ξ , where

$$\xi = \frac{(\gamma-1)}{2R} \sum_n i\omega\tau_n C_n / (1 + i\omega\tau_n),$$

thus we have

$$[\gamma(\omega)]^{1/2} = \gamma^{1/2} + \frac{(\gamma-1)}{2\gamma^{1/2}} \xi + O[\xi]^2 \cong \frac{1}{\gamma^{1/2}} \left[\gamma + \frac{(\gamma-1)^2}{4R} \sum_n \frac{i\omega\tau_n C_n}{1 + i\omega\tau_n} \right]. \quad (2.69)$$

Neglecting non-ideal gas effects, which are treated separately, the sound velocity is given by $c = \sqrt{\gamma(\omega)p/\rho}$. If we denote by ω_j the frequency that we

would obtain for the mode by using the static heat capacity ratio γ in place of $\gamma(\omega)$. we have

$$\omega_j^{rel} = \omega_j [\gamma(\omega)]^{1/2} / \gamma^{1/2}. \quad (2.70)$$

Inserting Eq. (69) into Eq. (70), we obtain,

$$\begin{aligned} \omega_j^{rel} &\equiv \omega_j \left[1 + \frac{(\gamma-1)^2}{4\gamma R} \sum_n \frac{i\omega\tau_n C_n}{1+i\omega\tau_n} \right] \\ &= \omega_j \left\{ 1 + \frac{(\gamma_0-1)^2}{4\gamma_0 R} \sum_{vib} \frac{i\omega\tau_n C_n}{1+i\omega\tau_n} + \frac{(\gamma_\infty-1)^2}{4\gamma_\infty R} \sum_{rot} \frac{i\omega\tau_n C_n}{1+i\omega\tau_n} \right\} \\ &\equiv \omega_j \left\{ 1 + \frac{\alpha_0}{2R} \sum_{vib} \frac{\omega^2 \tau_n^2 C_n}{1+\omega^2 \tau_n^2} + i \frac{\alpha_0}{2R} \sum_{vib} \frac{\omega\tau_n C_n}{1+\omega^2 \tau_n^2} + i \frac{\alpha_\infty}{2R} \sum_{rot} \omega\tau_n C_n \right\} \end{aligned} \quad (2.71)$$

where the sum has been split into a rotational and a vibrational term, with $\alpha_0 = (\gamma_0 - 1)^2 / 2\gamma_0$ and $\alpha_\infty = (\gamma_\infty - 1)^2 / 2\gamma_\infty$. γ_0 is the static heat capacity ratio and γ_∞ is the heat capacity ratio in the absence of vibrational degrees of freedom. There is no dispersion to first order in $\omega\tau_{rot}$, but the imaginary part of rotational relaxation losses remains. The real part of Eq. (71) is the frequency dispersion, which only has the vibrational terms,

$$\omega_j^{rel} = \text{Re } \omega_j^{rel} = \omega_j \left[1 + \frac{\alpha_0}{2R} \sum_{vib} \frac{\omega^2 \tau_n^2 C_n}{1+\omega^2 \tau_n^2} \right]; \quad (2.72)$$

the imaginary part is the relaxation dissipation of vibration and rotation. It will determine the half-width of the resonance profile given by

$$\Delta\omega_j^{rel} = 2 \text{Im } \omega_j^{rel} = \omega_j \left[\frac{\alpha_0}{R} \sum_{vib} \frac{\omega\tau_n C_n}{1+\omega^2 \tau_n^2} + \frac{\alpha_\infty}{R} \sum_{rot} \omega\tau_n C_n \right]. \quad (2.73)$$

2.4 Shifts of Frequency and Broadening of line-width

The overall Q factor for a resonance may be found by summing all the losses for that resonance, expressed as:

$$Q_{Tot,j}^{-1} = \sum_i Q_{i,j}^{-1}. \quad (2.74)$$

As we have calculated in the last section, there are three contributions: surface losses, volume losses and molecular relaxation parts. Thus we are able to obtain overall shift of the resonant frequency and the broadening of line width, which are experimental accessible, and from which we could extract molecular relaxation parameters.

The surface losses make a large contributions to resonant frequency shift as well as the broadening of the half width. The Q_{sur}^{-1} , Eq.(2.48), can be written as $Q_{sur,j}^{-1} = \alpha_j^{sur} p^{-1/2}$, where α_j^{sur} is a mode dependent constant and p the gas pressure. Thus,

$$\delta\omega_j^{sur} = -\frac{1}{2}\omega_j Q_{sur}^{-1} = -\frac{1}{2}\alpha_j^{sur}\omega_j p^{-1/2}, \quad (2.75)$$

and

$$\Delta\omega_j^{sur} = \omega_j Q_{sur}^{-1} = \alpha_j^{sur}\omega_j p^{-1/2}. \quad (2.76)$$

The volume losses generally amount to an insignificant source of energy dissipation. They are small when compared with surface losses, only in some extreme cases at low pressure it can make small contribution to the broadening of half width. They are usually neglected to the frequency dispersion since the magnitude of shift is a half of broadening. Similarly, the Q_{vol}^{-1} can be written as $Q_{vol,j}^{-1} = \alpha_j^{vol} p^{-1}$, where α_j^{vol} is a mode dependent constant and p the gas pressure.

The volumetric losses contribute to the broadening of half-width is then given by

$$\Delta\omega_j^{vol} = \omega_j Q_{vol}^{-1} = \alpha_j^{vol} \omega_j p^{-1}, \quad (2.77)$$

The correction for the deviation of the gas from the behavior of ideal gases on the resonant frequency, Eq.(2.51), loosely called Virial shift, can be written as

$$\delta\omega_j^{Vir} = -\alpha_j^{Vir} \omega_j p, \quad (2.78)$$

where α_j^{Vir} is a constant and p the gas pressure.

Adding Eq.(72), Eq.(75) and Eq.(78), we obtain the final expression for the resonance frequency that accounts for vibrational dispersion effects, the shifts of surface losses and nonideal behavior of the gas:

$$\begin{aligned} \omega_j^{all} &= \omega_j^{rel} + \delta\omega_j^{sur} + \delta\omega_j^{Vir} \\ &= \left\{ \left[1 + \frac{\alpha_0}{R} \sum_{vib} \frac{\omega^2 \tau_n^2 C_n}{1 + \omega^2 \tau_n^2} \right] - \frac{1}{2} \alpha_j^{sur} p^{-1/2} - \alpha_j^{Vir} p \right\} \omega_j, \end{aligned} \quad (2.79)$$

where $\alpha_0 = (\gamma - 1)^2 / 2\gamma$.

Adding Eq.(73), Eq.(76) and Eq.(77) together, we have the final formula for the half-width of the resonance profile which includes the contributions of both vibrational and rotational relaxation, surface and volume losses,

$$\begin{aligned} \Delta\omega_j &= \Delta\omega_j^{rel} + \Delta\omega_j^{sur} + \Delta\omega_j^{vol} \\ &= \left\{ \left[\frac{2\alpha_0}{R} \sum_{vib} \frac{\omega \tau_n C_n}{1 + \omega^2 \tau_n^2} + \frac{2\alpha_\infty}{R} \sum_{rot} \omega \tau_n C_n \right] + \alpha_j^{sur} p^{-1/2} + \alpha_j^{vol} p^{-1} \right\} \omega_j \end{aligned} \quad (2.80)$$

In all the above expressions, the relaxation times τ_n appear in conjunction with ω as a product $\omega\tau_n$. Although there are various effects that shift the frequency of the resonance, such as relaxation dispersion, Virial shifts, and boundary layer effects, it is still true that the frequency of a given resonance is nearly independent of pressure for the gases and pressure range considered in our experiment, the largest observed frequency shift being $\sim 1.8\%$ (in the case of SF_6). Thus we can simply use ω_j instead of ω in Eq.(79) and Eq.(80) to have explicit expressions of ω_j and $\Delta\omega_j$ as function of pressure in a good approximation. Therefore, observation of the dependence of the frequency shift and half width on pressure will mainly reflect the pressure dependence of τ_n . Since, at constant temperature, the product of pressure and relaxation time is constant, observation of the pressure dependence of the resonant frequency and half-width provides a means of determining the $(p\tau)$ product, although we loosely use the term relaxation time to denote one of the parameters of our experiment, we shall refer mostly to the $(p\tau)$ product. Like the vast majority of polyatomic molecules, SF_6 relaxes in a model of a single relaxation time, therefore simplifications could be made by eliminating the summations of vibration and rotation in Eq.(79) and Eq.(80).

2.5 General Considerations on Relaxation

This section deals with the case in which more than one relaxation time is present. This occurs in the collisions of polyatomic molecules which have several modes of vibration, with different vibrational frequencies, and even in a single degree of freedom in which the energy jumps do not all have the same

value, e.g., vibration versus rotation. In principle, one can distinguish three modes of excitation of several degrees of freedom:

- (a) Excitation in parallel. Each internal degree of freedom, independently of the others, exchanges energy with the external degrees of freedom. The objection has been made that many dispersion and absorption curves seem to cover all or nearly all of the vibrational energy, while vibrations with widely different frequencies should have widely different relaxation times, and therefore not a single dispersion-absorption region.
- (b) Excitation in series. Where a single relaxation time is observed and easily associated with a transition rate, was first recognized by Schäfer⁷. Even when the molecule contains several vibrational modes, if there is a "gating" mode through which the energy passes before it is quickly shared by the other modes, a single relaxation time is observed.
- (c) Excitation by complex collision. In this process there is, as in (b), feeding of one vibrational mode from another, but this process also can only occur in a collision, since the difference in the size of quanta is made up by exchange with translational energy. Therefore, a vibration may still be excited, even if the one from which it is normally "feeding" no longer exchanges energy directly with translation. While in scheme (b) the internal energy is preserved in the exchange between vibrations, in (c) the total number of quanta is preserved. Of course, in general, both types (a) and (b) will be present and it is only a question of which is the more effective.

Assuming that vibrational energy (or rotational) only is unable to equilibrate in the acoustic cycle, we may write $E'(T_{rr})$ as the value of the vibrational energy in equilibrium with the translational and rotational modes at a temperature T_{rr} . In general, in acoustic measurements we will observe a momentary value E' which is less than $E'(T_{rr})$. The relaxation equation is written in the form

$$-\frac{dE'}{dt} = \frac{1}{\tau} [E' - E'(T_{rr})]. \quad (2.81)$$

For small temperature changes starting with T_0

$$E' - E'_0 = C'(T' - T_0) \quad (2.82)$$

where C' is the internal heat capacity under equilibrium conditions and is $(C_0 - C_\infty)$.

Then the energy form of the relaxation equation can be converted to a temperature relation

$$-\frac{dT'}{dt} = \frac{1}{\tau} (T' - T_{rr}). \quad (2.83)$$

If the translational temperature is raised suddenly at $t = 0$ from T_0 to T_1 and if the external temperature is kept constant at T_1 after $t = 0$, we have a solution to above equation

$$T' = T_1 + (T_0 - T_1) \exp(-t/\tau) \quad (2.84)$$

We may re-write above equation as

$$T' - T_0 + \tau \frac{d(T' - T_0)}{dt} = T_{rr} - T_0$$

If the excess translational temperature $T_r - T_0$ is proportional to $\exp(i\omega t)$, the quantity $T' - T_0$ will also be proportional to $\exp(i\omega t)$. In the steady state this equation becomes

$$\frac{T' - T_0}{T_r - T_0} = \frac{1}{1 + i\omega\tau} \quad (2.85)$$

which can be rewritten

$$dT'/dT_r = 1/(1 + i\omega\tau) \quad (2.85')$$

The effective heat capacity suitable for the dispersion equation is obtained as the quantity dE/dT_r . The change in total internal energy

$$dE = C_\infty dT_r + C' dT' \quad \text{or} \quad C' dT' = \frac{C' dT_r}{1 + i\omega\tau}$$

we have

$$C_v^{eff} = C_\infty + \frac{C'}{1 + i\omega\tau} = C_\infty + \frac{C_0 - C_\infty}{1 + i\omega\tau} \quad (2.86)$$

2.5.1 Excitation in Parallel

Here we have two or more modes of different degrees of freedom fed independently from sources. We can describe this a set of equations

$$\frac{\partial E'_s}{\partial t} = -\frac{1}{\tau} [E'_s - E'_s(T_r)] \quad (2.87)$$

where the subscript s refers to the individual modes.

The temperature relaxation equations analogous to Eq.(87) above are then obtained for each mode

$$T'_s - T_0 = \frac{1}{1 + i\omega\tau} (T_r - T_0) \quad (2.88)$$

The value for the effective heat capacity then becomes

$$C_v^{\text{eff}} = C_\infty + \sum_s \frac{C'_s}{1 + i\omega\tau_s} \quad \text{and} \quad \sum C'_s = C' \quad (2.89)$$

In evaluating the dispersion for a system involving parallel excitation it is necessary to select the value of C'_s and τ_s which will fit Eq.(89); this can be done by successive approximation. If the values of τ_s are sufficiently different the regions of dispersion will be separated in steps and the problem of determining the individual τ_s will be simpler.

2.5.2 Excitation in Series

Here the energy is fed into the molecule via one mode and is redistributed from this mode to the others. It is simplest to consider a molecule with two modes only, one of which is activated directly from the excitation source with a relaxation time τ_1 . This approximation would also hold for a complex molecule in which all the other modes exchange energy with the first with a relaxation time τ_{12} .

If we write E'_1 as the energy of mode 1 and E'_2 as the energy of all other modes

$$E' = E'_1 + E'_2 \quad \text{and} \quad C' = C'_1 + C'_2 \quad (2.90)$$

Then the first of the relaxation equation is

$$-\frac{\partial E'_1}{\partial t} = \frac{1}{\tau_1} [E'_1 - E'_1(T_r)] - \frac{1}{\tau_{12}} [E'_2 - E'_2(T'_1)] \quad (2.91)$$

which can be rewritten

$$-\frac{\partial T'_1}{\partial t} = \frac{1}{\tau_1} [T'_1 - T_r] - \frac{C'_2}{C'_1} \frac{1}{\tau_{12}} [T'_2 - T'_1] \quad (2.92)$$

together with

$$-\frac{\partial T'_2}{\partial t} = \frac{1}{\tau_{12}} [T'_2 - T'_1] \quad (2.93)$$

Introducing the sinusoidal variation making $T_r - T_0$ proportional to $\exp(i\omega t)$, hence making $T'_1 - T_0$ and $T'_2 - T_0$ also proportional to $\exp(i\omega t)$, we can write the above equation as

$$i\omega\tau_1(T'_1 - T_0) = (T'_1 - T_0) - (T_r - T_0) - \frac{C'_2}{C'_1} \frac{1}{\tau_{12}} [T'_2 - T'_1] \quad (2.94)$$

and

$$-i\omega\tau_{12}(T'_2 - T_0) = (T'_2 - T_0) - (T'_1 - T_0) \quad (2.95)$$

From these we can derive

$$(T'_2 - T_0) = (T'_1 - T_0) / (1 + i\omega\tau_{12}) \quad (2.96)$$

and

$$(T'_1 - T_0) \left[1 + i\omega\tau_1 + \frac{C'_2}{C'_1} \frac{\tau_1}{\tau_{12}} \frac{i\omega\tau_{12}}{1 + i\omega\tau_{12}} \right] = (T_r - T_0) \quad (2.97)$$

The effective heat capacity, which is given by dE/dT_r , will be obtained from the equation summing the separate steps

$$C_v^{eff} (T_r - T_0) = C_\infty (T_r - T_0) + C'_1 (T'_1 - T_0) + C'_2 (T'_2 - T_0) \quad (2.98)$$

and can then be converted, using Eq.(87,88), to

$$C_v^{eff} = C_\infty + \frac{[(C'_1 + C'_2) + C'_1 i\omega\tau_{12}]}{[(1 + i\omega\tau_1)(1 + i\omega\tau_{12}) + (C'_2/C'_1) i\omega\tau_1]} \quad (2.99)$$

The most common series excitation observation in practice is that in which the rate of internal energy transfer is much more rapid than the rate of equilibration with translation. Under these conditions the relaxation time

$\tau_{12} \ll \tau_1$. If we rewrite the expression for the effective heat capacity ignoring terms in τ_{12} we get

$$C_v^{eff} = C_\infty + \frac{(C'_1 + C'_2)}{[(1 + i\omega\tau_1) + (C'_2/C'_1)i\omega\tau_1]} \quad (2.100)$$

This equation is identical with that for a single dispersion with a relaxation time τ , except that

$$\tau = \tau_1 \frac{C'_1 + C'_2}{C'_1} \quad (2.101)$$

In general for a polyatomic molecule in which a single mode is activated from the excitation source and rapid energy transfer to all the other modes follows, the measured τ is related to τ_1 , the relaxation time for the energy transfer process involving the first mode, by

$$\tau = \tau_1 \left(\sum_s C'_s / C'_1 \right), \quad (2.102)$$

which is also known as Schäfer equation⁷. Because τ_1 in this analysis refers to a relaxation process in which energy is fed into a further relaxing system, it is convenient to adopt a distinct symbol for this quantity. In the rest of this thesis we shall use the symbol β , where $\beta \equiv \tau_1$.

References to Chapter 2

- 2.1 P.M. Morse and K.U.Ingard, *Theoretical Acoustics*, (McGraw-Hill, New York, 1968).
- 2.2 L.B. Kreuzer, *Optoacoustic Spectroscopy and Detection*, edited by Y.H. Pao (Academic Press, 1977).
- 2.3 A. Karbach and P. Hess, *J. Chem. Phys.* **83**, 1075 (1985).
- 2.4 C.F. Dewey, Jr., R.D. Kamm, and C.E.Hackett, *Appl. Phys. Lett.* **23**, 633 (1973).
- 2.5 K. F. Herzfeld & T.A.Litovitz, *Absorption & Dissipation of Ultrasonic Waves*, (Academic Press, New York, 1959).
- 2.6 J. H. Dymond & E.B.Smith, *The Virial Coefficients of Gases*, (Claredon Press.Oxford.1969).
- 2.7 K. Z. Schäfer, *phys.Chem.* **b46**, 212(1940).

Chapter 3

Theories of Molecular Relaxation

In this Chapter, the theories of molecular vibrational-translational, vibrational-vibrational and rotational-translational energy transfers are outlined to back the interpretations of the experimental photoacoustic results, since photoacoustics deals with translational temperature, a final energy reservoir, ultimate destination of the relaxation of excited molecules through a number of intermediate states.

3.1 Molecular Collisions

Molecules usually gain and lose vibrational and rotational energy in collisions. polar molecules *can* be activated or deactivated by absorption or emission of radiation, but the radiative lifetime (which varies with ν^{-3}) is so long for infrared frequencies that this mechanism may be neglected under most conditions. The nature of the collision process is thus of fundamental importance.

Intermolecular potential energies A conventional representation of the intermolecular potential energy curve is given by the Lennard-Jones equation:

$$V(r) = 4\epsilon\left[\left(\frac{\sigma}{r}\right)^{12} - \left(\frac{\sigma}{r}\right)^6\right], \quad (3.1)$$

where $V(r)$ is the potential energy at separation r . This is shown graphically in Fig. 3.1. The second term $(\sigma/r)^6$, represents the long-range attractive forces

(London dispersion forces in the case of inert gases), and gives rise to the gentle decrease in $V(r)$ as molecules first approach. The first term, $(\sigma/r)^{12}$, represents the short-range repulsive forces (due to overlap of electron orbitals), and produces the much steeper rise in $V(r)$ as the molecules get closer. ϵ is the depth of the “potential well” at intermolecular distance r_m , where the repulsive forces take over from the attractive forces, and $V(r)$ presents its minimum. σ is the separation at zero energy, when $V(r)=0$, sometimes loosely called the “collision diameter”. r_c called “classical turning point” where the molecules being retarded by the steep repulsive potential and stop at a height $V(r) = \frac{1}{2}mv^2$ point. Potentials other than the Lennard-Jones often give a better fit for particular system, but all show the same general characteristics and use values for ϵ , r_m , and σ defined in the same way.

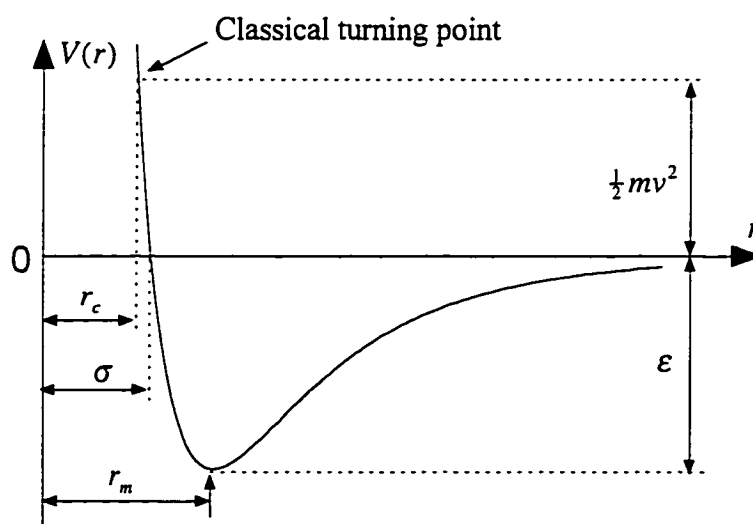


FIG. 3.1 The Lennard-Jones intermolecular potential.

For inert gas molecules, which have no internal degrees of freedom, the collisions can only be elastic. In any kind of elastic collision (head-on or not head-on) it

may be assumed that there is completely free interchange of translational energy between the collision partners, subject to the laws of conservation of energy and momentum. The rate of transfer of translational energy between molecules is thus effectively the gas kinetic collision rate.

For the diatomic and polyatomic gas molecules, the collisions involve vibrational and rotational degrees of freedom. Energy transfer occurs among all vibrational, rotational, and translational degrees of freedom. An elementary theory of vibrational energy transfer is the Landau-Teller theory,^{1,2} which assumed that only repulsive part of the intermolecular potential (Fig.3.1) is steep enough to influence energy transfer, so that the long-range attractive potential can be neglected. If the repulsive potential is represented by a simple exponential $V(r) = V_0 \exp(-\alpha r)$ (replacing the Lennard-Jones term $4\varepsilon(\sigma/r)^{12}$, where α is the exponential parameter in repulsive potential), the probability P_{10} for a $1 \rightarrow 0$ vibrational transfer occurring in a collision of velocity v , can be calculated by classical time-dependent perturbation theory on the assumption that probability P is proportional to the square of the Fourier component of the varying force at the oscillator frequency, ν . This assumes that all collisions have translational energy, $\frac{1}{2}mv^2 \gg h\nu$, and gives P_{10} proportional to $\exp(-4\pi^2 / \alpha v)$. The distribution of molecular speeds is given by the Boltzmann equations, and the proportion of the molecular with speed $\geq v$ is $\exp(-mv^2 / 2kT)$. Integration over the range of possible speeds gives the average probability of deactivation per collision at temperature T as:

$$P_{10} = \exp\left[-3\left(2\pi^4\mu v^2 / \alpha^2 kT\right)^{1/3}\right] \quad (3.2)$$

where μ is the reduced mass of a collision.

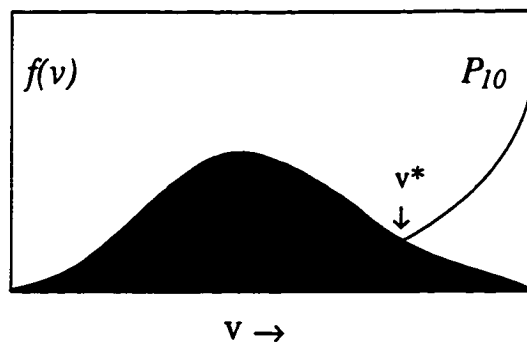


FIG.3.2 Schematic representation of the overlap between the distribution of molecular speeds $f(v)$, and the de-excitation probability P_{10} , as a function of molecular speed v .

The integration is represented graphically in the Fig.3.2, and it will be seen that, at each temperature, there is a speed v^* giving the highest transition probability. Eq.(3.2) is a surprisingly good approximation to the results of more sophisticated quantum mechanical treatments. In particular, a great many non-polar molecules show a linear Landau-Teller plot of $\log P_{10}$ against $T^{1/3}$ (or $\log P_{10}$ against $T^{1/3}$) over a large temperature range.

The Vibrational relaxation time Theoretical models, such as the Landau-Teller, give the value of P_{10} , the average probability per collision for a v ($1 \rightarrow 0$) to occur. In order to make a comparison with the experimental measurements this must be related to a transfer rate. The average number of collisions required for a molecule in the $v=1$ state to deactivate will be $Z_{10} = P_{10}^{-1}$, which is defined as the collision number for a v ($1 \rightarrow 0$) transfer. The gas kinetic collision rate is $Z = 4n\sigma^2(\pi kT/m)^{1/2}$, where m is the molecular mass and σ is the separation at zero energy, the collisions made by one molecule per second. The average time required for a molecule in state $v=1$ to deactivated is thus:

$$\tau = Z_{10}/Z = Z_{10}/4n\sigma^2(\pi kT/m)^{1/2} \quad (3.3)$$

τ is known as the vibrational relaxation time, and is the characteristic time for the establishment of equilibrium between translational motion and the intramolecular vibration. Since Z is proportional to the molecular concentration n , and hence to pressure, τ will vary inversely with pressure. For convenience relaxation times are always referred to a pressure of 1 atm. Eq.(3.3) is an approximation. A $\nu = 1 \rightarrow 0$ transfer can only occur when a molecule in the $\nu = 1$ state collides with another molecule in the $\nu = 0$ state. We have tacitly assumed that all the other n molecules are in this state. In fact there will be a Boltzmann distribution of molecules between the two levels. Further, the processes is reversible and, by the principle of detailed balancing, P_{01} for the reverse transfer must be given by

$$P_{01} = P_{10} \exp(-h\nu/kT)$$

where ν is the vibration frequency. Taking these factors into account, the correct form of relation Eq.(3.3) for a simple harmonic oscillator is:²

$$Z_{10} = Z\tau\{1 - \exp(-h\nu/kT)\} = P_{10}^{-1} \quad (3.4)$$

Experimental measurements usually give a relaxation time from t which P_{10} and Z_{10} may be calculated by Eq.(3.4). The collision number Z_{10} is the most convenient parameter to use.

An alternative way of expressing measurements is in terms of a rate constant k for energy transfer, defined by the relation

$$kp = \tau^{-1} \quad \text{or} \quad k = \tau^{-1} p^{-1} \quad (3.5)$$

p being the pressure. (k is usually expressed in the units $s^{-1} \text{ atm}^{-1}$, or $s^{-1} \text{ Torr}^{-1}$). The transfer rate may also be expressed in terms of a hypothetical energy transfer collision cross-section Q , defined by the relation

$$kp = 4n(kT/\pi m)^{1/2} Q \quad (3.6)$$

Both k and Q may be related to P_{10} by Eqs.(3.4~6). For experimental conditions where $h\nu \gg kT$ (e.g. most experiments involving diatomic molecules), Eq.(3.3) replaces Eq.(3.4), so that $Q/\pi\sigma^2 = P_{10}$, and the cross-section is a direct measure of transfer probability.

Any quantitative treatment for R-T transfer involves complicated geometrical factors. A further complication arises out of the fact that for most molecules the separation between lower rotational quantum levels is so small that, except at low temperature, a wide range of rotational energy levels will be populated under equilibrium conditions. This is in marked contrast with V-T transfer, where the majority of molecules are in the $n=0$ level, and only $\nu(0 \rightarrow 1)$ transitions are important. R-T transfer can be treated by a purely classical model, and Parker³ showed that rotational relaxation can be characterized by a single rotational relaxation time, τ_r , involving the whole of the rotational energy of the molecule, and corresponding to a rotational collision number Z_r . But neither τ_r nor Z_r can be related to a single rotational transition, $J_n \rightarrow J_m$.

3.2 Vibrational-Translational Transfer

3.2.1 The Transition Probability of the SSH Theory

The elementary discussion of inelastic collisions in § 3.1 has shown the difficulty of setting an exact and rigorous theory of energy transfer. Even if a completely satisfactory theory were available, its quantitative application would

be severely limited by the lack of accurate of realistic intermolecular potentials. The theory which has been most widely used for quantitative comparison with experimental measurements of vibrational relaxation is the Schwartz, Slawsky, and Herzfeld (SSH) theory⁴. It accounts semi-quantitatively for most of the principal features of vibrational energy transfer, and gives fair quantitative predictions for simple molecules. We shall use it to provide a basic theoretical framework, and to illustrate the relative importance of the various factors which influence transfer probabilities. It is a quantum-mechanical theory, and treats the collision as due to a parallel stream of molecules, which may be regarded as a de Broglie wave, falling on a molecule regarded as stationary.

Intermolecular potentials. The first requirement in any theory of energy transfer is to define an intermolecular potential $V(r)$. Analytical solutions of the collision problem require an exponential potential, as was used in the classical Landau-Teller theory. The potential used by SSH theory is

$$V(r) = U \exp(-\alpha r) - \epsilon \quad (3.7)$$

This is shown diagrammatically in Fig. 3.3, where it is compared with the Lennard-Jones potential. It is essentially a repulsive potential, and the attractive forces, represented by $-\epsilon$, are regarded as simple increasing the velocity of relative motion, thereby favoring a higher transition probability. Molecular collision parameters, have to derived from experimental measurements of transport properties and mostly expressed in terms of the Lennard-Jones potential: they have to be “fitted” to Eq.(3.7). There are two method to doing this,² which are illustrated in Fig. 3.3.

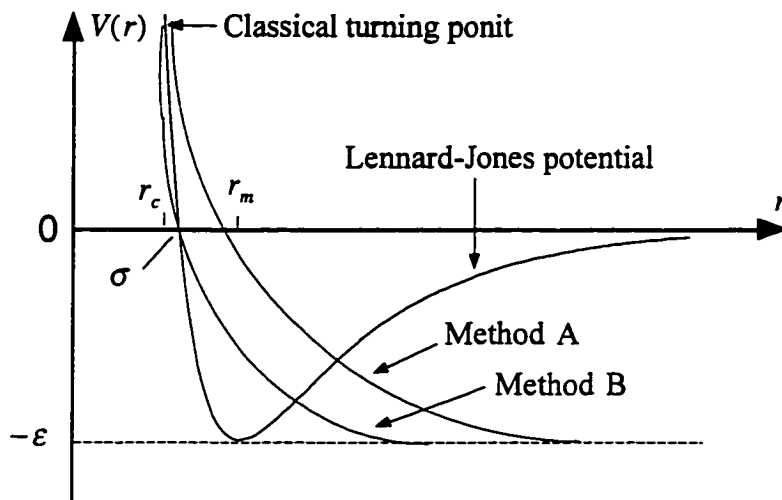


FIG. 3.3 "Fitting" of exponential potential.

Both methods equate the two potentials at classical turning point, r_c . Method A makes the exponential curve tangential to the Lennard-Jones curve at the classical turning point. Method B, which gives a larger value of α , is usually found to agree better with experiment. Both r_c and α will vary with the velocity of approach, and the value α' corresponding to the molecular speed with the highest transition probability, v^* , is used in Fig.3.2. Similar "fitting" techniques may be applied to potentials other than the Lennard-Jones.

Transition probabilities The probability that during a binary collision vibrational mode (a) of one molecule will change its quantum state from i to j , while simultaneously a second mode (b) in the other molecule will change its state from k to l , is given by SSH theory as ⁷

$$P_{k \rightarrow l}^{i \rightarrow j(a)} = P_0(a)P_0(b) [V^{ij}(a)]^2 [V^{kl}(b)]^2 \left(\frac{4\mu}{kT} \right) \exp\left(-\frac{\epsilon}{kT} \right) \left(\frac{8\pi^3 \mu \Delta E}{h^2} \right)^2 \int_0^\infty f(\bar{u}) d\bar{u} \quad (3.8)$$

where

$$f(\bar{u}) = \frac{\bar{u}}{\alpha^4} \left(\frac{r_c}{\sigma} \right)^2 \exp \left[-\frac{\mu \bar{u}^2}{2kT} \right] \left\{ \frac{\exp[L - L']}{(1 - \exp[L - L'])^2} \right\}$$

$$L = \frac{4\pi^2\mu}{\alpha h} \bar{u} \quad \text{and} \quad L' = \frac{4\pi^2\mu}{\alpha h} \bar{v}$$

μ is the reduced mass of the colliding pair which approach one another with an effective relative velocity \bar{u} and recede with velocity \bar{v} . The integration is over the thermal distribution at T of the molecular velocities assumed to be Maxwellian. ΔE is the amount of energy exchanged between the vibrational and translational degree of freedom:

$$-\Delta E = h\nu_a(i - j) + h\nu_b(k - l) = \mu(\bar{v}^2 - \bar{u}^2)/2$$

In a simple V-T transition, only mode (a) changes state, and $k = l$ so that the pre-exponential term $[V^k(b)]^2$ becomes unity. SSH calculations are best performed by making a numerical integration of Eq.(3.8).

When ΔE is large the integration can be solved analytically in terms of α' to give the formula deduced by Tanczos,⁵ which is valid for values of $\Delta E > 200$ cm^{-1} and forms a more convenient basis for discussing the influence of different factors on transition probability. Tanczos equation is

$$P_{k \rightarrow l(b)}^{i \rightarrow j(a)} = P_0(a)P_0(b) \left(\frac{r_c}{\sigma} \right) [V^{ij}(a)]^2 [V^{kl}(b)]^2 8 \left(\frac{\pi}{3} \right)^{1/2} \left(\frac{8\pi^3\mu\Delta E}{\alpha'^2 h^2} \right)^2 \zeta^{1/2} \exp \left(-3\zeta + \frac{\Delta E}{2kT} + \frac{\epsilon}{kT} \right) \quad (3.9)$$

where

$$\zeta = \frac{\mu u'^2}{2kT} = \left(\frac{\Delta E^2 \mu \pi^2}{2\alpha'^2 \hbar^2 kT} \right)^{1/3}$$

The Tanczos equation consists of four parts: (a) the geometrical, or steric, factor P_0 ; (b) the collision cross-reference factor $(r_c^*/\sigma)^2$, (c) the vibrational factor $[V]^2$; (d) the translational factor represented by the remainder of the equation.

(a) The steric factors, P_0 , are required to account for the fact that the molecules are not spherical symmetrical and that some collision orientations will be more effective than others. They are usually taken as $\frac{1}{3}$ (the average of $\cos^2 \theta$ taken over a sphere) for diatomic molecules and for longitudinal vibrations of linear polyatomic molecules. For non-linear polyatomic molecules and for bending modes of linear molecules, P_0 is taken as $\frac{2}{3}$. The theory takes no account of rotational transitions, and assumes the orientation to remain constant during a collision. These assumptions are invalid for hydrogen and hydrides where a very low moment of inertia is associated with rapid rotation and with wide spacing of rotational quantum levels; further discussion of these effects will be given later. The fact that certain orientations will be preferred for collisions involving polar molecules is also ignored, which limits the accuracy of the treatment for these molecules at low temperatures.

(b) The collision cross-reference factor, $(r_c^*/\sigma)^2$, is the ratio of the intermolecular separation at the classical turning point to the separation at zero energy, σ , which is used in calculating the gas kinetic collision number Z . It converts probabilities calculated for a collision cross-section πr_c^* , to the usual elastic cross-section of kinetic theory, $\pi \sigma^2$.

(c) The vibrational factor, $[V^{ij}(a)]^2$, is the square of the matrix element for the transition between the two vibrational state i , j of molecule (a). It represents the coupling of the initial and final states, i and j , of the oscillator under the

influence of the perturbation produced by collision, and correspond to the square of the Fourier component of the varying force at the oscillator frequency which is found in classical theory. It depends on the repulsion parameter a and the frequency and amplitude of the vibration.

(d) The transitional factor gives expression to the change in kinetic energy of transition involved in the inelastic collision. The parameters involved are the reduced mass of the collision, m , and the temperature T , which together determine the velocity of approach; ΔE , the amount of vibrational energy transferred in the collision, and the intermolecular repulsion parameter, a . It will be noted that all the terms involve ΔE^2 with the exception of the second exponential term, $\exp(-\Delta E/2kT)$. This alone will change sign for the reverse process, $P_{k \rightarrow l}^{i \rightarrow j(a)}$, and the two probabilities will differ by a factor $\exp(-\Delta E/kT)$ in accordance with the principle of detailed balancing.

The exponential term of the transition factor control the temperature dependence of P , since the whole the pre-exponential part of Eq.(3.9) is only weakly temperature dependent. The dominant term is usually the negative first exponential term, $\exp(-3\zeta)$. This predicts that $\log P$ will vary with $T^{1/3}$ as in the Landau-Teller expression. But for cases where the attractive potential (represented by $-\varepsilon$) is large the positive third exponential term $\exp(+\varepsilon/kT)$ can become dominant, give rise to a higher probability which will vary inversely with temperature. The SSH theory thus predicts qualitatively the minimum in the Landau-Teller plot ($\log P$ versus $T^{1/3}$) which is observed for strongly polar molecules, and the curvature observed for all other molecules at lower temperatures. Quantitative prediction under these conditions is unsuccessful

due to the failure of Eq.(3.8) to give adequate expression to the effect of the attractive potential, and the SSH theory consistently underestimates P for strongly polar molecules and at low temperatures.

3.2.2. V-R and V-(T,R) Transfer

The Attractive potential Two fundamental defects of the SSH theory have been pointed out before:

(a) Inadequate expression is given to the attractive part of the intermolecular potential. This becomes important for all molecules at low temperature, and for strong polar molecules at all temperature.

(b) The relative orientation of the molecules is regarded as constant during collision, and the possibility of simultaneous rotational transitions is disregarded. these assumptions are valid for molecules with large moments of inertia, but not for hydrides and deuterides. The followings will discuss modifications which take these factors into account.

Better account may be taken of the attractive forces for non-polar (approximately isotropic) molecules by using the Morse double exponential potential:

$$V(r) = \varepsilon \exp[-\alpha'(r - r_m)] - 2\varepsilon \exp[-\frac{1}{2}\alpha'(r - r_m)] \quad (3.10)$$

This allows an analytical solution, and leads to an alteration in the exponential factor in Eq. (3.9) which may be written,⁶

$$P(T) = A(T) \exp \left[-3\zeta + \frac{4}{\pi} \sqrt{\frac{\varepsilon\zeta}{kT}} + \frac{16\varepsilon}{3\pi^2 kT} + \frac{\Delta E}{2kT} \right] \quad (3.11)$$

where $A(T)$ represents the whole, weakly temperature dependent pre-exponential factor in Eq.(3.9). This assumes a spherical symmetrical potential and gives a good prediction for the temperature dependence of P for simple non-polar molecules at lower temperature. Eq.(3.11) is due to Shin.⁶ a calculation for N_2 , O_2 , and CO has been published by Calvert and Amme.⁷ The method can only be used when sufficient transport data are available to obtain the force constants for Eq.(3.10).

For polar molecules, which are strongly anisotropic, the angle dependence of the intermolecular potential must be taken into account, and also the predominance of preferred collisional orientations at lower temperatures, This requires modification of both the pre-exponential and the exponential terms in Eq.(3.9). Shin has derived an expression

$$P(T) = \frac{A}{16(a^2 - b^2)} \zeta^{3/2} \exp \left[-3\zeta + \frac{4}{\pi} \sqrt{\frac{\epsilon \zeta}{kT}} + \frac{16\epsilon}{3\pi^2 kT} + \frac{\Delta E}{kT} + 2a \right] \quad (3.12)$$

where $A = \sqrt{\frac{4\pi}{3}} \left(\frac{4\pi m \alpha \Delta E}{\hbar^2} \right)^2 X^2$ (X is the matrix element)

$$a = \frac{\mu^2}{\epsilon r_0^3} \left(\frac{\epsilon^{\frac{1}{2}} \zeta^{\frac{1}{2}}}{(kT)^{\frac{1}{2}}} \right), \quad b = \frac{\mu Q}{\epsilon r_0^4} \left(\frac{\epsilon^{\frac{1}{2}} \zeta^{\frac{1}{2}}}{(kT)^{\frac{1}{2}}} \right)$$

taking into account both dipole-dipole and dipole-quadrupole forces, (μQ) . This expression contains an additional positive exponential term $2a$, which also varies inversely with temperature and will be important for molecules with high dipole moment and small molecular diameter, such as NH_3 . It predicts with fair accuracy the inversion of the temperature-dependence of $P(T)$ observed at lower temperatures for molecules such as SO_2 .

Simultaneous rotational transitions: V-R and V-(t.R) transfer. Interaction between molecular vibration and rotation was proposed by Cottrell *et al.*⁸ in order to account for the observation that many deuterides show lower value of P_{10} than the corresponding hydrides, in spite of their substantially lower vibrational frequencies (which in simple SSH theory would correspond to faster relaxation). Cottrell suggested that, since the actual rotational velocity of the hydrogen atoms in most hydrides is larger than the translational velocity of the molecule, vibrational energy transfer into rotation will be more probable than transfer into translation. He produced a quantitative theory based on the model of interaction of a classical rotator and a quantized oscillator, which was further developed and applied to a wide range of molecules by Bradley Moore.⁹ It gives an expression for P_{10} which formally resembles the SSH expression Eq.(3.9), but with the important difference that, since the angular velocity of rotation rather than the translation velocity of the molecules plays important role, ωd is substituted for the translational velocity and I/d^2 for the reduced mass (ω is the angular velocity, d the bond length of the hydride molecules, and I the moment of inertia). The dominating negative exponential term ζ of the SSH Eq.(3.9), which may be written in the abbreviated form of Eq.(3.11) as

$$P(T) = A(T) \exp(-3\zeta) = A(T) \exp \left[-3 \left(\frac{\Delta E^2 \mu \pi^2}{2\alpha^2 \hbar^2 kT} \right)^{1/3} \right] \quad (3.13)$$

is thus replaced by a new term giving

$$P(T) = A(T) \exp \left[-3 \left(\frac{2\pi^2 I \Delta E^2}{d^2 \alpha^2 kT} \right)^{1/3} \right] \quad (3.14)$$

The gross effect of this change on the deuteride/hydride ratio may be seen from a simple example - CD_4/CH_4 . the ratio of moments of inertia is

$I_{CD_4}/I_{CH_4} = 6.38/3.19$, which is much larger than the ratio of molecular weights, $M_{CD_4}/M_{CH_4} = 20/16$, and this counteracts the favorable frequency ratio, $\nu_{CD_4}/\nu_{CH_4} = 2090/2886$, so that CH_4 relaxes faster. This theory, which treats vibrational relaxation as entirely due to V-R transfer, gives good prediction of the deuterides/hydride ratio, but predicts absolute rates which are general too low.

Shin¹⁰ has developed a classical collision theory for vibrational energy transfer in hydrogen halides. This solves the classical equations for the collision model of a “rotation-averaged oscillator and a rigid rotator, in which two hydrogen atoms interact strongly at close-in collisions”. It takes account of effects of both translational and rotational motion (i.e. of V-T and V-R transfer occurring simultaneously), and gives a good fit with experimental measurements for HCl, DCl, HBr, and HI over the temperature range 800~2000 K, where a ‘normal’ Landau-Teller temperature dependence is predicted and found.

Both the ‘pure’ semiclassical V-R theory and Shin’s classical V-(T,R) theory treat the rotational motion of the molecules as classical. This seems to be justified for molecules, such as the hydrogen halides, where the quantum vibrational level spacing are very much larger than the quantum rotational level spacings, but it breaks down for polyatomic molecules having much lower vibrational frequencies. If both energy modes are regarded as quantized, two competing factors have to be taken into account. A ΔJ transition, simultaneous with, and in opposite direction to a $\Delta \nu$ transition, will exert a favorable effect on the transition probability by decreasing ΔE_{int} , the amount of internal energy transferred to translation, since

$$\Delta E_{int} = \Delta E_{vib} - \Delta E_{rot}$$

This will tend to favor a large value of ΔJ and of ΔE_{rot} . This effect is balanced by the necessity for conservation of total angular momentum in collision, which favors a small value of ΔJ . Various theoretical calculations have been made, and all predict that a $\Delta v = \pm 1$ transfer will normally be accompanied by ΔJ transition of size depending on the mass and moment of inertia of the molecule. For a heavy molecule, such as I_2 , the momentum requirements are more easily met, and ΔJ values up to ± 14 (with an optimum at 6 to 8) are predicted theoretically and confirmed experimentally.¹¹ For lighter molecules such as O_2 and N_2 , $\Delta J = \pm 2$ is the most probable transition, being 50% more probable than $\Delta J = 0$, and three orders of magnitude more probable than $\Delta J = \pm 4$.¹² (The even number are required to maintain the symmetry of the total wavefunction for a homonuclear diatomic molecule.) This is confirmed by experimental work on Li_2 .¹³

3.2.3 Relaxation in pure Gases (Polyatomic)

The two major characteristics affecting the comparison between relaxation behavior of polyatomic gases and of diatomic are:

- (a) Polyatomic molecules possess several vibrational modes, each of which contributes to the molecular vibrational heat capacity, and can, in principle, relax independently.
- (b) Polyatomic molecules are structurally flexible and change their effective shape both during the normal vibration, and more important, during collision.

Consideration (a) turns out to be relatively undisturbing. The vast majority of polyatomic molecules show a single vibrational relaxation process involving the whole vibrational heat content of the molecule. This is due to rapid

intramolecular V-V transfer, which maintains continuous equilibrium of vibrational energy between the active fundamental modes. The whole vibrational heat content of the molecule will relaxes in a single V-T transfer via the lowest mode (which will usually have a higher V-T transfer rate than upper modes). This mechanism is characterized by a single overall relaxation time, τ , which may be related to τ_1 , the actual relaxation time of the lowest mode by the equation $\tau_1 = (C_1/C_s)\tau$, where C_s is the total vibrational heat content and C_1 the contribution to the lowest mode.¹⁴

The consequences of (b) are much more serious. For most polyatomic molecules even an approximately quantitative description of an elastic collision is at present impossible, while for inelastic collisions, first-order perturbation theory is inadequate. In consequence, the kind of theoretical treatment discussed in § 3.1 can only be applied qualitatively for most polyatomic molecules. The one gas to which quantitative calculations have been applied with some success is CH₄.

The role of V-(T,R) transfer. It was stated in § 3.2.2 that vibrational transition $\Delta v = \pm 1$ by molecules of moderate molecular weight are usually accompanied by simultaneous rotational transition, $\Delta J = \pm 2$. The amount of internal energy transferred to translation in a V-T,R transfer of this kind will be

$$\Delta E_{\text{int}} = \Delta E_{\text{vib}} \pm \Delta E_{\text{rot}}$$

If the rotational transition accompanying a $v = 1 \rightarrow 0$ vibrational transition is $\Delta J = \pm 2$, the energy level diagram for the relaxation of a state, $(v = 1)(J^*)$ will be as shown in Fig.3.4.

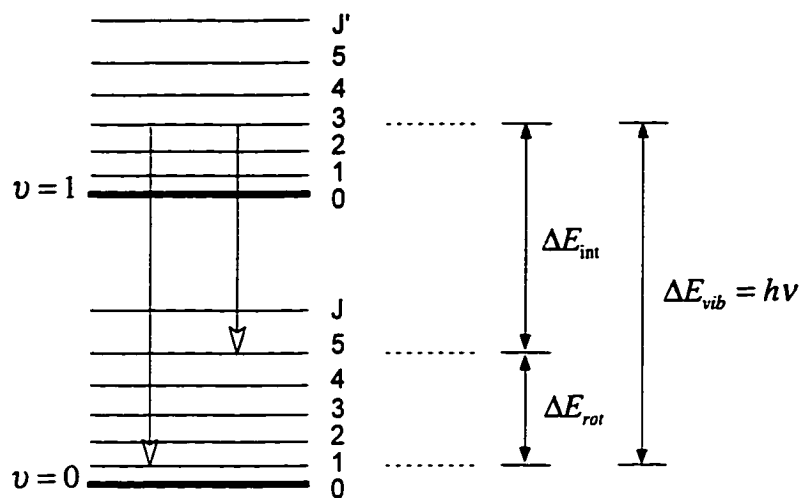


FIG. 3.4 Energy level diagram for simultaneous vibrational and rotational transitions.¹⁵

The most probable transition is likely to be that involving the smallest transfer to translation, i.e., from $(v=1)(J^*)$ to $(v=0)(J^*+2)$. For this transition,

$$\Delta E_{\text{int}} = \Delta E_{\text{vib}} - \Delta E_{\text{rot}} = h\nu - B(4J^* + 6)$$

so that the magnitude of the effect of the simultaneous rotational transition on the total relaxation process will depend critically on $B = h/8\pi^2 c I_B$, the rotational constant of the molecule. The slow V-(T,R) transfer in to the $(v=0)(J^*+2)$ level will be followed by very rapid thermal equilibration of the rotational levels in the $(v=0)$ state: i.e., if J^* is the most highly populated rotational level at the experimental temperature, there will be rapid R-T transfer, predominantly from (J^*+2) to J^* . The total effective transfer from internal to translational energy, as measured by acoustic or shock-tube experiments, will thus be ΔE_{vib} , but the rate-controlling step will be the slower V-(T,R) transfer involving the smaller quantity ΔE_{int} .

3.3 Vibrational-Vibrational Transfer

3.3.1 The SSH theory for non-resonant and resonant transfer

The SSH expression Eq.(3.8) for $P_{k-l(b)}^{i-j(a)}$, the probability that a vibrational mode (a) of one molecule will change its quantum state from i to j , while simultaneously a second mode (b) in the other molecule will change its state from k to l , applies equally to V-T transfer (where $k=l$) and to V-V transfer (where $k \neq l$). For the V-T case, ΔE , the energy exchanged between vibrational and translational degree of freedom, is

$$\Delta E = h\nu_a(i - j)$$

For the V-V case

$$\Delta E = h\nu_a(i - j) + h\nu_b(k - l)$$

Non-resonant V-V transfers are conveniently handled in terms of the analytical solution of Eq.(3.8) due to Tanczos (Eq.(3.9)), which was used as the basis for discussion of V-T transfer in § 3.1, and is valid for values of $\Delta E \geq 200\text{cm}^{-1}$. Similar criteria should apply for dependence on vibrational frequency, quantum number, single versus multiple quantum transfer, collision mass, temperature, and intermolecular potential.

For a V-V transfer between different molecular species the additional possibility arises of a resonant transition, where

$$h\nu_a(i - j) = h\nu_b(k - l)$$

and $\Delta E=0$. For resonant and near-resonant transfers a different analytical solution, also due to Tanczos, applies for values of $\Delta E \geq 50\text{cm}^{-1}$:

$$P_{k-l(b)}^{i-j(a)} = P_0(a)P_0(b) [V^{ij}(a)V^{kl}(b)]^2 \frac{64\pi^2 \mu kT}{\alpha^2 h^2} \exp\left(\frac{\varepsilon}{kT}\right)$$

Resonant transfers are much faster than non-resonant transfers, and there is no term in ΔE , so that all near-resonant transfers with $\Delta E \geq 50\text{cm}^{-1}$ behave as if they were resonant. Dependence on the frequency of the exchanging modes arises through the pre-exponential term $[V^{ij}(a)V^{kl}(b)]^2$. since each squared vibrational factor for a single quantum transition, $[V^{(i-1)-i}]^2$, is inversely proportional to the frequency in a single quantum jump, this gives rise to inverse dependence of P on the square of the frequency. Resonant transfers between high frequency modes will thus have a collision probability much smaller than unity. This is because, although there is no net energy transfer from vibration to translation, the change in vibrational quantum state can only be brought about by a time-dependent force. (The same factor also operates for non-resonant transfers.(3.9)), but will usually be far outweighed by the exponential dependence on ΔE). The last pre-exponential term predicts a weak positive dependence on temperature and a weak positive dependence on reduced mass. The only exponential term is that depending on the intermolecular attractive parameter, $\exp(\epsilon/kT)$, so that quite a small value of it will be sufficient to outweigh the pre-exponential term and produce an overall negative temperature dependence for resonant V-V transfer, which will in general be much more sensitive to intermolecular attractive forces than non-resonant transfer. Quantitative treatment of such transfers by SSH theory will again be unsatisfactory due to inadequacy of the assumed potential.

3.3.2 Intermode transfer in polyatomic gases

Single relaxation process. Intramolecular transfer of energy between different vibrational modes can only occur in collision, as the energy discrepancy

between the modes must be made up as translational energy. For a molecule with two active vibrational modes of frequency ν_1 and ν_2 there are three possible vibrational transitions, which are illustrated on the energy-level diagram in Fig.3.5

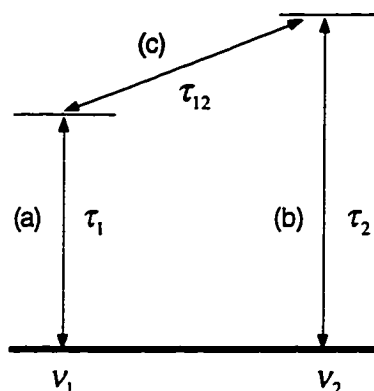
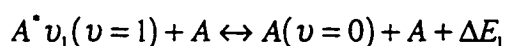
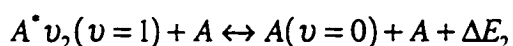


FIG. 3.5 Energy-level diagram showing transition for a molecule with two active vibrational modes.

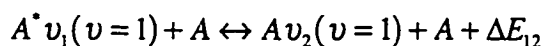
- (a) Transfer of translational energy into $0 \rightarrow 1$ excitation of the mode ν_1 , with relaxation time τ_1 :



- (b) Transfer of translational energy to $0 \rightarrow 1$ excitation of the mode ν_2 , with relaxation time τ_2 :



- (c) The complex transfer of one quantum of vibrational energy from mode ν_1 , plus the necessary increment of translational energy to give $0 \rightarrow 1$ excitation of the mode ν_2 , with relaxation time τ_{12} :



The values of τ_1 , τ_2 , and τ_{12} may, in principle, be calculated by SSH theory. Since only one molecule species is involved in all three processes, their relative

magnitudes will be mainly determined by the value of ΔE . For the model represented in Fig.3.5 the fastest relaxation process will be the complex transfer (c), and the slowest the V-T relaxation of mode ν_2 by process (b). This means that $\tau_2 > \tau_1 > \tau_{12}$. Vibrational energy thus enters the molecule via process (a), which is rate controlling, and rapidly flows in complex collisions via the faster process (c) to upper mode. Process (b) is too slow to play any role. This is known as a 'series' mechanism and is characterized by a single overall relaxation time τ , which can be related to τ_1 by $\tau_1 = (C_1/C_r)\tau$, where C_1 is the heat capacity contribution due to mode ν_1 alone, and C_r the total vibrational heat capacity.

This kind of behavior is known by the vast majority of polyatomic molecules. The most usual pattern of fundamental vibration frequencies is such that the energy gaps between the upper modes are much less than the energy level of the lowest mode. The general picture is that rapid vibration-vibration transfer maintains continuous equilibrium of vibrational energy between the various fundamental modes of the molecule, and that the whole of this energy relaxes in a single vibration-translation transfer process via the lowest mode.

Multiple relaxation process. A few polyatomic molecules have a large energy gap between the lowest and second lowest vibrational modes. The vibrational transitions for such a molecule, having two active vibrational modes ν_1 and ν_2 , are shown in Fig. 3.6(i), which may be contrasted with Fig.3.5. The same three transitions, (a), (b), and (c) are possible, but similar reasoning now gives the condition $\tau_2 \gg \tau_{12} > \tau_1$. Process (b) will again be too slow to play any role, and the upper mode will again relax by a series mechanism via the complex process (c), followed by (a). But (c) is now slower than (a) and becomes the rate-

determining step, so that the vibrational energy of the upper mode is transferred to translation with an effective relaxation time τ_{12} . The vibrational energy of the lowest mode relaxes independently by process (a) with the shorter relaxation time τ_1 . For the crude model shown in Fig.3.6(i) the criterion for multiple relaxation process of this kind would be the simple condition $\nu_2 > 2\nu_1$.

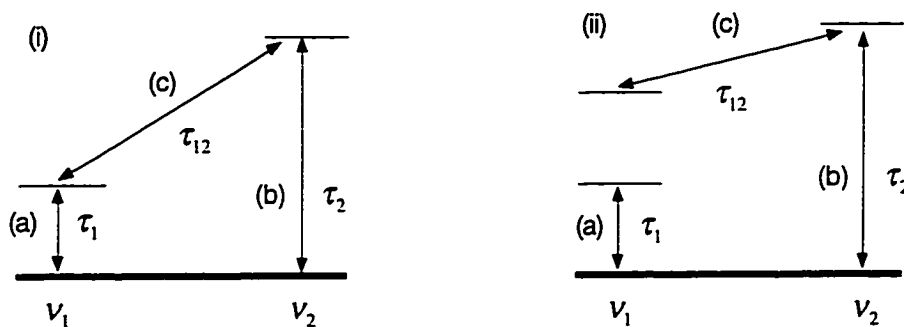
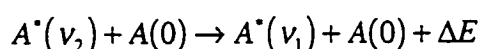
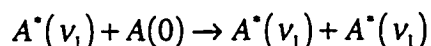


FIG. 3.6 Energy-level diagram for a molecule with two active vibrational modes, showing double relaxation process.

Actually the fastest complex process for relaxation of the upper mode will be a transition to the first harmonic ($2\nu_1$) of the lowest mode, as shown in Fig.3.6(ii):



followed by very rapid resonant single-quantum (intermolecular) transfer:



The first step is a two-quantum transition which is intrinsically slower than a one-quantum transition, but will still be faster than (a) for small values of $\Delta E = \nu_2 - 2\nu_1$, so that the criterion becomes $\nu_2 \gg 2\nu_1$.

3.4 Rotational-Translational Transfer

The general characteristics of R-T transfer, and how these differ in important respects from those of V-T transfer, were mentioned in § 3.1. Detailed theoretical treatments of rotationally inelastic collisions fall into three classes - quantum mechanical, classical, and semiclassical. The area of application of each method depends on the magnitudes of the rotational and translational quantum numbers involved. When both rotational and translational quantum numbers are small, as in collision involving H₂ and He, the quantum method is applicable. For systems specified by low rotational and high translational quantum numbers, e.g. HCl + Ar, the semiclassical method may be applied. For the very large number of systems involving heavy molecules with large moments of inertia, where both quantum numbers are large, the classical method is most suitable. Calculations based on all three methods require an accurate intermolecular potential, $V = V(r, \theta)$, particularly its angular dependence, which is only available for a few simple systems. Reviews of the theoretical treatment of R-T transfer can be found in the literatures.^{16,17,18} Here we only talk about classical theories.

The first classical treatment of rotational transfer was due to Parker,³ who investigated collisions between two homonuclear diatomic molecules, AB and CD. He adopted a potential function

$$V = a[\exp(-\alpha r_{AC}) + \exp(-\alpha r_{AD}) + \exp(-\alpha r_{BC}) + \exp(-\alpha r_{BD})] - b[\exp(-\frac{1}{2}\alpha R)]$$

containing both repulsive and attractive terms, and confined his attention to coplanar encounters with the initial rotational energy zero. Solution of the classical equations of motion showed that rotational relaxation could be

characterized by a single relaxation time, τ_r , involving the whole of the rotational energy of the molecule. This leads to a rotational collision number, Z_R , given by

$$Z_R = \frac{Z_R^\infty}{\left[1 + \frac{\pi^{3/2}}{2} \left(\frac{T^*}{T} \right)^{1/2} + \left(\frac{\pi^2}{4} + \pi \right) \left(\frac{T^*}{T} \right) \right]} \quad (3.15)$$

where $Z_R^\infty = \frac{1}{16}(\alpha d/\epsilon)^2$ and $T^* = \epsilon/k$. (a , d , and e are intermolecular potential parameters). Eq.(3.15) predicts a slight positive temperature dependence for Z_R (transfer becomes less efficient at higher temperatures and speeds of rotation), and gives fair predictions for O and N at 300 K. The Parker theory has been elaborated by Brau and Jonkman.¹⁹

Widom²⁰ used a classical ‘rough sphere’ model for the rotational relaxation of a spherical-top molecule in collision with an inert gas molecule, and found the simple expression

$$Z_R = \frac{3}{8}(1+b)^2/b \quad (3.16)$$

where $b = I/\mu a^2$, I being the moment of inertia, m the reduced mass of the collision, and a the molecular diameter. Eq.(3.16) predicts a minimum value $Z_R = 1.5$ when $I = \mu a^2$ and $b=1$, and it is analogous to an expression obtained earlier by Wang Chang and Uhlenbeck,²¹ who applied the same model to rotational relaxation of spherical-top molecules in self-collisions, and obtained a similar expression:

$$Z_R = \frac{3}{8}(1+2b)^2/b. \quad (3.17)$$

Both of these models neglect attractive forces entirely, and predict values of Z_R which are independent of temperature.

We shall here say a little bit about the mechanism of rotational excitation. The role of rotational excitation in the overall heating and cooling processes of heavier diatomic and polyatomic gases is uninteresting. R-T transfer is very rapid, multiple quantum transitions occur easily, and the rotational population distribution reaches equilibrium almost as quickly as the translational. For H and hydrides the picture is different; R-T transfer is much slower, also it plays a more important role in the overall heating and cooling processes, as vibrational modes of such molecules do not become active until relatively high temperatures. The rotational excitation process differs fundamentally from the vibrational because of the different ways in which the quantum levels are distributed: the energy gaps between successive vibrational levels become gradually smaller (owing to anharmonicity) as ν increases. This means that R-T transitions, $\Delta J = \pm 1$, become progressively less efficient as J and ΔE increase, while R-R transition, when involving neighboring levels, are nearly always non-resonant and inefficient. The kind of mechanism for vibrational excitation of cold gases—slow initial activation by V-T transfer to the $\nu = 1$ level, followed by rapid ‘staircase’ ascent by near-resonant V-V transfer - does not operate in rotational excitation. Instead, the initial R-T excitation of a cold gas from low J -level is rapid, but becomes progressively slower as J increases. Conversely, the initial rotational de-excitation of a hot gas, with rotational population peaking in a high J -level, will be very slow, but will become progressively faster as the rotational temperature drops. Very high rotational levels, sometimes produced in chemluminescent processes, may thus show a high degree of metastability. The rotational temperature of a hot gas, initially in Boltzmann equilibrium, cooling in a jet expansion can lag behind both translational and vibrational temperatures, giving

rise to a non-equilibrium distribution: $T_{rot} > T_{vib} > T_{Tran}$. In contrast, the temperature distribution in a cold gas, undergoing rapid heating in a shock-front, where rotational excitation will be much faster than vibrational, will be $T_{Tran} > T_{rot} > T_{vib}$. A detailed studies^{22, 23} has shown that the lower J-levels relax much faster than the upper J-levels.

It is interesting to note, in conclusion, that rotational de-excitation by emission of radiation follows an entirely different pattern. This can be important in interstellar clouds, where low temperature and extremely small molecular concentrations can render collisional relaxation extremely slow. the probability for radiative transition between the J' and $(J' - 1)$ levels varies with J^3 . The upper J-levels are therefore depopulated much more rapidly than the lower levels, and a population inversion builds up between the $J=1$ and $J=0$ levels.²⁴ This can lead to maser action.

References to Chapter 3

- 3.1. L. Landau & E. Teller, *Phys. Z. Sowj. Un.* **10**, 34(1936).
- 3.2. K.F. Herzfeld & T.A. Litovitz, *Absorption And Dispersion Of Ultrasonic Waves*, Academic Press, New York(1959).
- 3.3. J.G. Parker, *Physics Fluids*, **2**, 499(1959).
- 3.4. R.N. Schwartz, Z.I. Slawsky & K.F. Herzfeld, *J. Chem. Phys.*, **20**, 1591(1952).
- 3.5. F.L. Tanczos, *J. Chem. Phys.*, **25**, 439(1956).
- 3.6. H.K. Shin, *J. Am. Chem. Soc.*, **90**, 3029(1968).
- 3.7. J.B. Calvert & R.C. Amme, *J. Chem. Phys.*, **45**, 4710(1966).
- 3.8. T.L. Cottrell, *et al.*, *Trans. Faraday Soc.*, **60**, 241(1964).
- 3.9. C.B. Moore, *J. Chem. Phys.*, **43**, 2979(1965).
- 3.10. H.K. Shin, *J. Chem. Phys.*, **76**, 1079(1971).
- 3.11. Kurzel, R.B. *et al.*, *J. Chem. Phys.*, **55**, 4882(1971).
- 3.12. F.C. Hansen, *et al.*, *J. Chem. Phys.*, **53**, 2557(1970).
- 3.13. C.H. Ottinger, *et al.*, *Chem. Phys. Lett.*, **8**, 513(1971).
- 3.14. K. Z. Schäfer, *Phys. Chem.*, **B46**, 212(1940).
- 3.15. J.D. Lambert, *J. Chem. Soc. Faraday II*, **68**, 364(1972).
- 3.16. K. Takayanagi, *Adv. Atom. Molec. Phys.* **1**, 149(1965).
- 3.17. K. Takayanagi, *Comments At. & Mol. Phys.*, **4**, 59(1973).
- 3.18. D. A. Secrest, *Rev. Phys. Chem.*, **24**, 379(1973).
- 3.19. C.A. Brau, *et al.* *J. Chem. Phys.*, **52**, 477(1970).
- 3.20. B. Widom, *J. Chem. Phys.*, **32**, 913(1960).
- 3.21. Wang Chang, *et al.* Uni. Michigan Report, Cm-681, Project N-Ord-7249.

3.22. H. Rabitz, *et al.*, *J. Chem. Phys.* **63**, 3532(1975).

3.23. A.M.G. Ding, *et al.* *Chem. Phys.* **10**, 39(1975).

3.24. P. Goldsimth, *J. Astrophys.*, **176**, 597(1972).

Chapter 4

Experimental Apparatus

- Virtual Instrumentation of a Resonant Spectrophone

In this Chapter a description of the apparatus and technique is given, oriented toward developing a versatile and comprehensive instrumentation, which can perform the three tasks of tracing and monitoring gas molecules,¹⁻⁴ measuring molecular relaxation-time,^{5,6} and evaluating the rate constant and active energy of photo-induced chemical reaction in a resonator.⁷ The way to approach the ultimate goal is the usage of so-called Virtual Instrumentation (VI), in which software plays the key role played by hardware in traditional experimental setups. Through the GPIB(IEEE 488.2) interface, all instruments work as one virtual instrument that can be easily defined and application-oriented system.

4.1 Hardware Arrangement

The present experimental setup is illustrated in Figure 4.1, the main parts such as optical chopper, lock-in amplifier are used in the same way as in a traditional setup. A tunable CO₂ laser beam modulated by an optical chopper. The laser wavelength is coincident with an absorption line of the species. The beam is passed along the co-axis of the cylindrical cavity. The absorbed photon energy by the molecular species is converted into heat by the intermolecular collisions. This produces a periodic pressure rise at the modulation frequency,

that is, a sound wave, which may be detected by a sensitive microphone. The cavity was designed to minimize dissipation of the acoustic energy by modulating the laser beam spatially and temporally so as to promote acoustic resonance, the signal can be increased manifold.

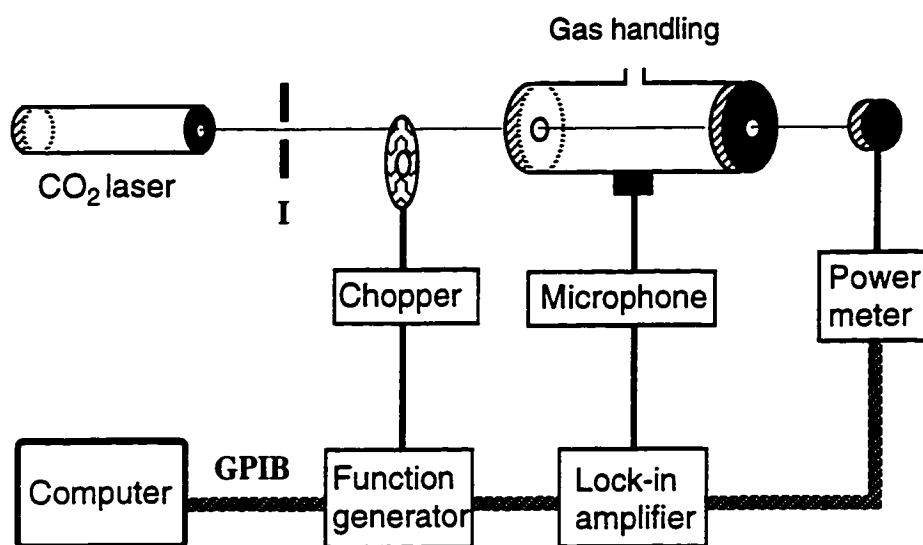


FIG. 4.1 Block diagram of the resonant spectrophone setup.

The CO₂ laser (*Laser Photonics CL35*) was grating tuned at the line P₂₀ with a power output about 0.5 Watts/line (see Appendix A: Data sheet of CO₂ waveguide laser) and the beam diameter was about 1.5 mm. The optical chopper, driven by a function generator (HP 3325A), can go up to 20 kHz. The photoacoustic signal, detected by a microphone, was processed by a lock-in analyzer. The laser power was measured with a power meter (*Molelectron MAX500D*) and was used for signal normalization. The setup was controlled by a Macintosh computer through GPIB(IEEE 488) interface. The acoustic signal was taken point by point at each discrete modulation frequency.

4.1.1 Cylindrical Cavity and Acoustic Modes

a. The Resonant Cavity

The resonator was constructed of brass to have a good heat conductivity, and nickel-plated to prevent potential chemical reaction. The cavity was cylindrical with a diameter of 10.16 cm and a length of $L \cong 2R = 10.16$ to minimize the ratio of surface area to volume for fixed volume. Figures 4.2 (a), (b), and (c) are the cross-sectional view of the window flange of the resonant cavity, the side view of the cavity, and the infrared laser window, respectively. The *Knowles* BT-1759 miniature electret microphone was mounted in the cylindrical wall halfway between the ends. The end plates were sealed with Viton O-rings. Two ZnSe windows with diameter 1.3 cm, were mounted in the centers of the two end plates, and were used as entry and exit of the laser beam. The heat $H(\vec{r}, t)$ introduced in the unit volume per unit time by the absorption of light acts as a source for the generation of sound. This can be described by ¹

$$\nabla^2 p - c^{-2} \partial^2 p / \partial t^2 = -[(\gamma - 1)/c^2] \partial H / \partial t \quad (4.1)$$

where c is the velocity of sound and $\gamma = C_p / C_v$, the ratio of specific heats of the gas. Eq.(1) is an inhomogeneous wave equation that may be solved by taking the time Fourier transform of both sides and expressing the solution p as an infinite series expansion of the normal mode solution p_i of the homogeneous wave equation, i.e. $p(\vec{r}, \omega) = \sum A_i(\omega) p_i(\vec{r})$. For a cylindrical cavity with rigid walls, the eigenfrequencies are given by ¹

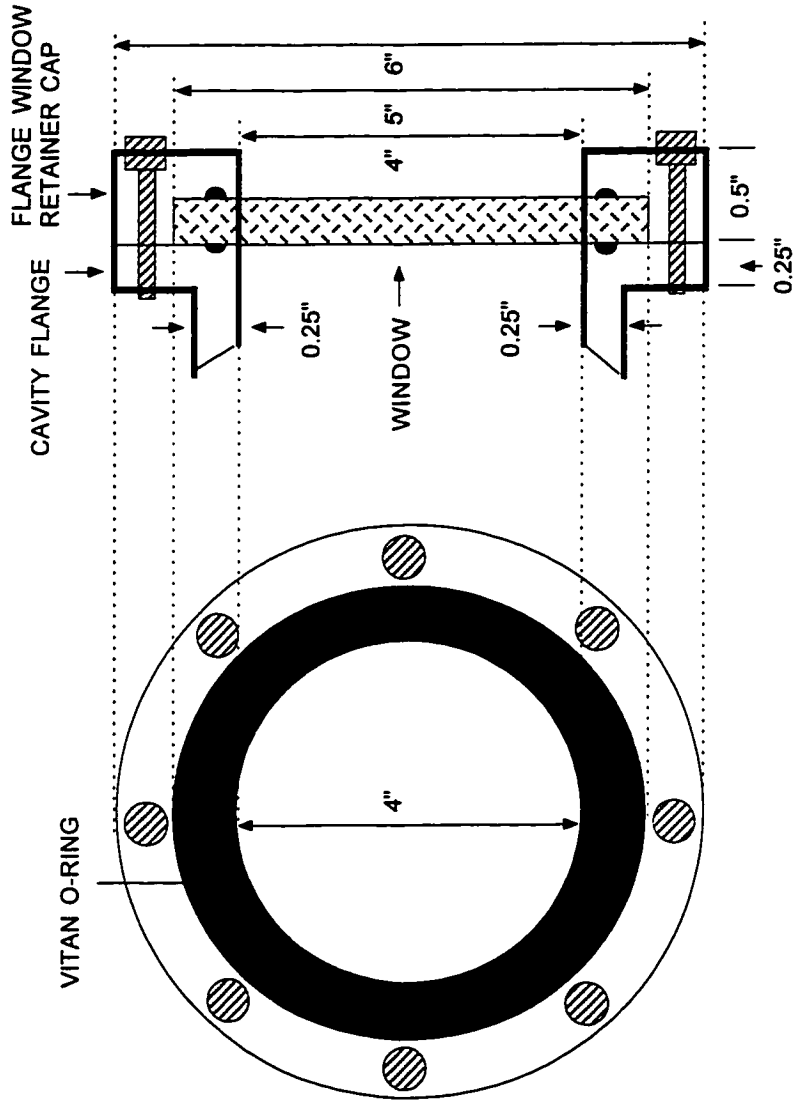


FIG.4.2(a) Cross-sectional view of the window flange of the resonant cavity

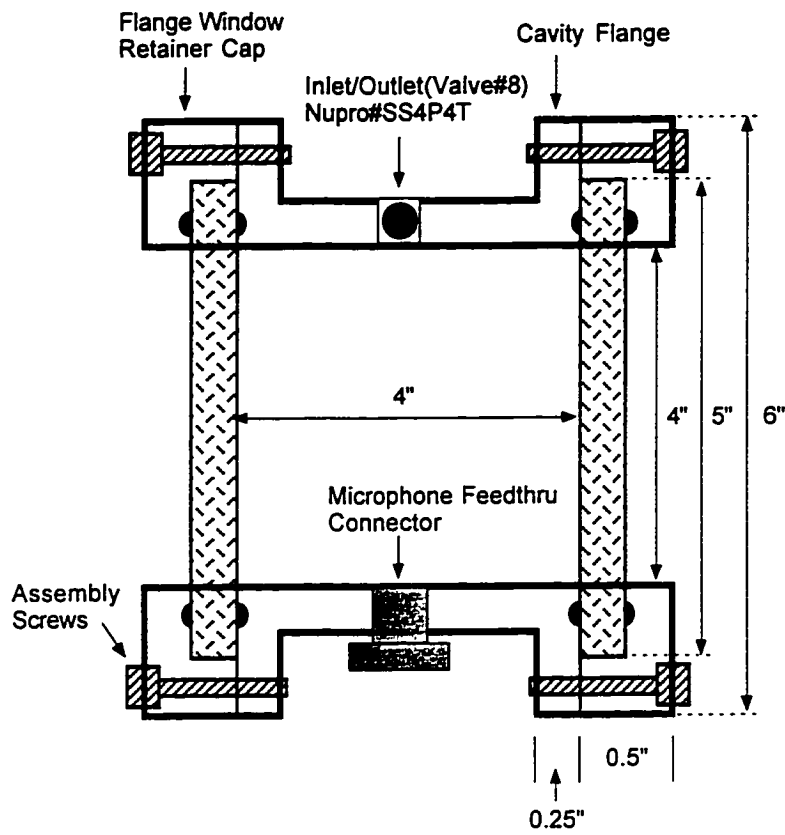


FIG.4.2 (b) Side view of the resonant cavity.

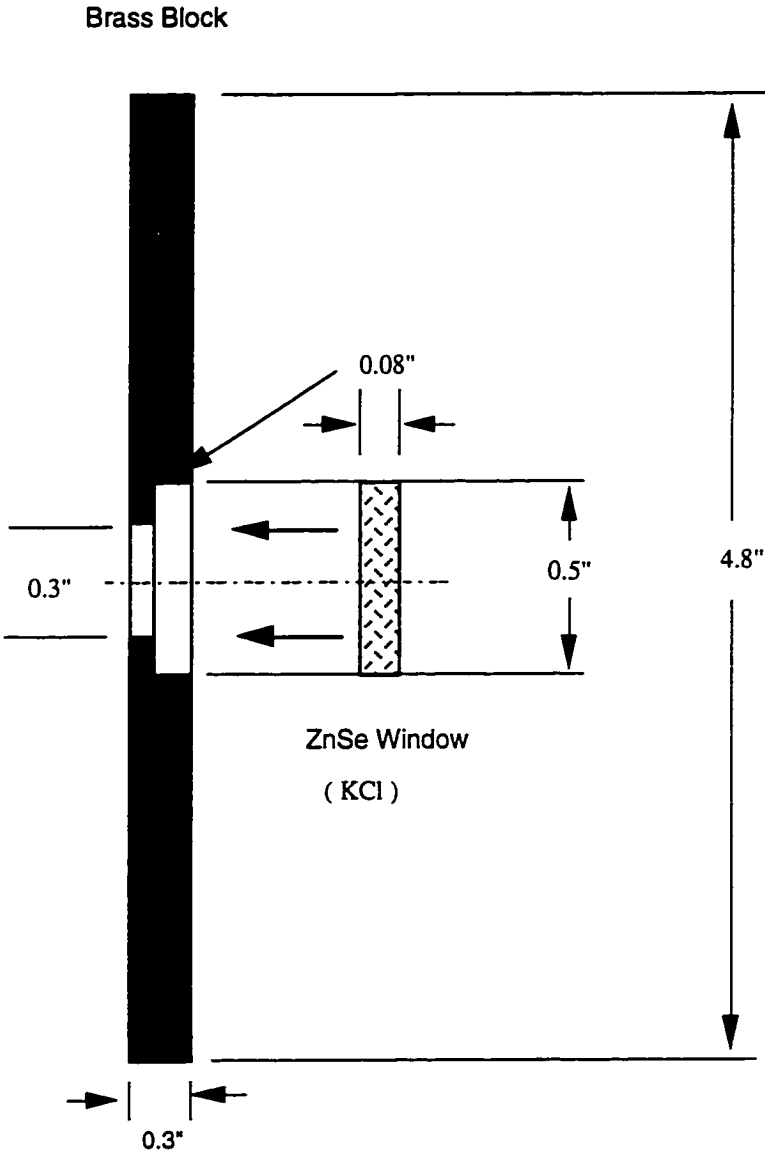


FIG.4.2(c) The side view of the cavity window

$$\omega_{mnl} = c \left[(\pi \alpha_{mn} / R)^2 + (\pi l / L)^2 \right]^{1/2} \quad (4.2)$$

The labels m , n and l refer to radial, azimuthal and longitudinal modes, respectively; R is the radius and L the length of the cavity, α_{mn} is the n th root of the derivative of the m th Bessel function. Figure 4.3 gives a pictorial view of these modes.

There are over 100 modes calculated by Eq.(4.2) for the cavity at a frequency range 0.6~10 kHz, and only about 40 modes are measurable (see Appendix C: The cavity modes data sheet), because the symmetry constraints imposed by laser excitation and microphone detection of the standing waves in the cavity has drastically reduced the number of the modes actually observed.

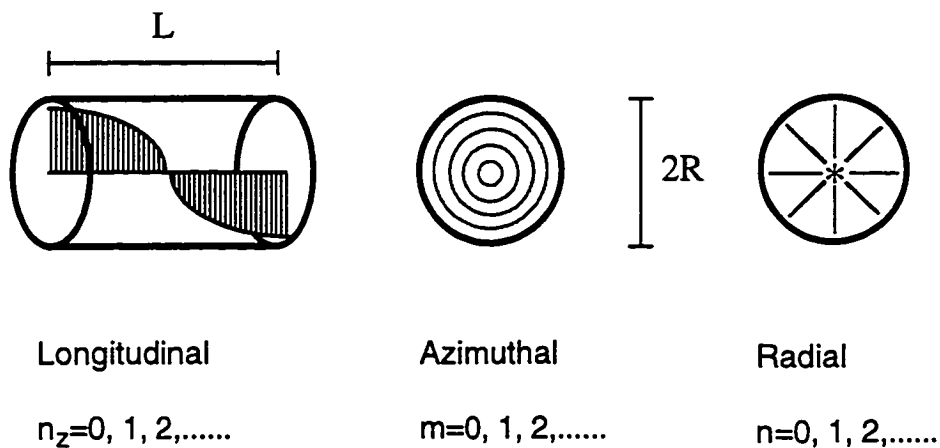


FIG. 4.3 Pictorial view of resonant acoustic longitudinal, azimuthal, and radial modes.

The mode amplitudes, where the losses are taken into account by the usage of a mode dependent quality factor Q_j , can be represented as follows ¹

$$A_j(\omega) = -\frac{i\omega \left[(\gamma-1) / V_c \right] \int p_j^* H dV}{\omega_j^2 \left[1 - \omega^2 / \omega_j^2 - i\omega / \omega_j Q_j \right]} \quad (4.3)$$

where V_c is the volume of the gas container and p_j is the normal mode solution. The root of complex conjugation of Eq.(4.3) is the pressure distribution in the cylinder, which is a symmetric Lorentzian profile, i.e.

$$A_j(f) = \frac{A_j}{\sqrt{(f_j^4/f^2) - 2f_j^2 + f^2 + \Delta f_j^2}} \quad (4.4)$$

where resonant frequency $f_j = \omega_j / 2\pi$, half-width of the resonant profile $\Delta f_j = f_j / Q_j$, and $A_j = \left[(\gamma-1) / V_c \right] \int p_j^* H dV$ is the amplitude.

b. The Microphone

A *Knowles* Electric model BT-1759 subminiature electret (condenser) microphone was used to detect the acoustic signals, see Figure 4.4.

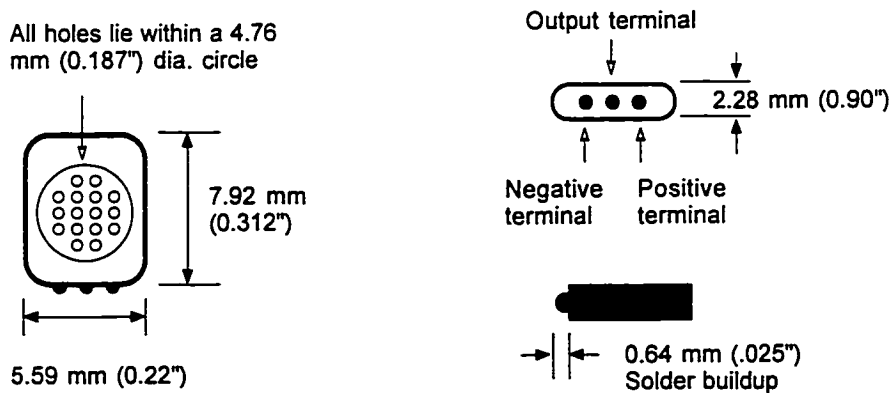
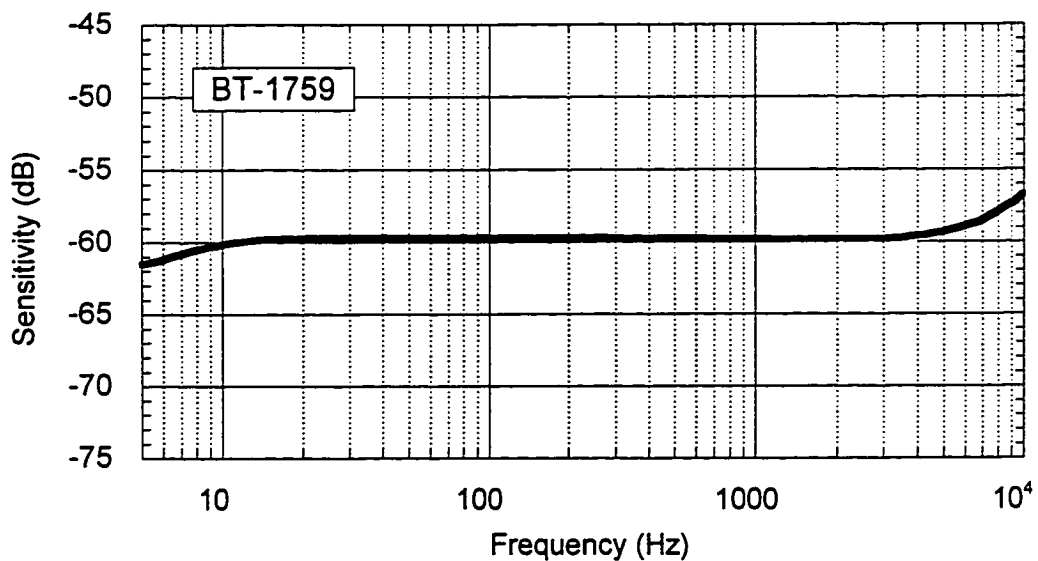


FIG.4.4 The dimensions of *Knowles* BT-1759 microphone

It has a built in FET preamplifier, which permits its use in applications requiring high sensitivity, small size (total nominal weight 2.3 gram), high resistance to mechanical shock and low current drain. The choice of a miniature microphone is particularly advantageous since it can be readily incorporated in the resonant cavity without significantly degrading the cavity factor Q . The microphone is mounted against the end of a brass plug which fits snugly into a port on the side of the cavity. The mount is sealed against the cavity wall by a O-ring. The microphone leads pass through the plug, and are insulated and sealed by means of *Devkon* Pk 20 epoxy cement. The leads are carefully soldered to the solder lugs on the end of the microphone to hold the microphone in place. The battery, power switch, and BNC output connector are contained in a shielded box attached directly to the microphone mount. Figure 4.5 gives the performance specification of *Knowles* model BT-1759 microphone.



1. Open circuit sensitivity in dB relative to 1.0 volt/microbar (0.1 N/m^2)
2. DC supply: 1.3 V

3. Amplifier current drain: 50 μ A max.
4. Output impedance: 2,000 to 6,000 Ω (3,500 Ω nominal)
5. Case connected to negative terminal
6. Sensitivity change on reducing supply to 0.9 Vdc: 3 dB max.
7. "A" weighted noise (1 kHz equivalent SPL): 30 dB max.
- 8.

Frequency	Sensitivity			Device Conformity	
	Min.	Nom.	Max.	Range of Deviation from 1 kHz	
100	---	-60.5	---	-4.0	+1.0
1000	-63.0	-60.0	-57.0	0.0	0.0
10000	---	-56.5	---	-1.0	+9.5

FIG.4.5 Performace specification of *Knowles* BT-1759 microphone.

c. The Gas Handling System

The gas handling system, Figure 4.x, was designed to introduce or evacuate the gas sample into or out the resonant cavity. Most of the components are demountable and made of glass. All the glasses to glass connections were made with a clamped O-ring joint (joint size I.D. 7 mm, O-ring EPR 112). A mechanical vacuum pump (Vac Torr 25 Precision Scientific) was employed and connected with system by a high vacuum rubber tubing. The pump can go down to the pressure of 20 millitorr.

The manifold of the gas handling system has 6 take-offs equipped with high vacuum Teflon valves (Kontes K-826500). The valve #1 positioned between the manifold and vacuum pump served as the out-gate of the system; the valve #2

was connected to the gas cylindrical tank as the in-gate of gas flow. The valve #3 connected to a large flask with large volume served as a reservoir, and to protect the microphone from any sudden change of pressure. The valve #4 and #5 were connected to a mm Hg pressure gauge and a thermocouple fine vacuum gauge (Varian 531) which measures millitorr range pressure. The valve #6 was connected to a long glass tubing, which in turn was connected to a Fusion Connector, the outer diameter of which has been reduced from $\frac{3}{8}$ " to $\frac{1}{4}$ " in order to make a glass-metal connection possible. This was done by using a brass union tube fitting (Swagelok B 44-6) with Teflon ferrules on the glass side and brass ferrules on the metal side, and the metallic part is a flexible stainless steel tubing (Cajon 321-4-X-U). The other end of flexible tubing was connected to the in-out plug valve of the cavity through a union tube fitting.

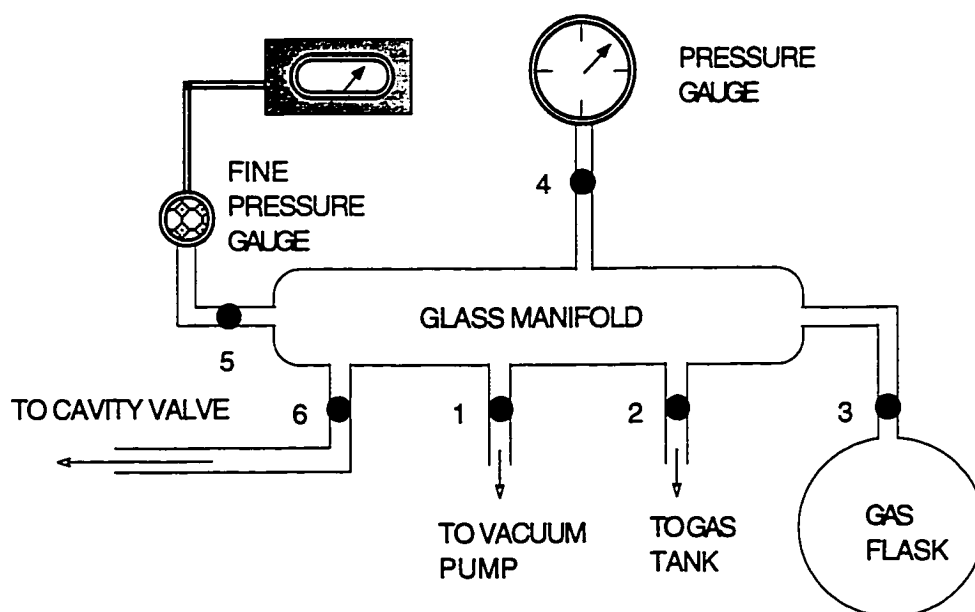


FIG.4.6 The manifold of gas handling system.

4.1.2 The Instruments

a. Chopper

An essential part of a photoacoustic device is the chopper and the electronics controlling the chopper frequency. In the present experiments the chopper (*Scitec 300CD*) works in its external mode, in which the frequency control is used to set the proportionality between input dc voltage and chopping frequency; this DC voltage is applied by a function generator (*HP 3325A*) controlled by a personal computer via GPIB interface. The actual chopper frequency is measured with a light gate at the chopper blade using a photodiode and a LED display gives a directly read-out of the chopping frequency. A square wave reference signal, which is a standard 5V TTL pulse, at the chopping frequency and having constant phase relative to the chopping action fed into the Lock-in analyzer (*EG&G 5210*).

Even though the frequency stability of the chopper is better than $\pm 0.2\%$ of reading within 10 to 100% of maximum frequency, the mechanical chopper limits the accuracy in the high pressure region, where sharp resonance with very high quality factor Q are observed. These problems can be avoided with a more expensive electro-optic modulation device, such as a Pockel-Cell, in which the modulation system can be regulated directly by the synthesizer with high precision. To investigate a potential cross talk between chopper and resonator, we performed measurements in the whole pressure range without laser radiation; we found that the acoustic signals caused by the chopper noise and other external noise sources were below the detection limit of the apparatus.

b. Lock-in amplifier

An EG&G model 5210 lock-in analyzer was employed for the phase sensitive rectification and amplification of the microphone signal. The signal from the microphone is made to appear at a reference frequency, then amplified and applied to a phase sensitive detector operated at the reference frequency. Because of the frequency selection effects of the phase sensitive detector, the result is a detector output that includes a value representing the amplitude of the signal of interest as well as the ac components that may be due to noise and interference. Direct measurement of dc signals with an electrometer are often plagued by drift. By modulating the experimental input at a frequency that is also fed to the lock-in amplifier as a reference input, dc drift is eliminated and very high rejection of interfering frequencies is achieved. This rejection can be improved to any arbitrary degree by increasing the time constant of the measurement.

c. Computer Interface

The present experimental setup employed a NB-GPIB-P/TNT interface board (*National Instruments*) to perform the basic IEEE 488 Talker, Listener, and controller functions required by the most recent GPIB standard, IEEE 488.2, between a Apple Macintosh NuBus computer (*Power Macintosh 6100/66*), and the lock-in amplifier and function generator. On this board, the FIFO (First-Out-Memory Buffer) buffers to decouple GPIB transfers from NuBus transfers, and 16-bit NuBus interface with byte-to-word packing and unpacking. The NB-GPIB-P/TNT can sustain data transfer rates of 1.3 Mbytes/s, and also implements a high-speed GPIB protocol (HS488), so that one basically can have data transfers

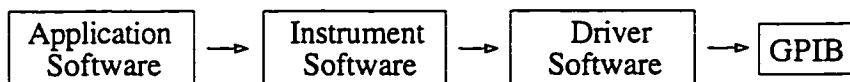
up to 1.6 Mbytes/s, though the actual rates depend upon system configuration and instrument capabilities. Each board can be hook up to 14 instruments with standard IEEE 488 cables and 24-pin I/O connector.

4.2 Software Virtualization

The software paves the way for new types of instruments-Virtual Instruments (VI), in which the user, not the vendor, defines the ultimate functionality of the instruments, and their appearance and operation imitate actual instruments. A full definition of Virtual Instruments (VI) is "A layer of software and/or hardware added to a general-purpose computer in such a fashion that users can interact with the computer as though it were their own custom-designed traditional electronic instrument".

4.2.1 The Operation System

The proliferation of operating system of the spectrophone is as the following,



We employed an application program called LabVIEW (*National Instruments*) which takes care of all aspects of an instrumentation system, including data acquisition, instrument control and data analysis; below it are the instrument drivers that contain high-level functions for interactively controlling specific instruments and verifying the communication; the driver software NI 488.2 transforms the Macintosh commands from the instrument driver to a GPIB

controller with complete communications and bus management capability, it comes also with an interactive GPIB control utility and the Microsoft QuickBASIC, Macintosh Programmer's Workshop (MPW) C and THINK C, and HyperTalk language interface.

4.2.2 The VI Programming

We constructed our program of the resonant spectrophone VI in the way as the block diagram in the Figure 4.7 shows.

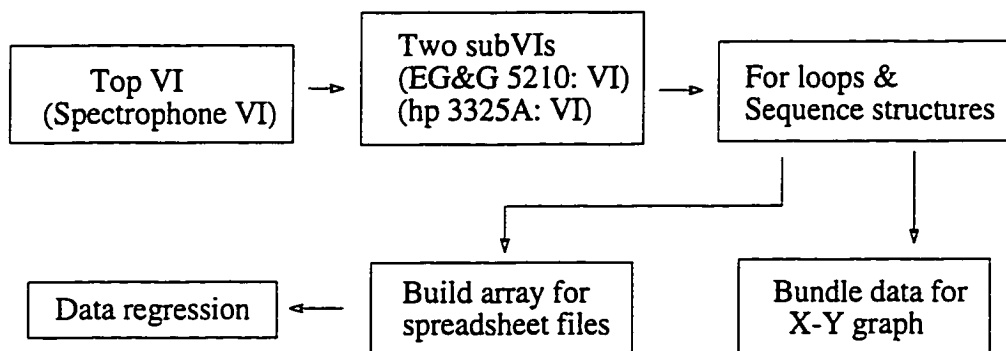


FIG. 4.7 The program block diagram of the resonant spectrophone VI .

The top VI of the spectrophone followed by the two subVIs of instrument driver, EG&G 5210.VI and HP 3325.VI (see Appendix D: Instrument driver programs). The structure of the program based on the for loops, the iteration number of the for loop corresponds to the data points aqisited; inside the loop, there are four sequences executes one after another sequentially, which carry out the tasks of configuration of the instruments, time waiting, GPIB write and GPIB read. The Bundle function assembles the data collected in all iterations into a single cluster for a X-Y graph, and the Build Array function concatenates to top-

bottom order, two dimension array for spreadsheet file. Finally is the data regression. Figure 4.8 is a part of the laser resonant spectrophone VI.

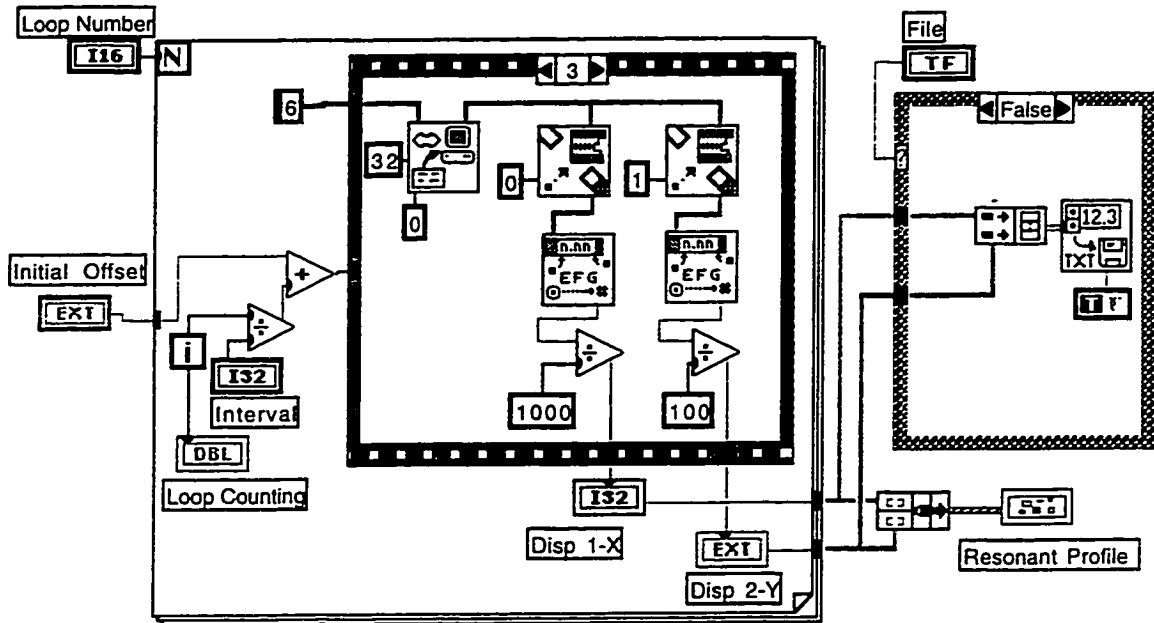


FIG. 4.8 The block diagram of the laser resonant spectrophone VI at the 3th sequence.

The Labview programming is a pictorial solution to a programming problem. The block diagram is also the source code for the VI. One constructs a program in *graphical* language by wiring the icons together according to its rules. The following are some of VIs, functions and structures used in the photoacoustic spectrophone VI.

1. GPIB Read vi



The GPIB Read VI reads a specified number of bytes from the GPIB

device at the specified address string. The data is returned in a string. One has to convert the data string to a numeric data type before it can be process, e.g. to graph it.

2. *Pick line & Append*



The Pick line & Append function chooses a line from a multi-line string and appends that line to a string.

3. *From Exponential/Fract/Eng*



The From Exponential/Fract/Eng function converts a string containing valid numeric characters (0 to 9, +, -, e, E and period) to a number. The function starts scanning the string at offset. The first character offset is zero.

4. *Bundle*



The Bundle cluster function assembles all the individual input components into a single cluster or changes the values of wired components. The input parameters of this function are polymorphic - they can be of any data type.

5. *Build Array*



The Build Array function appends any number of array or element inputs in top-to-bottom order to *create array with appended element*.

6. Write to Spreadsheet File VI



The Write to Spreadsheet File VI converts the two-dimensional array to a spreadsheet string and writes it to a file. If no path name is specified, then a file dialog box will pop up and prompt for a file name. The Write to Spreadsheet File will write either a one- or two-dimensional array to file.

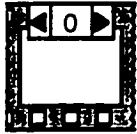
7. For Loop Structures



One use the For Loop to control repetitive operations, until a specified number of iterations have completed. A For Loop executes its subdiagram count times, where the count equals the value contained in the count terminal. One can set the count explicitly by wiring a value from outside the loop to the left or top side of the count terminal, or one can set the count implicitly with auto-indexing. The outer edges of the count terminal are exposed to the inside of the loop so that one can access the count internally. The iteration terminal contains the current number of completed iterations; 0 during the first iteration, 1 during the second, and so on up to N-1. Both the count and iteration terminals are signed long integers with a range of 0 through $2^{31}-1$. If one wire a floating-point number to the count terminal, LabVIEW rounds it, if necessary, and coerces it to within range. If one wire 0 to the count terminal, the loop does not execute. The For Loop is equivalent to the following pseudo-code: for $i = 0$ to N-1. The for loop can have terminals

called shift registers that one use for passing data from the current iteration to the next iteration.

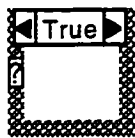
8. *Sequence structures*



The Sequence structure, which looks like a frame of film, consists of one or more subdiagrams, or frames, that execute sequentially. Determining the execution order of a program by arranging its elements in sequence is called control flow. BASIC, C, and most other programming languages have inherent control flow, because statements execute in the order in which they appear in the program. The Sequence structure is the LabVIEW way of obtaining control flow within a dataflow framework. A Sequence structure executes frame 0, followed by frame 1, then frame 2, until the last frame executes. Only when the last frame completes does data leave the structure. Within each frame, as in the rest of the block diagram, data dependency determines the execution order of nodes. One use the Sequence structure to control the order of execution of nodes that are not data-dependent. A node that gets its data directly or indirectly from another node has a data dependency on the other node and always executes after the other node completes. One do not need to use the Sequence structure when data dependency exists or when the execution order is unimportant. If one part of a block diagram must execute before another part can begin, but data dependency does not exist between them, the Sequence structure can establish the correct execution order. This situation occurs often with GPIB applications. One may need to write a command to an instrument before

taking a reading; however, the Receive VI does not use data from the Send VI and thus has no data dependency on it. Without the Sequence structure, the Receive VI may execute first, causing errors. By placing the Send VI in frame 0 of a Sequence structure and the Receive VI in frame 1, as shown in the following illustration, one can enforce the proper execution order. Output tunnels of Sequence structures can have only one data source, unlike Case structures. The output can emit from any frame, but keep in mind that data leaves the structure only when it completes execution entirely, not when the individual frames finish. Data at input tunnels is available to all frames, as with Case structures. To pass data from one frame to any subsequent frame, use a terminal called a sequence local. To obtain a sequence local, choose Add Sequence Local from the structure border pop-up menu. This option is not available if one pop up too close to another sequence local or over the subdiagram display window. One can drag the terminal to any unoccupied location on the border. Use the Remove command from the sequence local pop-up menu to remove a terminal. An outward-pointing arrow appears in the sequence local terminal of the frame containing the data source. The terminal in subsequent frames contains an inward-pointing arrow, indicating that the terminal is a source for that frame. In frames before the source frame, one cannot use the sequence local, and it appears as a dimmed rectangle.

9. Case Structure



The Case structure has two or more subdiagrams, or cases, exactly one of which executes when the structure executes. This depends on the

value of the Boolean or numeric scalar one wire to the external side of the selection terminal or selector. If a Boolean is wired to the selector, the structure has two cases, False and True. If a numeric is wired to the selector, the structure can have from 0 to 215-1 cases. Initially, only the 0 and 1 cases are available.

4.2.3 The Front Panel of the VI

Figure 4.9 is the front panel of the resonant spectrophone VI, the interactive user interface.

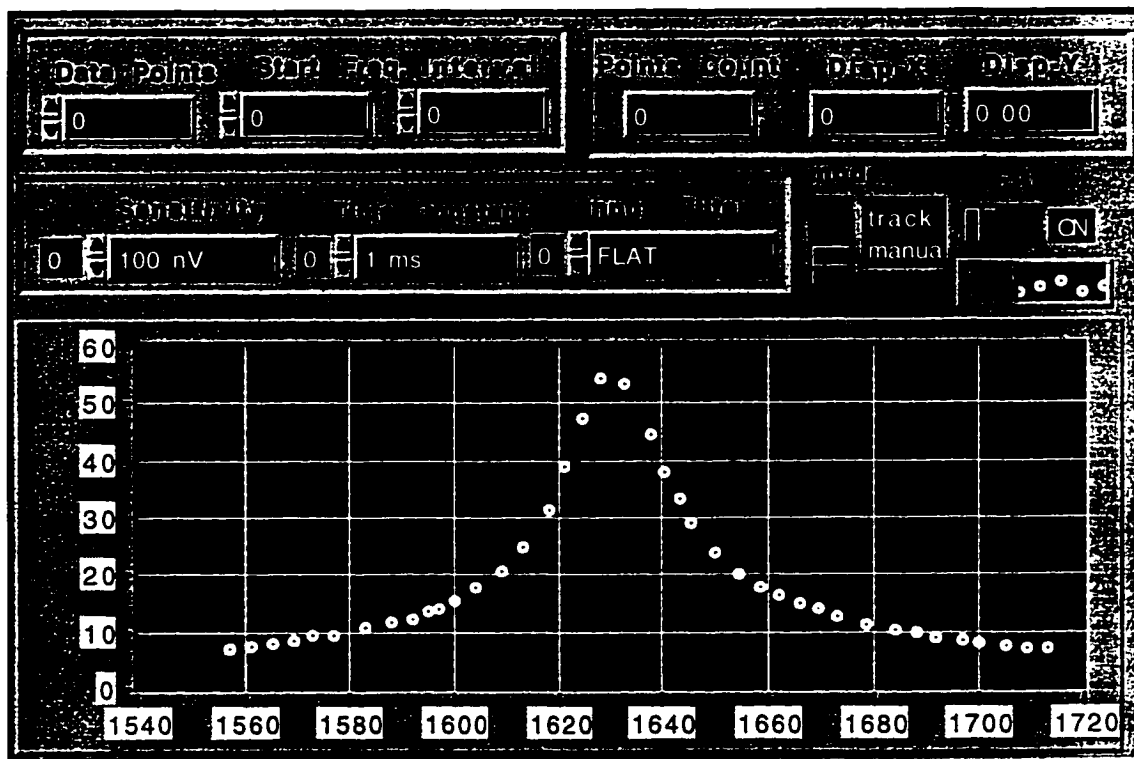


FIG. 4.9 The front panel of the resonant spectrophone VI.

It consisted of three groups of the digital controller and indicator, two slide switches and a X-Y graph display. The up-left group digital controller is used to set up the starting frequency, the number and interval of data points of the sweeping parameters of the VI. The up-right group are three digital indicators to display the n th of the data point and its values of frequency (X) and acoustic pressure amplitude in real time. The next lower group are three digital controllers to be use to configure the sensitivity, time constant and tracking filter mode of the resonant spectrophone VI. The horizontal slide switch is used to switch on or off to let the VI automatically create a spreadsheet file readable by most spreadsheet programs, and the vertical slide switch is used to select the filter to track or manual mode. Finally, after collecting all points required in the Data Points controller, the X-Y graph display automatically plots all measured data points.

4.3 Experimental Results

Two typical resonance curves shown in the Figure 4.10 and 4.11, which obtained by the excitation of the ν_3 (940 cm^{-1}) mode of SF_6 molecule with the line P₂₀ of a tunable CO_2 waveguide laser. The black dots are the experimental data and the solid resonance curves are the non-linear fitted curves in which the symmetric Lorentzian profile Eq.(4.4) was applied to fit the data using the Levenberg-Marquardt algorithm. The fitting parameters were the resonant frequency $f_j (= \omega_j / 2\pi)$, the half-width $\Delta f_j (= Q_j^{-1} f_j)$, and the amplitude A_j where the Q_j is the quality factor of the cylindrical cavity.

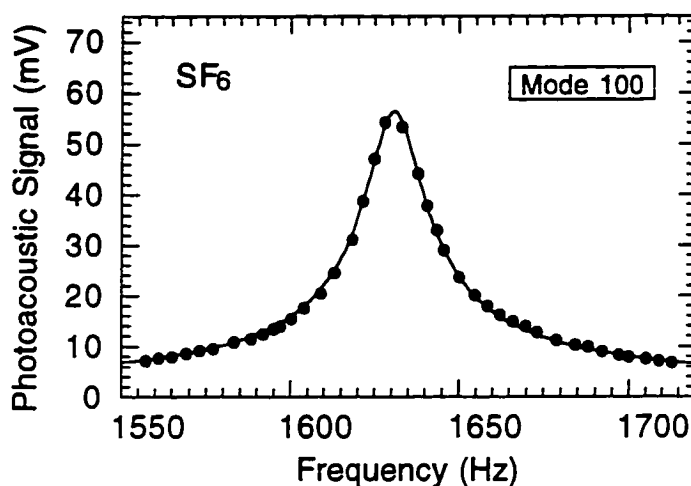


FIG. 4.10 The resonant profile of the first radial mode (100) of SF₆ at pressure 40 Torr and temperature T=295 K.

Figure 4.9 is the resonant profile of the first radial mode (100) of SF₆ at pressure 40 Torr and temperature 295 K. The percent error at the final iteration of the fitting was 0.044 and the curve fit results and the standard error values of the parameters are a resonant frequency of $f_j = 1630.8 \pm 0.08$, a half-width of $\Delta f_j = 17.3 \pm 0.3$, and amplitude of $A_j = 954.9 \pm 14.9$ with the Pearson's correlation coefficient (without weights) $R = 0.99866$. Figure 4.10 is The resonant profile of the second longitudinal mode (002) of SF₆ at pressure 600 Torr and temperature 289 K. The percent error at the final iteration of the fitting was 0.058 and the curve fit results and the standard error values of the parameters are a resonant frequency of $f_j = 1329.9 \pm 0.024$, a half-width of $\Delta f_j = 5.16 \pm 0.07$, and a amplitude of $A_j = 581.4 \pm 6.1$ with the Pearson's correlation coefficient (without weights) $R = 0.99915$.

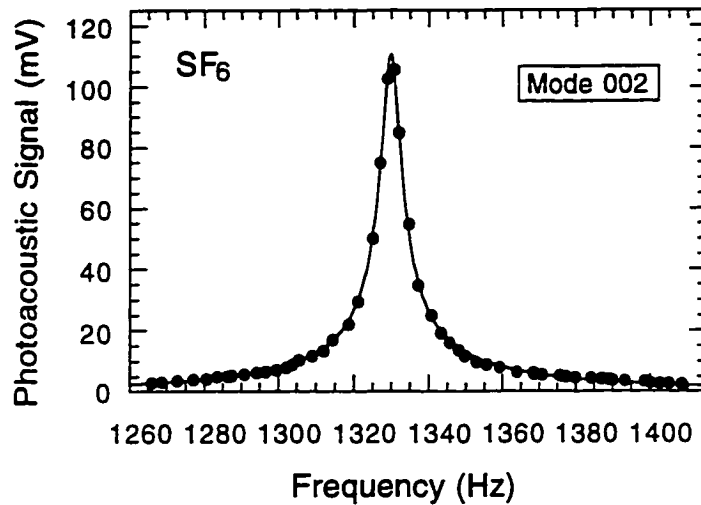


FIG. 4.11 The resonant profile of the second longitudinal mode (002) of SF₆ at pressure 600 Torr and T=289 K.

The equation used to calculate the Pearson's correlation coefficient (without weights) is

$$R = \frac{\sum_i^N (x_i - \bar{x})(y_i - \bar{y})}{\sqrt{\sum_i^N (x_i - \bar{x})^2} \sqrt{\sum_i^N (y_i - \bar{y})^2}} \quad (4.5)$$

where the y_i and \bar{y} are the actual value and the mean of actual value, the x_i and \bar{x} are the calculated value and the mean of calculated value.

The resonant profiles are shown to be well described by a Lorentzian shape. This implies the resonant spectrophone can perform a very accurate measurements of resonant profile at low (40 Torr) or high (600 Torr) pressure. The statistical error here may be due to the power instability of the CO₂ waveguide laser. The resonant method, which comprises the optical and acoustic

methods by measuring the resonance frequency instead of measuring the sound velocity, i.e. the line position and line width are determined by frequency measurements, which has substantially improved the accuracy of measurements.

As we have mentioned before, the resonant spectrophone can be used for a number of applications such as tracing and monitoring atmosphere pollutants, gas absorption coefficients α , in which the absorption intensity of the detecting species, i.e. the acoustic mode amplitude A_j is most concerned; for the study of the rate constant and activation of chemical reaction, and molecular energy transfers in gases, in which the resonant frequency f_j and half-width Δf_j are studied as a function of pressure in the dispersion region. With the present virtualized resonant spectrophone, a completely application-oriented system, one do not need any change in hardware setup, all are just matter of modified the spectrophone VI in software. Which greatly not only enhance the system performance on flexibility, reusability and reconfigurability, but also reduce the development and maintenance costs.

References to Chapter 4

- 4.1. L.B.Kreuzer, J. Appl. Phys., 42, 2934(1971).
- 4.2. C.F.Dewey Jr., R.D.Kamm & C.E.Hackett,
Appl.Phys.Lett., 23, No.11, 633(1973).
- 4.3. P.D.Goldan & K.Goto, J. Appl. Phys., 45(10), 4350(1974).
- 4.4. P.L.Meyer & M.W.Sigrist, Rev.Sci. Instrum., 61(7), 1779(1990).
- 4.5. A.Karbach et al, J. Chem Phys., 83(3), 1075(1985).
- 4.6. R.H.Johnson et al, Applied Optics, 21(1), 81(1982).
- 4.7. M.Fiedler & P.Hess, J. Chem. Phys., 93(12), 8693(1990).
- 4.8. P.M.Morse and K.U.Ingard, "Theoretical Acoustics"
(McGraw-Hill, New York, 1968).
- 4.9. Yoh-Han Pao, "Optoacoustic Spectroscopy and Detection"
(Academic Press, 1977).

Chapter 5

Relaxation and Losses of SF₆

- Measurement of Rotational and Vibrational Relaxation in Gases by Photoacoustic Resonance: Application to SF₆

A thorough study of molecular relaxation on the cavity mode (034) has been presented in this Chapter. The profile of the acoustic resonance, excited by the vibrational mode ν_3 of gas sample SF₆ with a CO₂ laser, was measured as a function of pressure between 1~800 Torr. The analysis of the experimental data yields a value of vibrational relaxation time $(p\tau)_{v-T} = 0.21 \pm 0.01 \mu\text{s atm}$, and a value of $(p\tau)_{R-T} = 0.09 \pm 0.06 \text{ ns atm}$ for the rotational relaxation time of SF₆ at T=295 K.

5.1 Sulfur Hexafluoride Molecules

Electron diffraction measurements first strongly suggested that in sulfur hexafluoride the sulfur atom occupies the center of a regular octahedron whose corners are occupied by the fluorine atoms. This highly symmetrical structure has been fully confirmed by Raman and infrared investigations.¹ It belongs to the O_h point group, that has in addition to the symmetry elements of O a center of symmetry i , as well as several other symmetry elements necessitated by it. Therefore, for each symmetry type of O there are two in O_h , one that is symmetric and one that is antisymmetric with respect to i . As an example, in FIG.5.1 the normal vibrations of an octahedral XY_6 molecule (SF_6) are illustrated.

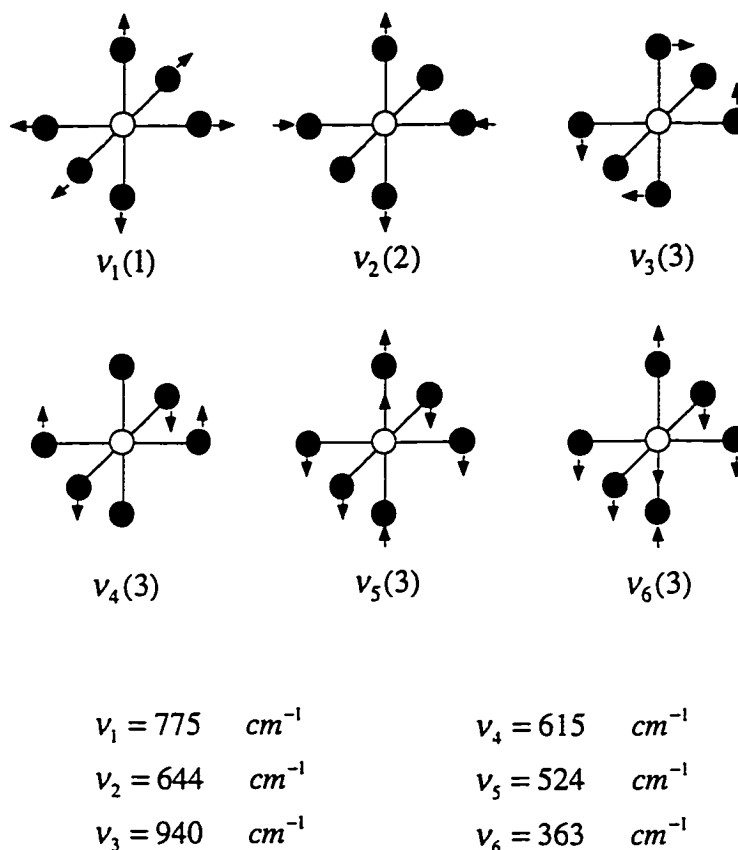


FIG. 5.1 The normal vibrations of an octahedral XY_6 molecule (SF_6) with corresponding degeneracy factors (g), and wave numbers (cm^{-1}).

The choice of SF₆ as a model system is attributable primarily to its intense infrared absorption at the 940 cm^{-1} laser frequency and the ease of handling this material. These factors have doubtless led to over a dozen different 3ser radiation on SF₆, which are:²

- (1) Self Q switching of a CO₂ laser by incorporating a cell containing SF₆ into laser cavity;
- (2) passive mode locking of a CO₂ laser, by the same technique;
- (3) self-induced transparency of SF₆ to CO₂ laser pulses;

- (4) infrared photon echo in SF₆;
- (5) transmission of CO₂ laser pulses through SF₆;
- (6) saturation of infrared absorption in SF₆ by a cw CO₂ laser beam;
- (7) fluorescence of excited by a CO₂ laser pulse;
- (8) adiabatic inversion of vibrational level populations;
- (9) transient notation impressed onto CO₂ laser pulses by SF₆, although the origin of this effect has been questioned;
- (10) use of SF₆ in a CO₂ laser cavity to tune the output wavelength;
- (11) cross saturation of laser signals by SF₆;
- (12) cavity dumping by saturable resonators.

A thorough study of the relaxation behavior of SF₆ is thus required, if for no other reason than to provide an interpretation to all these (sometime conflicting) experimental studies.

5.2. Photoacoustic Resonance in a Cylindrical Cavity

The initial interest in laser photoacoustic resonance was primarily due to the high sensitivities attainable in the detection of trace amounts of gaseous molecules by monitoring their vibrational spectra in the infrared region.³⁻⁵ This has, however, led to an increasing number of applications, such as molecular relaxation processes⁶⁻⁸, photon-induced chemical reactions⁹ and gas absorption line profiles,¹⁰ mainly due to its high sensitivity and the capability of dealing with the non-radiative processes. The measurements of the rate constants of energy transfer between different degrees of freedom are carried out by analyzing the characteristics of a acoustically resonant curve (a Lorentzian profile), such as the

resonant frequency and the half-width as a function of pressure. The advantage of this method is that it utilized both the optical and acoustic methods by measuring the resonance frequency instead of measuring the sound velocity in the dispersion region. The accuracy of measurements, therefore, could be substantially improved. The disadvantage is that the photoacoustic signal in a resonator depends also on the various losses present in the cavity and the deviation of the gas from the ideal condition. One has to, therefore, take into account all of these factors in order to extract the information related to the relaxation processes from the data. Since a large set of experimental data has to be collected, an automatic data acquisition system seems to be necessary.

For a cylindrical cavity with rigid walls, the resonant frequencies are given by ¹¹

$$\omega_{mnl} = c \left[(\pi \alpha_{mn} / R)^2 + (\pi l / L)^2 \right]^{1/2} \quad (5.1)$$

where the labels m , n and l refer to radial, azimuthal and longitudinal modes, respectively. R is the radius and L the length of the cavity, α_{mn} is the n th zero of the derivative of the m th Bessel function divided by π . One may retain the assumption of complete wall rigidity (i.e., that there is no phase shift of the acoustic wave on reflection from the cavity walls either due to wall compliance or boundary layer effects). It is, however, certainly not a delta function singularity at each discrete resonant frequency of Eq.(5.1). In actual fact, it is comprised of a narrow band of frequencies, described by a *Lorentzian* profile,¹²

$$A_j(\omega) = -\frac{i\omega}{\omega_j^2} \frac{A_j^0}{\left[1 - \omega^2/\omega_j^2 - i\omega/\omega_j Q_j\right]}, \quad (5.2)$$

around the resonant frequency ω_j (j refers a mode n,m,l) over which appreciable excitation can occur. The important sources of this smearing out of the sharp frequency of oscillation are the dissipation of energy by a number of loss mechanisms, such as cavity losses, molecular relaxation effects, and non-ideal behavior of the gas. These losses can be taken into account by the use of a mode dependent quality factor Q_j . The sharpness and position of the resonance profiles will contain the information of the various losses and the molecular relaxation. Losses due to thermal conduction and viscosity can be separated into surface and volume losses.

a) surface losses, due to wave interactions with cavity walls, account for a large part of energy dissipation. Viscous and thermal dissipation in the boundary layer is the dominant surface loss mechanism, whose quality factor Q_{sur}^{-1} for a mode (034) of a cylinder cavity is given by⁸

$$Q_{sur}^{-1} = \frac{1}{R} \left[d_v + (\gamma - 1) d_h \left(1 + \frac{2L}{R} \right) \right] \quad (5.3)$$

where $d_v = \sqrt{2\eta RT/M\omega p}$ and $d_h = \sqrt{2\kappa RT/\omega p C_p}$ are the viscous and thermal boundary layer thicknesses, η is the shear viscosity, κ is the thermal conductivity, M is the mass per mole, and R is the gas constant. The corresponding frequency shift $\delta\omega$ and half-width broadening $\Delta\omega$ are given by:

$$\delta\omega^{sur} = -\frac{1}{2} Q_{sur}^{-1} \omega_j = -\frac{1}{2} \alpha_{sur} \omega_j p^{-1/2} \quad (5.4)$$

$$\Delta\omega^{sur} = Q_{sur}^{-1} \omega_j = \alpha_{sur} \omega_j p^{-1/2} . \quad (5.5)$$

b) volume losses make a small contribution to the broadening of the half-width at low pressure. The friction due to compression motion and

transformation of organized energy into heat caused by temperature gradients are responsible for this free space viscous and thermal losses (Stokes-Kirchoff). The quality factor Q_{vol}^{-1} is given by¹¹

$$Q_{vol}^{-1} = \left(\frac{\omega}{\gamma p} \right) \left[\frac{4}{3} \eta + (\gamma - 1) \frac{\kappa M}{C_p} \right], \quad (5.6)$$

and the contribution to the broadening of half-width is then given by:

$$\Delta\omega^{vol} = \omega_j Q_{vol}^{-1} = \alpha_{vol} \omega_j p^{-1} \quad (5.7)$$

c) *Virial shift*, gases exhibit non-ideal behavior at high pressures where intermolecular forces give rise to a change in the compressibility and, consequently, in the sound velocity. The shift of the resonant frequency due to this non-ideal behavior is given by¹³

$$\delta\omega^{vir} = \frac{p\omega_j}{RT} \left[B + \frac{RT}{C_v} \frac{dB}{dT} + \frac{(RT)^2}{2C_v C_p} \frac{d^2B}{dT^2} \right] = \alpha_{vir} \omega_j p, \quad (5.8)$$

where R is the gas constant and B the second Virial coefficient.

d) *Molecular relaxation effects* arise because of the finite time required for the internal degrees of freedom of the molecules to come into thermal equilibrium with the translational degrees of freedom, as described by:

$$\frac{dE_n}{dt} = - \frac{(E_n - E_n^e)}{\tau_n} \quad (5.9)$$

where E_n is the ensemble average energy in the n th mode of the molecule, E_n^e is its equilibrium value, and τ_n is the relaxation time for that mode. If E_n varies as a

harmonic function of time, $E_n = E_0 e^{i\omega t}$, the solution of above differential equation leads us to the dynamic heat capacity $C_n(\omega)$ for the n th mode,

$$C_n(\omega) = \frac{dE_n(\omega)}{dT} = \frac{C_n}{1 + i\omega\tau_n}. \quad (5.10)$$

thus, the dynamic heat capacity ratio is,

$$\begin{aligned} \gamma(\omega) &= \frac{C_p(\omega)}{C_v(\omega)} = \frac{C_p - \frac{1}{2} \sum_n [i\omega\tau_n C_n / (1 + i\omega\tau_n)]}{C_v - \frac{1}{2} \sum_n [i\omega\tau_n C_n / (1 + i\omega\tau_n)]} \\ &= \frac{\gamma - \frac{(\gamma-1)}{2R} \sum_n [i\omega\tau_n C_n / (1 + i\omega\tau_n)]}{1 - \frac{(\gamma-1)}{2R} \sum_n [i\omega\tau_n C_n / (1 + i\omega\tau_n)]} \end{aligned} \quad (5.11)$$

where C_p and C_v are the molar static heat capacities. Since the C_n 's for the vibrational modes are small at room temperatures, we can expand the fraction of Eq. (5.11) for these terms, but we cannot neglect the higher orders of $\omega\tau_n$. The root square of Eq. (5.11) can be approximated to the first power in $[\frac{(\gamma-1)}{2R} \sum_n i\omega\tau_n C_n / (1 + i\omega\tau_n)]$. We have, then,

$$[\gamma(\omega)]^{1/2} \cong \frac{1}{\gamma^{1/2}} \left[\gamma + \frac{(\gamma-1)^2}{4R} \sum_n \frac{i\omega\tau_n C_n}{1 + i\omega\tau_n} \right]. \quad (5.12)$$

Neglecting non-ideal gas effects, which will be treated separately, the sound velocity is given by $c = \sqrt{\gamma(\omega)p/\rho}$. If we denote by ω_j the frequency that we would obtain for the mode by using the static heat capacity ratio γ in place of $\gamma(\omega)$. we have

$$\omega_j^{rel} = \omega_j [\gamma(\omega)]^{1/2} / \gamma^{1/2}. \quad (5.13)$$

Inserting Eq. (5.12) into Eq. (5.13), we obtain,

$$\begin{aligned}
 \omega_j^{rel} &\equiv \omega_j \left[1 + \frac{(\gamma-1)^2}{4\gamma R} \sum_n \frac{i\omega\tau_n C_n}{1+i\omega\tau_n} \right] \\
 &= \omega_j \left\{ 1 + \frac{(\gamma_0-1)^2}{4\gamma_0 R} \sum_{vib} \frac{i\omega\tau_n C_n}{1+i\omega\tau_n} + \frac{(\gamma_\infty-1)^2}{4\gamma_\infty R} \sum_{rot} \frac{i\omega\tau_n C_n}{1+i\omega\tau_n} \right\} \\
 &\equiv \omega_j \left\{ 1 + \frac{\alpha_0}{2R} \sum_{vib} \frac{\omega^2 \tau_n^2 C_n}{1+\omega^2 \tau_n^2} + i \frac{\alpha_0}{2R} \sum_{vib} \frac{\omega\tau_n C_n}{1+\omega^2 \tau_n^2} + i \frac{\alpha_\infty}{2R} \sum_{rot} \omega\tau_n C_n \right\} \quad (5.14)
 \end{aligned}$$

where the sum has been split into a rotational and a vibrational term, with $\alpha_0 = (\gamma_0 - 1)^2 / 2\gamma_0$ and $\alpha_\infty = (\gamma_\infty - 1)^2 / 2\gamma_\infty$. γ_0 is the static heat capacity ratio and γ_∞ is the heat capacity ratio in the absence of vibrational degrees of freedom. There is no dispersion to first order in $\omega\tau_{rot}$, but the imaginary part of rotational relaxation losses remains. The real part of Eq. (5.14) is the frequency dispersion, which only has the vibrational terms,

$$\omega_j^{rel} = \text{Re } \omega_j^{rel} = \omega_j \left[1 + \frac{\alpha_0}{2R} \sum_{vib} \frac{\omega^2 \tau_n^2 C_n}{1+\omega^2 \tau_n^2} \right]; \quad (5.15)$$

the imaginary part is the relaxation dissipation of vibration and rotation. It will determine the half-width of the resonance profile given by

$$\Delta\omega_j^{rel} = 2 \text{Im } \omega_j^{rel} = \omega_j \left[\frac{\alpha_0}{R} \sum_{vib} \frac{\omega\tau_n C_n}{1+\omega^2 \tau_n^2} + \frac{\alpha_\infty}{R} \sum_{rot} \omega\tau_n C_n \right]. \quad (5.16)$$

Adding Eq. (5.15), (5.4) and (5.8), we obtain the final expression for the resonance frequency that accounts for vibrational dispersion effects, the shifts of surface losses and non-ideal behavior of the gas:

$$\omega_j(\omega) = \omega_j^{rel} + \delta\omega_j^{sur} + \delta\omega_j^{vir}$$

$$= \left\{ \left[1 + \frac{\alpha_0}{2R} \sum_{vib} \frac{\omega^2 \tau_n^2 C_n}{1 + \omega^2 \tau_n^2} \right] - \frac{1}{2} \alpha_{sur} p^{-1/2} + \alpha_{vir} p \right\} \omega_j \quad (5.17)$$

adding Eq. (5.16), (5.5) and (5.7) together, we have the final expression for the half-width of the resonance profile which includes the contributions of both vibrational and rotational relaxation, surface and volume losses,

$$\begin{aligned} \Delta\omega_j(\omega) &= \Delta\omega_j^{rel} + \Delta\omega_j^{sur} + \Delta\omega_j^{vol} \\ &= \left\{ \left[\frac{\alpha_0}{R} \sum_{vib} \frac{\omega \tau_n C_n}{1 + \omega^2 \tau_n^2} + \frac{\alpha_\infty}{R} \sum_{rot} \omega \tau_n C_n \right] + \alpha_{sur} p^{-1/2} + \alpha_{vol} p^{-1} \right\} \omega_j. \end{aligned} \quad (5.18)$$

We should mention the following points:

a). Both Eq. (5.17) and (5.18) appear to be implicit equations for ω in terms of itself, even α_{sur} and α_{vol} are function of ω . Although there are various effects that shift the resonant frequency, however, the total shifts are still relatively small (in the case of SF₆, the total shifts $\sim 1.8\%$), to have explicit equations one may simply substitute ω_j for ω in Eq. (5.17) and (5.18) without significant loss of accuracy.

b). For many polyatomic molecules the vibrational relaxation can be characterized by a single relaxation time,¹² and so is more valid for rotational relaxation. So, simplifications could be made by eliminating the summations of vibration and rotation in Eq.(5.17) and (5.18).

c). Since, at constant temperature, the product of pressure and relaxation time is constant, observation of the pressure dependence of the resonant frequency and half-width provides a means of determining the $(p\tau)$ product.

Although we loosely use the term relaxation time to denote one of the parameters of the experiment, we shall refer mostly to the $(p\tau)$ product.

5.3 Experimental results and data handling

A typical photoacoustic setup with automatic data acquisition was employed to excite and detect acoustic resonance in a cylindrical cavity. An infrared beam from a CO₂ laser to excite a gas sample is chopped at an acoustic frequency that may coincide with a natural frequency of the cavity to promote a resonance, and propagates along the co-axis of the cylinder to a laser power meter for signal normalization. The photoacoustic signal detected by a microphone was amplified by a lock-in analyzer (*EG&G 5210*), and the CO₂ laser (*Laser Photonics, CL35*) was grating tuned and emitted 0.5~2 W/line with a beam diameter ~1.5 mm. The optical chopper (*Scitec 300CD*) was driven by a function generator (*HP 3325A*) which can operate as high as 20 kHz. The resonant cavity was constructed of brass and nickel-plated with a diameter of 10.16 cm and a length of $L \cong 2R = 10.16$ cm to minimize the ratio of surface area to volume for a fixed volume. The miniature electret microphone (*Knowles BT-1759*) was mounted in the cylindrical wall halfway between the ends. Two ZnSe windows with diameter 1.3 cm mounted in the centers of two end plates. The setup was completely controlled by a computer through a GPIB interface. A NB-GPIB-P/TNT interface board (*National Instruments*) was employed to perform the basic IEEE 488 Talker, Listener, and Controller functions required by the most recent GPIB standard, IEEE 488.2, between an Apple NuBus computer and the GPIB instruments. An application software called *LabVIEW* was employed for the

instrument control and data acquisition through the design of the so-called virtual instrument. More details can be found elsewhere.¹⁴

The measurements were made at the pressure range of 1~800 Torr and ambient temperature typically around 295 K. Often, a particular resonant mode of the cavity was scanned several times at the same pressure to assess the reproducibility. The acoustic signal was taken point by point at each discrete modulation frequency. A commercial SF₆ gas sample with a stated purity of 99.8% was used without further purification. There are over 100 modes predicted by Eq. (1) in the cavity at a frequency range 0.6~10 kHz, but only about 30 modes are measurable, because the symmetry constraints imposed by laser excitation and microphone detection of the standing waves in the cavity has drastically reduced the number of the modes actually observed. We chose the combination mode (034) because it was the best undisturbed mode in the resonator.

An overview of the observed resonance curves of the mode (034) as a function of pressure is shown in the 3D surface plot of Fig. 5.1. With the pressure decreasing, the resonant frequency shifts up and down through the vibrational dispersion region, and the accumulated energy in the mode spreads out, resulting in an increase of the half-widths, namely the quality factors Q_j decreases.

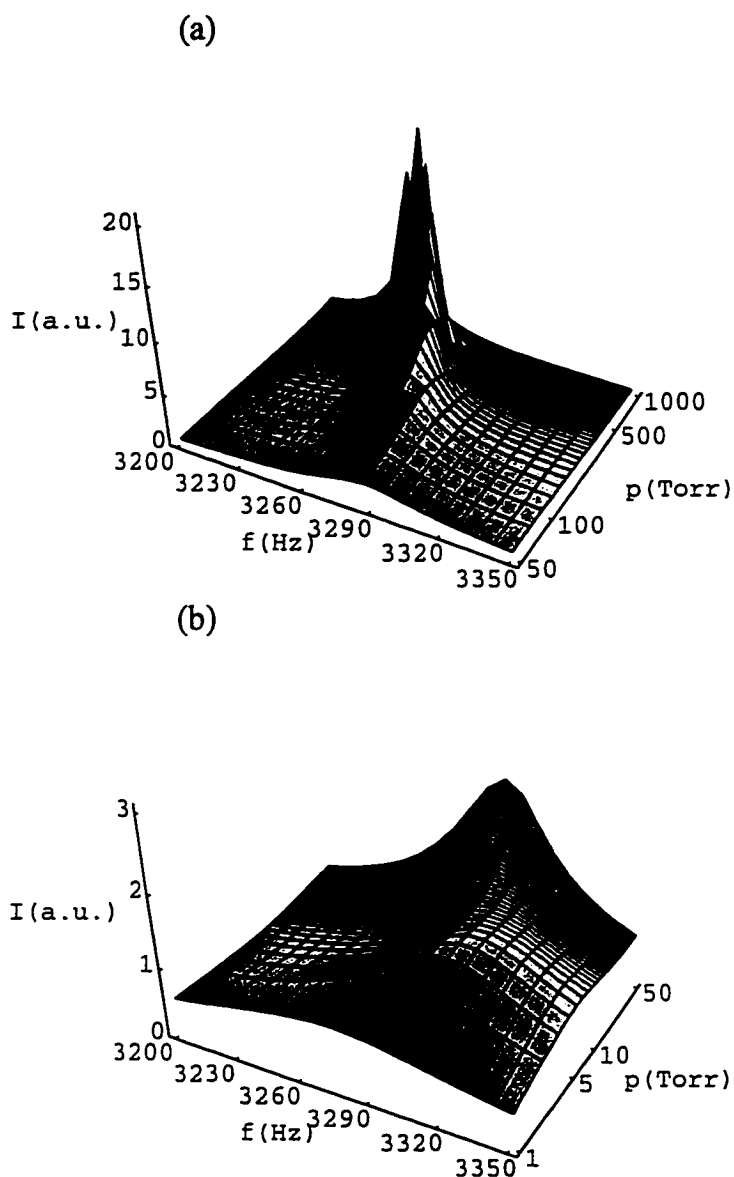


FIG. 5.2 An overview of the resonance profile of the mode (034) of SF₆ as function of pressure, (a) 50~1000 Torr, (b) 1~50 Torr. With the pressure decreasing, the resonant frequency shifts up and down through the vibrational dispersion region, and the accumulated energy in the mode spreads out, resulting in an increase of the half-widths.

The data analysis was done according the following procedures. In first step, a symmetric Lorentzian profile, the square root of the complex conjugate of Eq.(5.2),

$$A_j(f) = \frac{A_j}{\sqrt{(f_j^4/f^2) - 2f_j^2 + f^2 + \Delta f_j^2}}, \quad (5.19)$$

was used to fit the data of the photoacoustic signal vs. frequency at each fixed pressure, to determine the resonant frequency $f_j (= \omega_j / 2\pi)$ and the half-width $\Delta f_j (= Q_j^{-1} f_j)$. The black dots in Fig. 5.3 and 5.4 show the behavior of the obtained resonant frequencies f_j and half-width Δf_j versus pressure, respectively. Next, Eq.(5.17) was used to fit the resonant frequency f_j data in Fig.5.3 to determine the vibrational relaxation time, i.e.,

$$\begin{aligned} \delta\omega_j &= \omega_j^{rel} + \delta\omega_j^{sur} + \delta\omega_j^{vir} \\ &= \left\{ \left[1 + \frac{\alpha_0}{R} \sum_{vib} \frac{\omega^2 \tau_n^2 C_n}{1 + \omega^2 \tau_n^2} \right] - \frac{1}{2} \alpha_j^{sur} p^{-1/2} - \alpha_j^{vir} p \right\} \omega_j. \end{aligned} \quad (5.17')$$

The value of vibrational specific heat capacity C_{vib} was calculated by the Planck-Einstein formula with the following frequencies for the six fundamental modes:

$$\begin{aligned} \nu_1 &= 775 \text{ cm}^{-1}(1), & \nu_2 &= 644 \text{ cm}^{-1}(2), & \nu_3 &= 940 \text{ cm}^{-1}(3), \\ \nu_4 &= 615 \text{ cm}^{-1}(3), & \nu_5 &= 524 \text{ cm}^{-1}(3), & \nu_6 &= 363 \text{ cm}^{-1}(3), \end{aligned}$$

$$\text{i.e.,} \quad C_{vib}/R = \sum_n g_n \left(\frac{h\nu_n}{kT} \right)^2 \frac{e^{h\nu_n/kT}}{(e^{h\nu_n/kT} - 1)^2}. \quad (5.21)$$

The numbers in the brackets are the corresponding degeneracy factor (g), and $C_{vib} = 7.5235R$ was obtained at 295 K. The rest of parameters are given in Table 1. Since, like vast majority of polyatomic molecules, SF₆ shows a single V-T transfer via the lowest mode ν_6 involving the whole vibrational heat capacity,^{2,15,16} the

obtained vibrational relaxation time has to be modified, to give a molecular transition probability of the mode. By the Schäfer equation,¹⁷ $\tau_{vib} = \tau_{vib} (g_6 C_6 / C_{vib})$, where τ_{vib} is the observed overall vibrational relaxation time from the frequency dispersion, C_{vib} is the total vibrational heat capacity, and C_6 and g_6 are the heat capacity and degeneracy of the lowest mode ν_6 . The resulting vibrational relaxation time was found to be $(p\tau)_{v-T} = 0.21 \pm 0.01 \mu\text{s atm}$. Eq. (5.17) fits the data very well, and an error of $2.33 \times 10^{-4}\%$ was reached at the final iterations of the fitting. The calculated individual contributions to the resonant frequency shifts are also indicated in Fig. 5.3. The upper S-shaped curve represents the vibrational frequency dispersion, and the two downward shifts of surface losses and non-ideal correction of the gas make their large contributions at the low and high pressure regions, respectively.

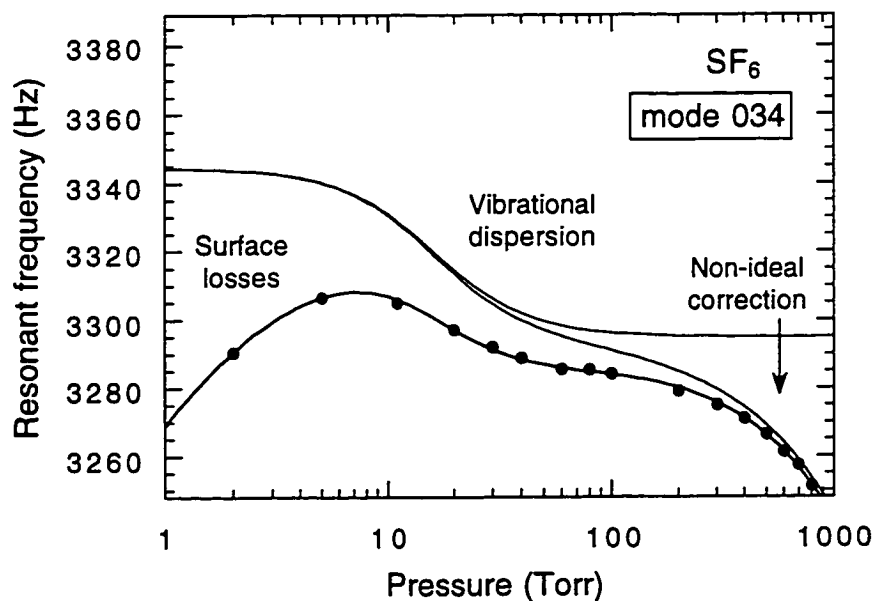


FIG. 5.3 The pressure dependence of resonant frequency of the combination mode (034) for SF₆. The upper S-shaped thin curve is the calculated vibrational dispersion, the surface losses make large contribution at low pressure, and the non-ideal correction becomes significant at high pressure.

Finally, Eq. (5.18) was used to fit the half-width Δf_j data in Fig. 5.4 to determine the rotational relaxation time, i.e.,

$$\Delta\omega_j = \Delta\omega_j^{rel} + \Delta\omega_j^{sur} + \Delta\omega_j^{vol}$$

$$= \left\{ \left[\frac{2\alpha_0}{R} \sum_{vib} \frac{\omega\tau_n C_n}{1 + \omega^2\tau_n^2} + \frac{2\alpha_0}{R} \sum_{rot} \omega\tau_n C_n \right] + \alpha_j^{sur} p^{-1/2} + \alpha_j^{vol} p^{-1} \right\} \omega_j. \quad (5.18')$$

The rotational heat capacity was simply taken as $C_{rot} = \frac{3}{2}R$. Since the rotational energy levels are much more closely spaced and highly populated, it is more valid that R-T transfer can be characterized by a single rotational relaxation time.¹⁸ The observed rotational relaxation time may be modified by a factor of $\frac{1}{3}$. The resulting rotational relaxation time was found to be $(p\tau)_{R-T} = 0.09 \pm 0.06$ ns atm. The fitting had an error of 2.8% at the final iterations.

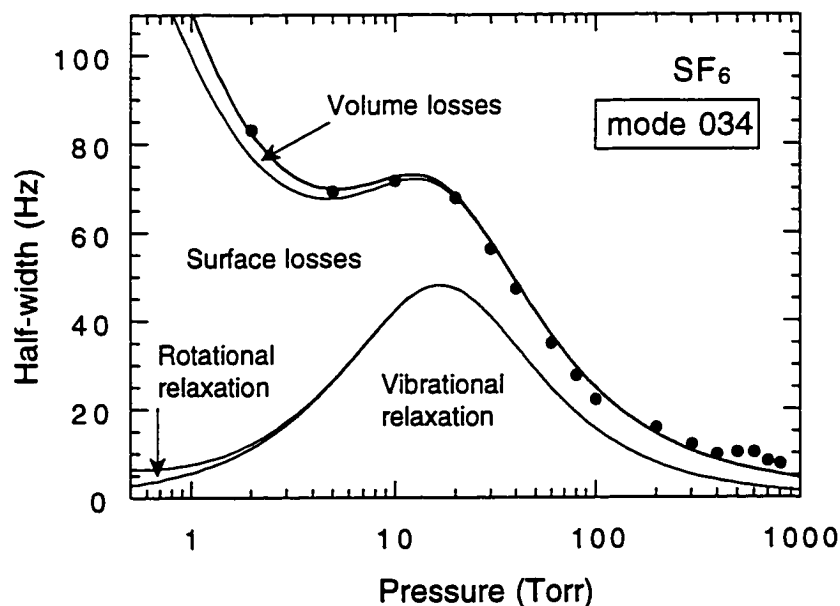


FIG.5.4 The pressure dependence of the half-width of the combination mode (034) for SF₆. The lower bell-shaped thin curve is the calculated vibrational relaxation and the difference on its left wing as pointed by an arrow is the rotational relaxation contribution. The surface losses make a large contribution to the half-width, and the volume losses make its correction at low pressure.

As it is indicated by the calculated curves in Fig.5.4, for the much faster rotational relaxation, only the right wing of the bell-shaped relaxation dissipation curve is noticeable, even at the lowest pressure studied. The contributions of volume losses, surface losses, and vibrational relaxation to the broadening of half-widths are all illustrated in the Fig. 5.4. Table 1 summarizes all the constants used to evaluate Eq. (5.17) and (5.18).^{19,20} The fittings were carried out using the Kaleidagraph data analysis/graphics application, which uses the Levenberg-Marquardt algorithm for non-linear least squares fitting.

Table 5.1. Summary of the constants used to evaluate Eq.(5.17) and Eq.(5.18).^{19,20}

Mode	α_0	α_∞	α_{sur} (Torr ^{1/2})	α_{vir} (Torr ⁻¹)	α_{vol} (Torr)
034	4.01×10^{-3}	4.17×10^{-2}	4.62×10^{-2}	-1.57×10^{-5}	3.22×10^{-3}

5.4 Discussion of the Results

5.4.1 Molecular Relaxation times

The vibrational relaxation time of SF₆ has been measured by a variety of methods. The present value of 0.21 μ s atm (295 K) agrees fairly well with the ultrasonic absorption results of 0.18 μ s atm (309K)¹⁶, and 0.24 μ s atm (301K)¹⁸. It is also in agreement with the laser spectroscopic result of 0.16 μ s atm (300 K)². The observed overall vibrational relaxation time of 1.03 μ s atm is about 23% higher than the result of 0.84 μ s atm (298 K)⁷ obtained by the same kind photoacoustic resonance method. The reason for this discrepancy is probably due to the fact that the vibrational dispersion term of $\omega^2 \tau_n^2$ has been neglected in

their theoretical considerations. The rotational relaxation time of SF₆ has been measured by laser induced spectroscopic method with a value of 0.05 ns atm at (163~178 K)^{21,22}, and by the temperature dependent ultrasonic absorption with a value of 0.6 ns atm (284 K)²³. The present result of $(p\tau)_{R-T} = 0.09 \pm 0.06$ ns atm is in agreement with the spectroscopic results within the experimental error, and it may be considered the first reported result obtained by photoacoustic resonance method for SF₆.

5.4.2 Losses Mechanism

Surface and volume losses are the two major damping parameters in a cavity. The surface loss occurs in a thin region near the walls which may be considered to composed of two layers, thermal and viscous boundary layers. The physical interpretation of the thermal boundary layers' contribution to the frequency shift is easy to see. In the bulk of the gas, sound propagates adiabatically with a velocity $\sqrt{\gamma p/\rho}$. The gas in the boundary layer, however, is in good thermal contact with the walls, and, therefore, as one approaches the wall, the sound velocity approaches its isothermal value $\sqrt{p/\rho}$. This reduction in sound velocity in the boundary layer is like an increase in the dimensions of the resonator and produces a downward shift in the frequency. The viscous boundary layer shift, while less intuitively obvious, is generally of comparable magnitude. The shifts are inversely proportional to the root square of pressure, as it shown in the Fig.5.3. The surface losses would also make a large contribution to the half-width broadening. The thermal dissipation process occurs because the expansion and compression of the gas do not occur adiabatically near the walls. The isothermal process in the boundary layers leads

to heat conduction responsible for the thermal losses. The viscous dissipation is also due to the boundary conditions imposed by the walls; at the surface, the tangential component of acoustic velocity is zero, whereas in the interior of the cavity it is proportional to the acoustic pressure gradient. The contributions of broadening are also inversely proportional to the root square of pressure as it is presented in the Fig.5.4.

The friction due to compression motion and transformation of organized energy into heat caused by temperature gradients is responsible for a free space viscous and thermal losses, i.e. volume losses (Stokes-Kirchoff losses). They make small contributions to the broadening of half-width. It is inversely proportional to the pressure as shown in the Fig.5.4.

5.4.3 Nonideality of Gases

Corrections for the deviation of the gas from the behavior of ideal gases results in a shift of the resonant frequency, called "Virial shift". It is proportional to pressure p , represented in the Fig.5.3. This is because at high pressures intermolecular forces give rise to a change in the compressibility and consequently in the sound velocity.

5.4.4 Relaxation Model in SF₆

In the photoacoustic effect the energy fed into the molecule via the specific mode probably relaxes through the entire heat capacity to the translational modes. The system was not sensitive to the details of processes by which molecules were removed from these levels. The experimental results seem to support the generalized effective two-state relaxation model^{2,24} as illustrated in

Fig. 5.5. The generalization consists of treating the vibrationally excited molecules as not exclusively in $\nu_3 = 1$, but in a complete distribution of vibrational states from $\nu_6 = 1$ on up, all of which are in very rapid equilibrium with each other. These levels can thus be described by an effective vibrational temperature, which need not be the same as the translational and rotational temperature of the system.

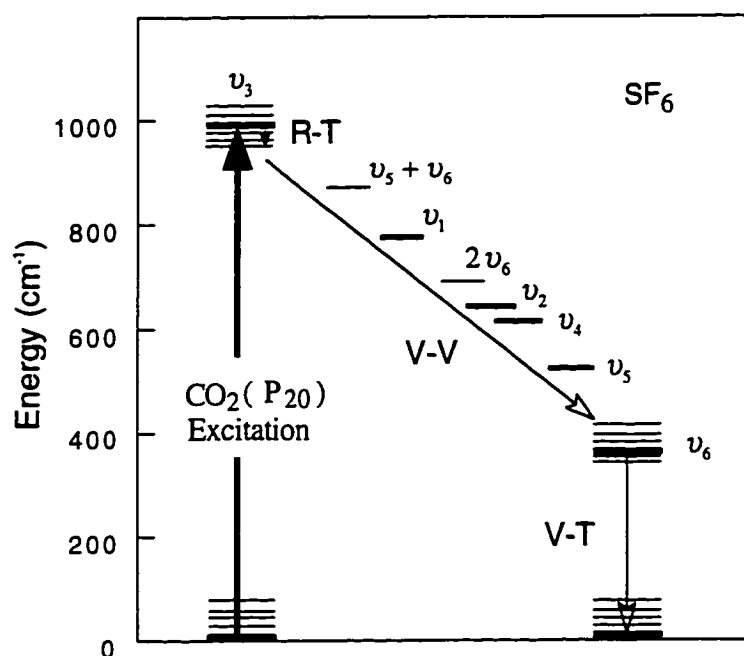


FIG. 5.5 The effective two-states relaxation model of SF₆, following the CO₂ (P₂₀) laser excitation of the ν_3 vibrational mode, the system relaxes by rapid R-T to translational and V-V down to the lowest vibrational ν_6 level; the whole excess vibrational temperature relaxes via a slow rate V-T transfer process from ν_6 level to the translational temperature, and heat the entire gas translationally.

The experiment we are carrying out thus consists of:

- (i) Laser-pumping a small fraction of the SF₆ molecules to a specified rotational level (s) of the $\nu_3 = 1$ state.

- (ii) these levels are rapidly coupled by both rotation-translation and near resonant vibration-vibration energy transfer processes to the complete set of excited vibrational levels in SF₆.
- (iii) The excess vibrational temperature relaxes back to the translational temperature, and the rate limiting process for this to occur is the vibration-translation deactivation of the ν_6 level at 363 cm^{-1} .
- (iv) Meanwhile, the energy released in step (ii) and (iii) has heated the entire gas translationally; this cools back to the ambient temperature by some combination of diffusion and conduction, giving rise to the long relaxation time seen in the system.

The photoacoustic resonance method has been used to measure the relaxation times in SF₆ for both vibration and rotation. The agreements with the ultrasonic and spectroscopic results on the vibrational relaxation time are about as good as can be expected. The present photoacoustic result on rotational relaxation time seems to back the spectroscopic results rather than that obtained by ultrasonic measurements. The theoretical treatment and the effective two-state relaxation model that we used here for the relaxation processes in a photoacoustic resonator seem reasonable in the context of the present knowledge of energy transfer. We believe that this work appears promising as a basis for developing versatile and comprehensive instruments that can carry out measurements of trace gas analysis, of molecular relaxation-times, and of rate constant and reactive energy of a photo-induced chemical reaction in a resonator.

References to Chapter 5

- 5.1 G. Herzberg, "Molecular Spectra and Molecular Structure"
(D. Van Nostrand Company, Inc., New York, 1945)
- 5.2 J. I. Steinfeld, I. Burak, D. G. Sutton and A.V. Nowak,
J. Chem. Phys. **52**, 5421 (1970).
- 5.3 L.B.Kreuzer, J. Appl. Phys. **42**, 2934 (1971).
- 5.4 C.F.Dewey, Jr., R.D. Kamm, and C.E.Hackett, Appl. Phys. Lett. **23**, 633 (1973).
- 5.5 Roger D.Kamm, J. Appl. Phys. **47**, 3550 (1976).
- 5.6 K. Frank and P. Hess, Chem. Phys. Lett. **68**, 540 (1979).
- 5.7 R.H.Johnson, R.Gerlach, L.J.Thomas III and N.M.Amer,
Applied Optics **21**, 81 (1982).
- 5.8 A.Karbach and P. Hess, J. Chem. Phys. **83**, 1075 (1985).
- 5.9 M.Fiedler & P.Hess, J. Chem. Phys. **93**, 8693 (1990).
- 5.10 R.P.Fiegel, P.B.Hays & W.M.Wright, Applied Optics **28**, 1401 (1989).
- 5.11 P.M.Morse and K.U.Ingard, *Theoretical Acoustics*,
(McGraw-Hill, New York, 1968).
- 5.12 L.B.Kreuzer, *Optoacoustic Spectroscopy and Detection* edited by Y.H.Pao
(Academic Press, 1977).
- 5.13 K.F.Herzfeld & T.A.Litovitz, *Absorption & Dissipation of Ultrasonic Waves*,
(Academic Press, New York, 1959).
- 5.14 G. Lei and B. Di Bartolo, Rev. Sci. Instrum. **66**, 5102(1995).
- 5.15 R. D. Bates, J.T. Knudtson and G.W. Flynn, J. Chem. Phys. **57**, 4174 (1972).
- 5.16 C.L. O'Connor, J. Acoust. Soc. Amer. **26**, 361 (1954).
- 5.17 K. Schäfer, Z. Physik. Chem. **B46**, 212 (1940).

- 5.18 T.L.Cottrell and J.C. McCoubrey, *Molecular Energy Transfer in Gases*, (Butterworths, London, 1961).
- 5.19 W. Braker and A.L.Mossman, *Matheson Gas Data Book*, (Matheson Press, 1980).
- 5.20 J.H.Dymond & E.B.Smith, *The Virial Coefficients of Gases*, (Claredon Press.Oxford.1969).
- 5.21 M. Dubs, D. Harradine, E. Schweitzer, and J. I. Steinfeld, *J. Chem. Phys.* **77**, 3824 (1982).
- 5.22 P. F. Moulton, D. M. Larsen, J.N.Walpole, and A.Mooradian, *Optics Letters* **1**, 51 (1977).
- 5.23 E.U. Haebel, *Acoustica*, **20**, 65 (1968).
- 5.24 R. D. Bates, J.T. Knudtson and G.W. Flynn, *J. Chem. Phys.* **57**, 4174 (1972).

Chapter 6

Conclusions and Future Work

This Chapter will summarize the results and conclusions of this thesis, present the reasons for continuing research on these types of studies, and put forward suggestions for future works.

6.1 Summary of the Thesis Works

This thesis has demonstrated that the photoacoustic resonance method can be used to measure the rate constants of both vibrational and rotational molecular relaxation with high precision. The results on the SF_6 molecular system show a very satisfying degree of consistency with the results obtained by other methods, such as laser induced spectroscopy and ultrasound. The rotational relaxation time obtained here may be considered the first reported value for SF_6 by the photoacoustic resonance method. The work can be summarized as follows:

- (i) A general theoretical treatment of vibrational and rotational relaxation based on the acoustically resonant characteristics of molecular gases was made in detail. In particular, the resonant frequency and broadening of the half-width was examined, with care taken to account for the surface and volume losses in the cavity, and the nonideality of the gas. This

theoretical treatment was used to frame the discussion of the relaxation processes following the vibrational excitation.

- (ii) The effective two-state relaxation model that we used here for the relaxation processes in the photoacoustic resonator seems reasonable in the context of the present knowledge of energy transfer. Through the model, the association has been made between the observed "overall relaxation times" and the internal energy transition rates of a molecular mode of the gas.
- (iii) The analysis of the experimental data yields a value for the vibrational relaxation time $(p\tau)_{V-T} = 0.21 \pm 0.01 \mu\text{s atm}$, and a value of $(p\tau)_{R-T} = 0.09 \pm 0.06 \text{ ns atm}$ for the rotational relaxation time of SF_6 at $T=295 \text{ K}$. The agreement between our results with the ultrasonic and spectroscopic results on the vibrational relaxation time is excellent. The photoacoustic result on rotational relaxation time backs the spectroscopic results rather than that obtained by ultrasonic measurements which often had limitation to deal with such a fast process. The rotational relaxation is, to the best of the author's knowledge, the first such measurement obtained by the photoacoustic resonant method.
- (iv) The research work has, in a comprehensive manner, brought all aspects of the pressure dependence of photoacoustic resonance to the application of relaxation time measurements for the first time. The theory is sound, and the experimental results agree well with those obtained by other methods (i.e., spectroscopy and ultrasound).

- (v) An infrared laser photoacoustic resonant spectrophone has been constructed during the course of this thesis work. The apparatus was completely controlled by a PC computer with virtualized instrumentation and data acquisition system. This has thoroughly established the ground work to fulfill the goal of developing a versatile instrument capable of tracing and monitoring gas species, measuring relaxation times, and evaluating the rate constant and reactive energy of photo-induced chemical reaction in a resonator.

6.2 Problems of Continuing Interest and Suggestions for Future Work

The thesis work has put forth a detailed study of molecular relaxation for a gas sample of SF_6 . The resonant frequency dispersion and broadening of half-width as a function of pressure has been studied. There is much that needs to be done in terms of studying other aspects of the resonant profile. The mode amplitude A_j , for instance, is relevant for the study of tracing and monitoring gaseous species; the pressure and temperature dependence of the resonant frequency, f_j , and half-width, Δf_j , would provide information on the kinetics of a photo-induced chemical reaction. If we consider the present work as phase I, then the next phase of the research could be the following with respect to developing the versatile instrumentation.

- (i) For tracing and monitoring gaseous species, we need an IR laser with high enough power (~ 0.5 Watt) and tunability in wavelength to cover the absorption features of the molecular species of interest. The recently commercialized high power diode IR laser seem to match these needs.

Ideally the tuning would be automatic through GPIB, Series or VXI bus. Either of these can easily be handled with the present setup.

- (ii) Utilizing a UV or Visible laser, and automatic thermal cavity temperature detection, measurements could be performed on the kinetics of photo-induced chemical reactions. The feasibility of employing "pump and probe" techniques seems promising for chemical reaction kinetics studies.
- (iii) The present system has utilized much less automation than its capability. If the gas handling system (i.e., the vacuum pump and gauge) and the laser tuning step motor were automated, experiments could be done from a remote location through the existing internet by a Ethernet-GPIB controller. Alternatively, through a wireless modem, the experiment could be controlled on a lunched balloon from a ground based station.

APPENDIX A:**CO₂ Waveguide Laser Line Data Sheet (¹²C¹⁶O₂)****10 Microns: P Branch** (24 °C, Temp. Set Pt. 4.0~6.5)

Line	Wavelengths (μm)	Power (Watts)	Mode	Micrometer Setting	Temp. Set Point
P(6)	10.46	1.5	00	7.981	4.46
P(8)	10.48	1.5	00	8.083	6.34
P(10)					
P(12)					
P(14)	10.53	2.5	00	8.362	4.62
P(16)					
P(18)	10.57	2.0	00	8.531	5.94, 6.24
P(20)	10.59	2.5	Tem 00	8.691	5.94, 6.24
P(22)					
P(24)	10.63	2.0	00	8.914	5.94, 6.24
P(26)	10.65	1.5	00	9.001	5.94, 6.24
P(28)					
P(30)	10.70	2.0	00	9.206	5.94, 6.24
P(32)	10.72	2.0	00	9.371	5.94, 6.24
P(34)	10.74	1.5	00	9.501	5.94, 6.24
P(36)	10.77	2.0	00	9.618	4.62
P(38)					
P(40)					
P(42)		1.0	00	10.001	4.62

APPENDIX A:**CO₂ Waveguide Laser Line Data Sheet (¹²C¹⁶O₂)****10 Microns: R Branch** (24 °C, Temp. Set Pt. 4.0~6.5)

Line	Wavelengths (μm)	Power (Watts)	Mode	Micrometer Setting	Temp. Set Point
R(6)					
R(8)	10.33	1.5	Tem 00	7.375	5.94, 6.2
R(10)					
R(12)	10.30	2.0	00	7.174	5.94, 6.2
R(14)	10.29	1.5	00	7.107	6.14
R(16)	10.28	2.5		7.038	5.94, 6.2
R(18)	10.26	1.5	00	6.942	5.94, 6.2
R(20)	10.25	1.0	Tem 00	6.931	7.0
R(22)		1.0	00	6.822	5.94, 6.2
R(24)	10.22	1.5	00	6.751	4.46, 6.2
R(26)	10.21	1.5	00	6.734	5.94, 6.2
R(28)		1.6	00	6.652	4.46
R(30)	10.18	2.5	00	6.585	5.94, 6.2
R(32)	10.17	2.5	00	6.515	3.84
R(34)	10.16	1.5	00	6.471	6.0
R(36)					
R(38)					
R(40)					
R(42)					

APPENDIX A:**CO₂ Waveguide Laser Line Data Sheet (¹²C¹⁶O₂)****9 Microns: P Branch (24 °C, Temp. Set Pt. 5.0~6.5)**

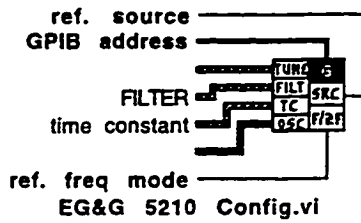
Line	Wavelengths (μm)	Power (Watts)	Mode	Micrometer Setting	Temp. Set Point
P(6)					
P(8)					
P(10)					
P(12)					
P(14)					
P(16)	9.52	1.0	00	3.555	5.28
P(18)					
P(20)					
P(22)	9.57	1.5	00	3.764	5.94, 6.24
P(24)	9.59	2.0	00	3.865	5.94, 6.24
P(26)	9.60	1.0	00	3.901	5.28
P(28)	9.62	2.0	00	4.002	5.94, 6.24
P(30)					
P(32)					
P(34)					
P(36)	9.69	1.5	00	4.333	6.24
P(38)					
P(40)					
P(42)					

APPENDIX B: Resonant Frequency (SF₆)						
<i>(c=138.4 m/s, R=0.0508, L=0.1016 m)</i>						
Calculated		Locatable	Measured	Calculated		Locatable
mode	frequency			mode	frequency	
OO1	681			2O2	3333	
O1O	798	791	791	OO5	3406	
O11	1049		1320	130	3475	
O2O	1324	1320	1620	O15	3498	
OO2	1362		2090	131	3542	
O21	1489		2637	123	3554	
O12	1579		3090	O44	3569	
1OO	1661	1620	3240	114	3573	
1O1	1796		3670	O25	3654	
O3O	1822		3980	2O3	3665	3670
O22	1900		4280	21O	3697	
O31	1945		4500	132	3733	
OO3	2043	2090	4940	211	3759	
1O2	2149		5040	1O5	3789	
O13	2194		5270	O35	3862	
O32	2275		5500	124	3985	3980
O4O	2306		5770	14O	4025	
11O	2312		5830	2O4	4084	
O41	2404		6040	OO6	4087	
111	2410		6140	O45	4113	
O23	2435		6200	115	4116	
1O3	2634	2637	6290	O16	4164	
O42	2678		6400	O26	4296	4280
112	2683		6490	3OO	4411	
OO4	2724		6570	106	4412	
O33	2738		6620	3O1	4464	
O14	2839		6800	O36	4474	4500
12O	2908			OO7	4768	
121	2987			O17	4834	
O24	3029			O27	4948	4940
2OO	3042			OO8	5449	
O34	3081			O18	5507	5500
113	3085	3090		4OO	5777	5770
2O1	3117			OO9	6130	6140
1O4	3191			O19	6182	6200
122	3211			O1O	6811	6800
O34	3277	3240				

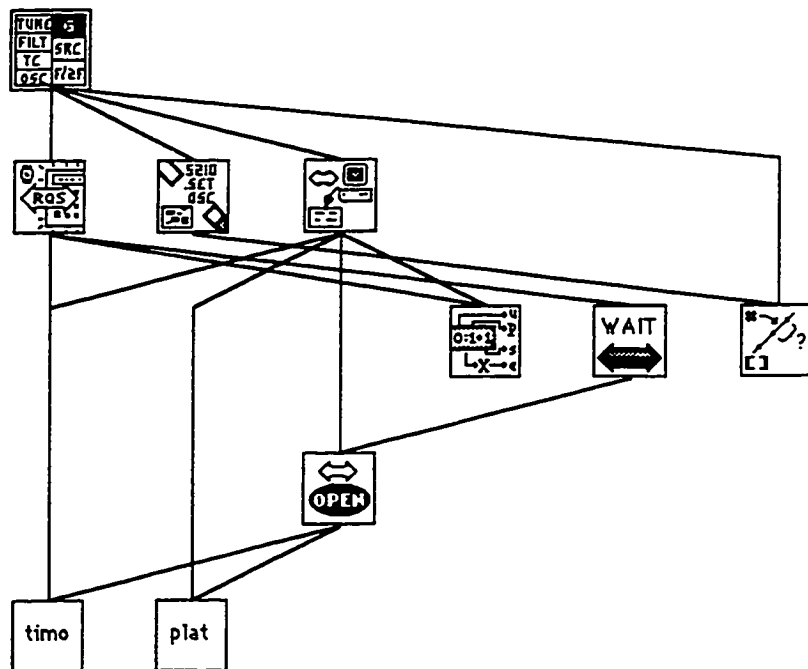
APPENDIX C: INSTRUMENT DRIVER PROGRAMS

C-1. EG&G 5210 Lock-in

Connector Pane







Position in Hierarchy



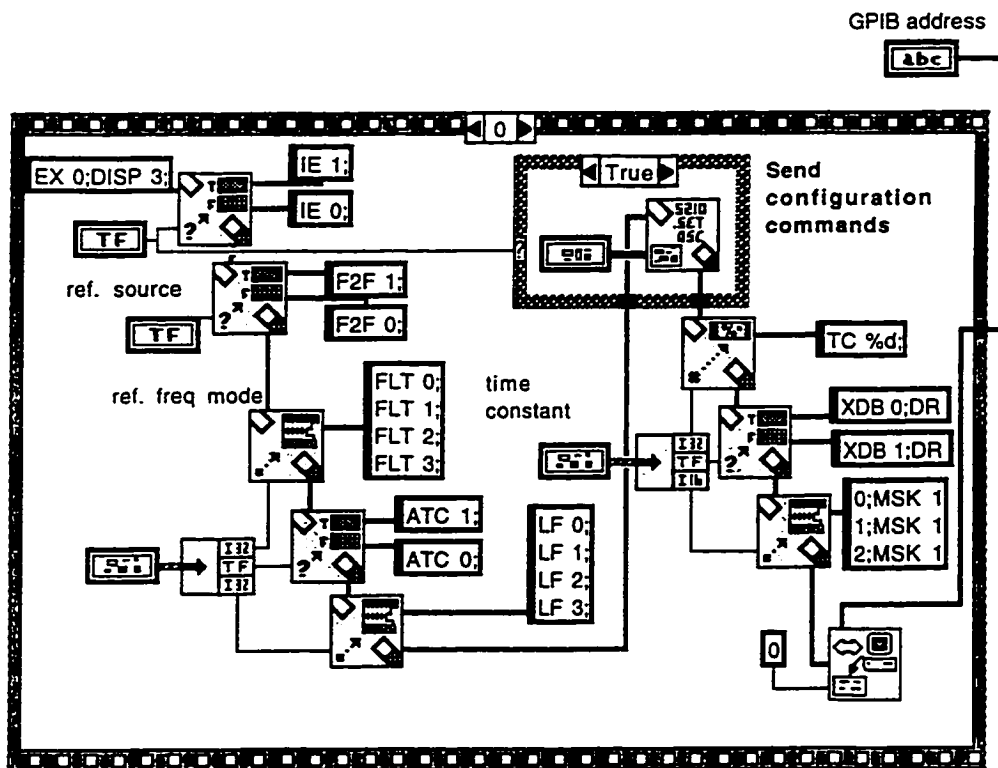
APPENDIX C: INSTRUMENT DRIVER PROGRAMS

C-1. EG&G 5210 Lock-in

List of SubVIs

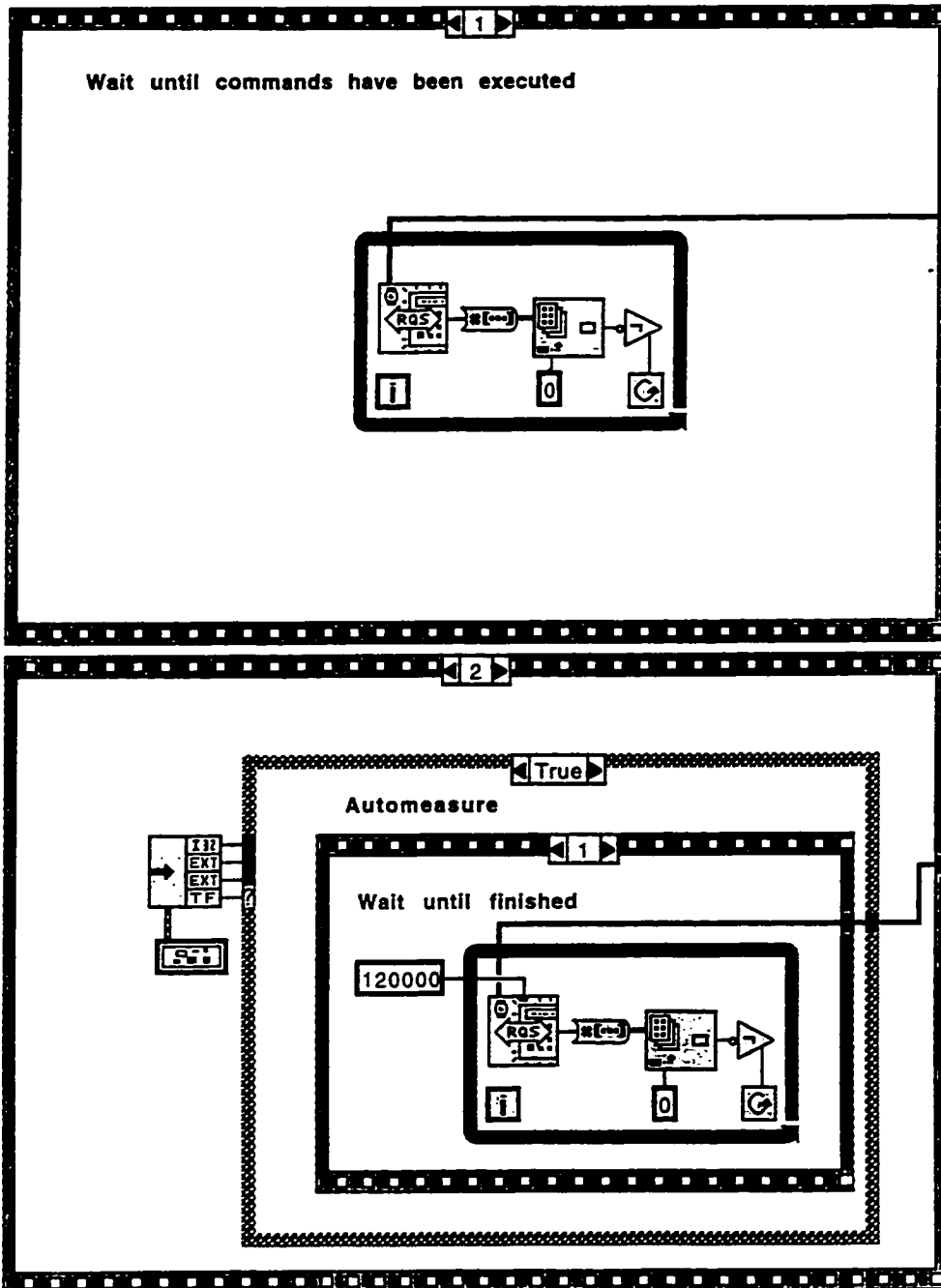
- 
GPIB Write.vi
 PowerMac:Photoacoustic Lab.:LabVIEW 3.1.1:vi.lib:Instr:gpi trad.lib:GPIB Write.vi
- 
EG&G 5210 Set Osc.vi
 PowerMac:Photoacoustic Lab.:Instrument-drivers:egg5210.lib:EG&G 5210 Set Osc.vi
- 
Find Array Index.vi
 PowerMac:Photoacoustic Lab.:Instrument-drivers:egg5210.lib:Find Array Index.vi
- 
Wait for GPIB RQS.vi
 PowerMac:Photoacoustic Lab.:LabVIEW 3.1.1:vi.lib:Instr:gpi trad.lib:Wait for GPIB RQS.vi

Block Diagram



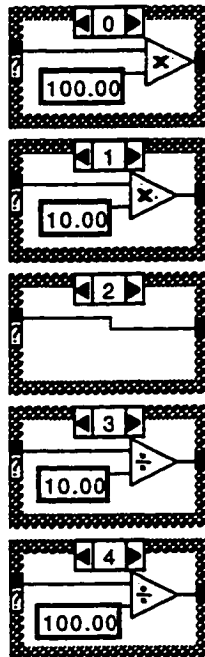
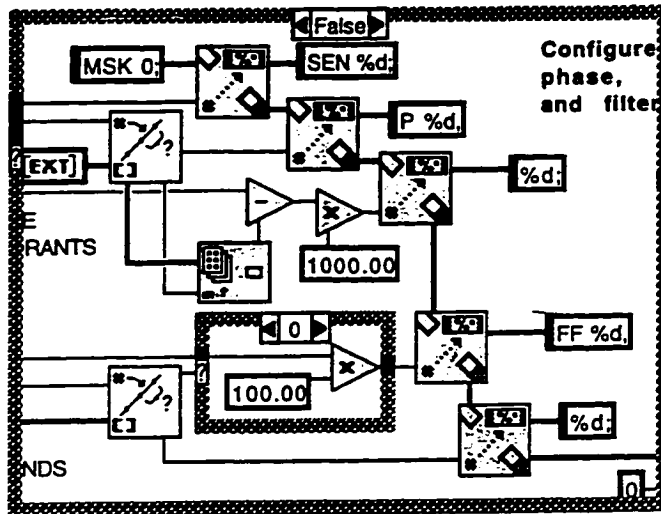
APPENDIX C: INSTRUMENT DRIVER PROGRAMS

C-1. EG&G 5210 Lock-in



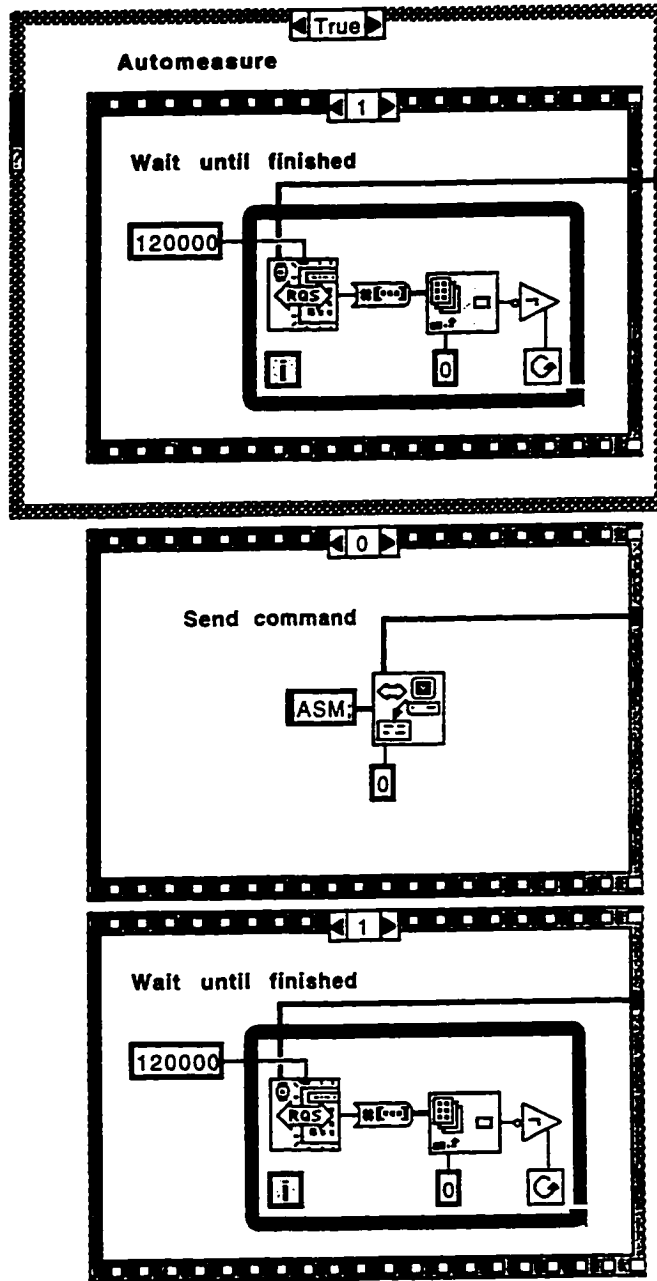
APPENDIX C: INSTRUMENT DRIVER PROGRAMS

C-1. EG&G 5210 Lock-in



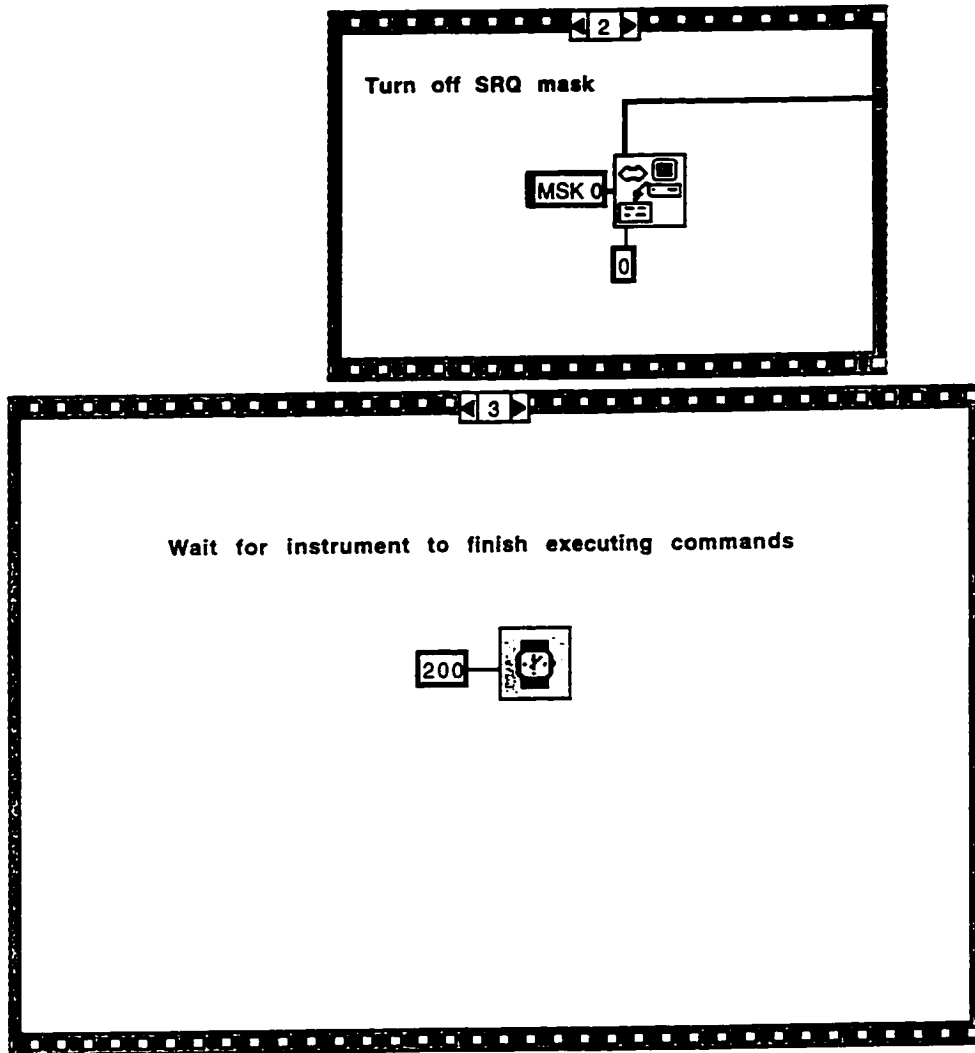
APPENDIX C: INSTRUMENT DRIVER PROGRAMS

C-1. EG&G 5210 Lock-in



APPENDIX C: INSTRUMENT DRIVER PROGRAMS

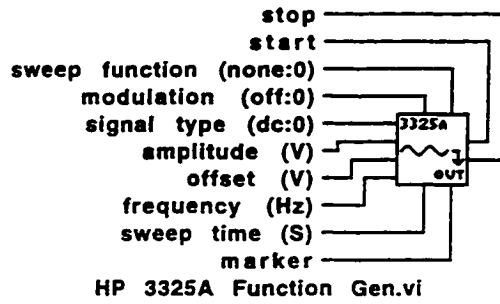
C-1. EG&G 5210 Lock-in



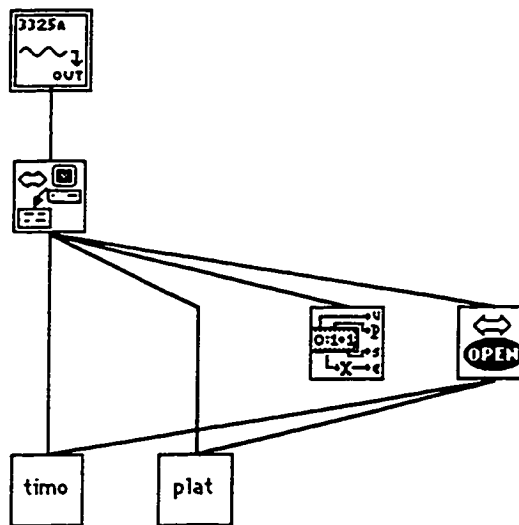
APPENDIX C: INSTRUMENT DRIVER PROGRAMS

C-2. HP 3325A Synthesizer/Function Generator

Connector Pane



Position in Hierarchy



List of SubVIs



GPIB Write.vi
PowerMac:Photoacoustic Lab.:LabVIEW 3.1.1.vi.lib:Instr:gpi trad.lib:GPIB Write.vi

APPENDIX D INSTRUMENT DRIVER PROGRAMS

D-2. HP 3325A Synthesizer/Function Generator

